RICE UNIVERSITY

High-Yield Synthesis and Applications of Anisotropic Gold Nanoparticles

by

Leonid Vigderman

A THESIS SUBMITTED
IN PARTIAL FULFILLMENT OF THE
REQUIREMENTS FOR THE DEGREE

Doctor of Philosophy

APPROVED, THESIS COMMITTEE

Eugene R. Zubarev, Chair
Associate Professor of Chemistry

Stephan Link
Assistant Professor of Chemistry,
Electrical and Computer Engineering

Kevin F. Kelly
Associate Professor of Electrical and
Computer Engineering

HOUSTON, TEXAS
February 2013

ABSTRACT

High-Yield Synthesis and Applications of Anisotropic Gold Nanoparticles

by

Leonid Vigderman

This work will describe research directed towards the synthesis of anisotropic gold nanoparticles as well as their functionalization and biological applications. The thesis will begin by describing a new technique for the high-yield synthesis of gold nanorods using hydroquinone as a reducing agent. This addresses important limitations of the traditional nanorod synthesis including low yield of gold ions conversion to metallic form and inability to produce rods with longitudinal surface plasmon peak above 850 nm. The use of hydroquinone was also found to improve the synthesis of gold nanowires via the nanorod-seed mediated procedure developed in our lab. The thesis will next present the synthesis of novel starfruit-shaped nanorods, mesorods, and nanowires using a modified nanorod-seed mediated procedure. The starfruit particles displayed increased activity as surface-enhanced Raman spectroscopy (SERS) substrates as compared to smooth structures. Next, a method for the functionalization of gold nanorods using a cationic thiol, 16-mercaptohexadecyltrimethylammonium bromide (MTAB), will be described. By using this thiol, we were able to demonstrate the complete removal of

toxic surfactant from the nanorods and were also able to precisely quantify the grafting density of thiol molecules on the nanorod surface through a combination of several analytical techniques. Finally, this thesis will show that MTAB-functionalized nanorods are nontoxic and can be taken up in extremely high numbers into cancer cells. The thesis will conclude by describing the surprising uptake of larger mesorods and nanowires functionalized with MTAB into cells in high quantities.

Acknowledgments

Frist, I would like to thank my advisor, Prof. Eugene Zubarev, for his help throughout my studies. I have appreciated the balance of direct guidance as well as freedom to explore that he granted me throughout my studies, allowing me to grow as a scientist while keeping me on the right track along the way.

Thanks to my committee members, Prof. Stephan Link and Prof. Kevin Kelly, for finding the time in their busy schedules to take part in my PhD defense. In addition, my collaboration with Prof. Link has been fruitful and I learned much during Prof. Kelly's class.

I have been lucky to have great coworkers in the Zubarev group including Bishnu Khanal, Jacob Gibson, Pramit Manna, and Paul Derry, who were great collaborators and friends. They made my stay at Rice much more enjoyable even when there were only two of us in the lab.

Finally, I wanted to express my sincere gratitude to my parents, Oleg and Alla, and my brother Constantine, without whose support I would have never made it to this point, and to my girlfriend Eliona Kulla, for bringing me so much happiness during this time.

Contents

List of Figures

Introduction

High-Yield Synthesis of Gold Nanorods Using Hydroquinone as a Reducing Agent

Nanorod Overgrowth: Synthesis of Smooth and Branched Nanostructures

List of Tables

High-Yield Synthesis of Gold Nanorods Using Hydroquinone as a Reducing Agent

Nomenclature

AA	Ascorbic Acid
Au	Gold
CTAB	Cetyltrimethylammonium Bromide
HQ	Hydroquinone
ICP-OES	Inductively Coupled Plasma - Optical Emission Spectroscopy
IR	Infrared
MTAB	16-mercaptohexadecyltrimethylammonium bromide
MUTAB	16-mercaptoundecyltrimethylammonium bromide
MR	Mesorod
NMR	Nuclear Magnetic Resonance
NR	Nanorod
NW	Nanowire
PEG	Polyethylene Glycol
PNR	Pentahedrally-Twinned Nanorod
SEM	Scanning Electron Microscopy
SERS	Surface-enhanced Raman Spectroscopy
SPR	Surface Plasmon Resonance
TEM	Transmission Electron Microscopy
TGA	Thermogravimetric Analysis
UV-Vis	Ultraviolet-Visible

Chapter 1

Introduction

1.1. Gold Nanoparticles

The fascinating size-dependent properties of noble metal nanoparticles (also known as gold colloids) have created a great promise for their use in a variety of electronic, optical, and biomedical applications. Gold nanoparticles, specifically, have received a great deal of attention due to their unusual physical properties. They are generally simple to synthesize, requiring only a gold salt, reducing agent(s), and a surfactant. Synthesis can be carried out in organic or aqueous environments without the need for any moisture- or oxygen-free techniques. The stability of gold nanoparticles is also quite high as compared to other noble metal systems such as silver or copper, which are highly prone to oxidation. In addition, the nanoscale confinement of electrons on the surface of gold nanoparticles grants them shape- and size-dependent properties not seen in larger particles.[1,2] Initially,

spherical or quasi-spherical gold nanoparticles received the most attention due to the ease of synthesis of such structures. This is perhaps unsurprising given that the spherical shape is often the most thermodynamically favorable morphology.

Gold nanoparticles were actually first used in the 5th century BC as a rose coloring for glass. The synthesis of colloidal suspensions of spherical gold nanoparticles was first described scientifically by Michael Faraday in the 1850s utilizing phosphorus as a reducing agent for gold chloride[3] and since then has gained popularity rapidly. The most popular modern methods of synthesis were developed by Turkevich in 1951[4] and further refined by Frens in 1973[5] and utilized citric acid or tannic acid as dual-purpose reducing and stabilizing agents. Such procedures produce water-soluble, quasi-spherical nanoparticles with size from 5-100 nm and the highest monodispersity in the 10-20 nm size range. Such nanoparticles are stabilized by weakly-binding surfactants which can be exchanged for more strongly binding molecules such as thiols. On the other hand, reduction of gold directly in the presence of thiolated molecules, which bind strongly to the gold surface forming a self-assembled monolayer,[6] leads to the formation of much smaller nanoparticles of 1-5 nm in diameter which are generally soluble in organic media.[7,8] These nanoparticles have been very popular due to their high stability and the possibility for further reaction[9–14] or exchange of the organic surface coating[7,15–17] to modify them for a particular application.[18] For more detailed information, the reader is directed to one of the many reviews on the synthesis, functionalization, and application of gold nanoparticles.[15,19–28]

1.2. Moving Away from Isotropic Growth

As mentioned previously, the optical and electronic properties of gold nanoparticles are largely determined by their shape and size. Thus, having access to only isotropic, spherically-shaped particles provides a significant limitation on their usefulness. For instance, one of the most important properties of gold nanoparticles is their optical absorption in the visible region due the presence of surface plasmon resonance (SPR), the collective oscillation of electrons on the particle surface. Spherical nanoparticles show limited tunability of this SPR absorption ranging from about 520 to 575 nm corresponding to diameters from 5 to 100 nm, respectively, which explains their red solution color.[28] This is a significant limitation, especially for biomedical applications, as the biological tissue has very low transparency in the visible region.[29] Furthermore, nanoparticles with a smaller diameter do not display any appreciable SPR effect.

In order to access more complicated structures, it is necessary to find reaction conditions which can break the propensity towards isotropic growth and, instead, direct the nanoparticle growth in an anisotropic fashion. The first class of anisotropic nanoparticles to gain the most popularity has been gold nanorods (NRs), which were first synthesized in the mid-1990s through an approach based on electrochemical reduction into rod-shaped templates.[30,31] Due to the limitations of this technique, such as the low total yield of the procedure, more widespread adoption of gold NRs into research did not occur until the advent of wet-chemistry synthetic techniques, which did not appear until Murphy and coworkers‘ seminal

work published in 2001.[32] Continued improvements in synthetic methodology have led to better reliability and have increased the shape-wise yield of rods to above 90 percent.

As synthetic capabilities improved, so did the understanding of the physical properties of NRs, including their anisotropic optical and electronic properties. Excellent reviews have been published that describe the origins and modeling of the physical properties of gold NRs.[33–35] As noted earlier, the position and intensity of SPR bands can be highly shape- and size-dependent.[33–38] Due to the anisotropic shape of gold NRs, they display two separate SPR bands corresponding to their width and length known as the transverse (TSPR) and longitudinal surface plasmon bands (LSPR). The TSPR is located at just above 500 nm while the LSPR varies widely according to the NR aspect ratio and the overall size. Modeling of the optical properties of gold NRs is generally carried out using Gans theory which describes the optical properties of ellipsoidal particles.[33] The relationship between the rod aspect ratio and the LSPR has been empirically determined to fit the equation:[33]

$$\lambda_{max} = 95AR + 420$$

However, the exact LSPR position and intensity is dependent on a variety of factors including the size, dielectric constant of the surrounding media, and small variations in morphology deviating from a perfect rod shape.[33,39–41] Through careful synthesis, it is possible to create single crystalline gold NRs with an LSPR anywhere

from the visible (600 nm) all the way into the near IR (1100+ nm) portion of the electromagnetic spectrum.

1.3. Applications of Gold Nanorods

The ability of NRs to absorb near IR light makes them particularly well-suited to biomedical applications since the absorbance of the biological tissue in this region is low, with several excellent reviews having been published on the topic.[29,33,42–44] One of the most prominent application of gold NRs, as well as other near-IR absorbing morphologies such as gold nanoshells and nanocages, has been their use in photothermal cancer therapy.[44–47] This technique is based on the ability of gold nanoparticles to absorb energy in the form of light and emit it in the form of heat. Gold NRs are delivered to the vicinity of a cancer and irradiated with a near-IR laser, to which the body is mostly transparent. This induces rapid, localized heating around the rods, destroying any tissue in the vicinity. Another application for gold NRs is as an imaging agent in biological systems due to their very high light scattering ability[33,48] as well as their two-photon luminescence properties.[49,50] Both of these can be utilized to provide high signal above the relatively high level of noise that is present in biological systems.

However, several issues exist for the clinical application of such systems. First, there is a need to address the cytotoxicity of gold NRs which is related to their surface coating. Recent literature has supported the idea that it is the NR surfactant rather than the gold core which is cytotoxic.[51] Chapter 5 will discuss this issue in

more detail by presenting a unique system to mitigate this cytotoxicity. Second, targeted delivery to the cancer site is very important to maximize the therapeutic efficacy.[43] Targeted delivery of nanoparticles in the body can be accomplished in various ways, but the most promising way appears to be the conjugation of antibodies to the nanoparticle,[44,52,53] which has been demonstrated in rods,[33,54] although application of these systems *in vivo* is still limited. Cell uptake of the rods once they reach the desired location in the body may also be important to maximize their activity especially for drug or gene delivery,[20] an issue which will be addressed in Chapter 5. Finally, the clearance and long-term effects of gold NRs are not well understood at this time, although the functionalization of nanoparticles with polyethylene glycol is generally known to inhibit cell uptake and improve clearance from the body.[43]

Outside the biomedical realm, gold NRs have shown much promise for the sensing of a variety of analytes including environmental toxins[55–57] and biomarkers,[58,59] which has been covered extensively in a recent review.[60] Changes in the optical absorbance of gold NRs, usually LSPR position or intensity, can be a sensitive marker of surface chemistry as well as orientation of gold NRs. Binding of analytes can be monitored directly[61–64] or through induced rod assembly. [56,65–69] Similarly, the efficient light-scattering of rods[33,70] can be taken advantage of to design systems with low limits of detection through the use of dynamic light scattering.[56,71] The use of assemblies of gold nanoparticles, including NR and other received a great deal of attention due to the possibility of sensing with extremely

low detection limits and with access to analyte structural information.[72–79] Using gold NRs allows the creation of unique assays based on the anisotropic structure and assembly of the rods,[80–82] as we have demonstrated with the use of NR supercrystal arrays for ultrasensitive detection of prions.[83] Finally, recent studies have demonstrated the potential of capturing high-energy electrons generated during rod plasmonic excitation with possible applications in light detection and photovoltaics.[84–86]

1.4. Gold Nanorod Synthesis

There are various methods to produce gold NRs with different structures. The first class of synthetic techniques that will be discussed are the various aqueous wet-chemical CTAB-mediated synthetic procedures which have become the most popular as originated by Murphy et al[32] and El-Sayed et al.[87] While all of these techniques produce crystalline NRs, they can be subdivided into those that lead to rods with single-crystalline or pentahedrally-twinned structure. This is an important distinction as the purity, length-scale, and further manipulations can depend highly on this difference. The second class of techniques are those based on reduction of gold inside a template of some sort, most often an anodized aluminum oxide (AAO) membrane, which produces polycrystalline structures in limited quantities.

1.4.1. Silver-Mediated Synthesis of Single-Crystalline Nanorods

1.4.1.1. Electrochemical Synthesis

The first report of reasonably high quality gold NRs used an electrochemical approach which was the precursor of the most common seed-mediated procedure.[88,89] Reported by Wang and coworkers, this approach utilized a two-electrode electrochemical cell in which the gold anode provided the gold source for the reaction while the template for rod-growth was a mixed surfactant system of CTAB and tetradodecylammonium bromide (TDTAB). Small amounts of acetone and hexane additives were also present and the entire setup was sonicated throughout the reaction. The presence of a silver plate, which was theorized to produce silver ions in solution, led to increased rod yield and length.[89] NRs were synthesized with aspect ratios anywhere from 1 to 7 with a corresponding longitudinal plasmon as high as 1050 nm with rod diameters of about 10 nm. Although the exact mechanism was not known, it was theorized that TDTAB was the rod-directing agent and that growth may have occurred on the surface of the electrode, with sonication responsible for freeing the rods into solution.

1.4.1.2. Seed-Mediated Synthesis

The next advance from Murphy and coworkers was to replace the gold electrode as the source of gold and move to a chemical source, chloroauric acid.[32] Electrochemical reduction was replaced with chemical reduction using a weak reducing agent (ascorbic acid) and silver nitrate. Finally, instead of using a co-

surfactant system containing CTAB and TDTAB, only CTAB was used during the synthesis, although hexane and acetone were still added. The ascorbic acid used in this synthesis is unable to reduce gold to the metallic state under the high CTAB concentration and low pH (~2.5), and instead reduces it to Au(I) state.[91] However, addition of small seed particles of about 3 nm in diameter into the Au(I) solution resulted in reduction to metallic gold, which is catalyzed by the surface of the seeds and leads to the gradual change in shape from quasi-spherical to rod-like crystal. It was determined that addition of less seed generally led to higher aspect ratio rods. However, the shape-yield of NRs was still relatively low and a large amount of spheroidal particles was present. It is possible to estimate the relative abundance of rods versus other shapes by comparing the LSPR peak with the low wavelength maximum at around 500 nm, which comes from a combination of the TSPR of NRs and the absorbance of spheroidal particles. A peak closer to 550 nm usually corresponds to the presence of cubic particles. One can estimate that a 4:1 ratio of longitudinal to transverse peak corresponds to 90% or higher content of rods of aspect ratio around 4 (LSPR~800 nm). In the early work on NRs synthesis, this ratio appeared to be closer to 1.5:1, which indicated a relatively high content of spheroidal impurities.[32]

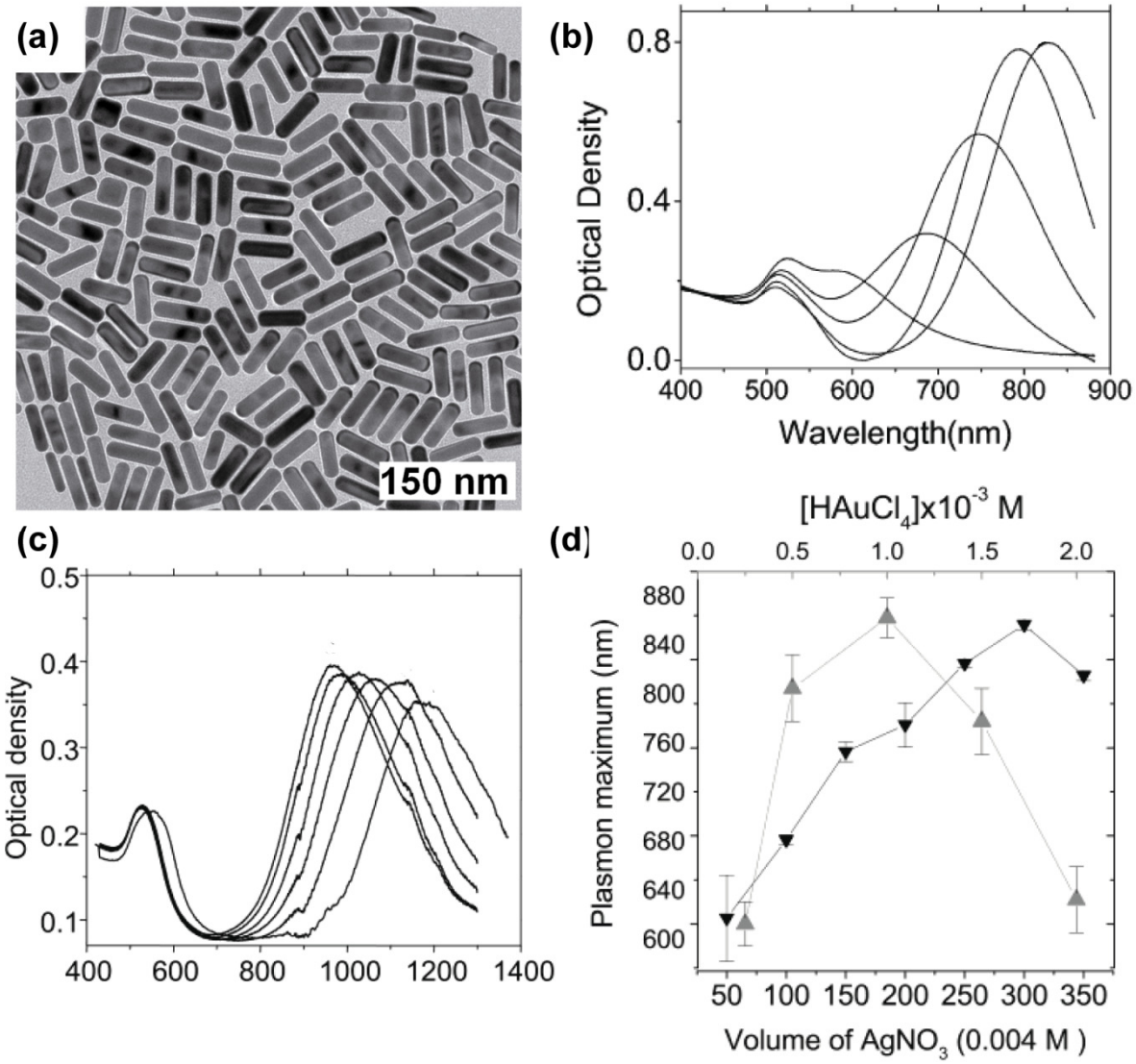

Figure 1.1. Gold NR synthesis using the procedure of El-Sayed et al.[87] (a) TEM image of NRs synthesized in our lab following this procedure. (b) UV-Vis absorbance spectrum of rods synthesized with increasing amounts of silver nitrate, from left to right, leading to higher LSPR wavelength. (c) UV-Vis absorbance spectrum demonstrating the increase in LSPR wavelength of rods synthesized in a CTAB/BDAC surfactant mixture with successive gold addition, from left to right. (d) Graph showing the dependence of rod LSPR on silver (black) and gold (grey) concentration in the growth solution.

Significant improvement of this method was achieved by El-Sayed et al. who were able to minimize the formation of spheroidal particles and produce rod-like

morphology in high yield in terms of shape.[87] This change was achieved by utilizing CTAB-capped seeds rather than the citrate-capped seed particles used before. A TEM image of gold NRs synthesized by this procedure is shown in Figure 1.1a. Two surfactant systems were explored, including a single CTAB surfactant system and a dual-surfactant system containing CTAB and benzyldimethylhexadecylammonium bromide (BDAC), both of which did not use any organic additives such as hexane or acetone. The single-surfactant system coupled with CTAB-capped seed and an appropriate amount of silver nitrate (~10-20 mol. %) routinely gives greater than 95% shape-yield of rods and allows one to reach aspect ratios up to 4.5 and LSPR peak close to 850 nm (Figure 1.1b). The use of the dual-surfactant system can generate NRs with an aspect ratio as high as 10 and LSPR up to 1300 nm through either aging of the growth solution or slow addition of gold ions after the initial growth (Figure 1.1c). However, the level of spheroidal impurity appears to be significantly higher, as evidenced by absorbance peak ratio of less than 4:1 compared to 10:1 for the CTAB-only method.

A partial control of the plasmon peak location is possible by altering the concentration of silver nitrate and gold chloride. Increasing these concentrations led to higher wavelength LSPR peaks, but only up to a certain point, after which the opposite trend was observed, as seen in Figure 1.1d.[87] In practice, we and others have found that batch to batch variability in LSPRs can be significant and is dependent on several factors.[92,93] In particular, proper synthesis of the seed is critically important as slightly increased amounts of added borohydride can lead to

increased seed particle sizes and ultimately to much larger amounts of spheroidal impurities.[94–96] This can be observed through the presence of a reddish hue in the seed solution. Furthermore, slight variations in the ratio of ascorbic acid to gold chloride concentration in the growth solution can lead to large differences in the final LSPR peak position: an increase in this ratio was found to generate shorter rods and lower wavelength LSPR.[97] Similarly, an increase in the proportion of seed to total gold ions concentration leads to shorter rods while a decrease in the total amount of CTAB has a similar effect, but the shape-yield of rods is reduced drastically.[97] Another method to obtain NRs with a particular LSPR was proposed by Wei and coworkers who were able to arrest NR growth with the addition of sodium sulfide.[93] Since the NR synthesis only consumes about 20-30 % of gold ions present in solution, slow reduction of gold onto the rod surface after their initial formation leads to a slow increase in diameter and a concomitant blue shift of LSPR on the time scale of several days. Addition of sodium sulfide was shown to effectively suppress the post-synthesis drifting of the LSPR peak.[93] Recently, Murray and coworkers demonstrated tuning of LSPR through addition of aromatic salicylate additives as well as hydrochloric acid, which was explained through an effect on the micellar structure of CTAB during rod growth.[98] This method can produce higher aspect-ratio gold NRs with fewer spherical impurities, as can be seen in

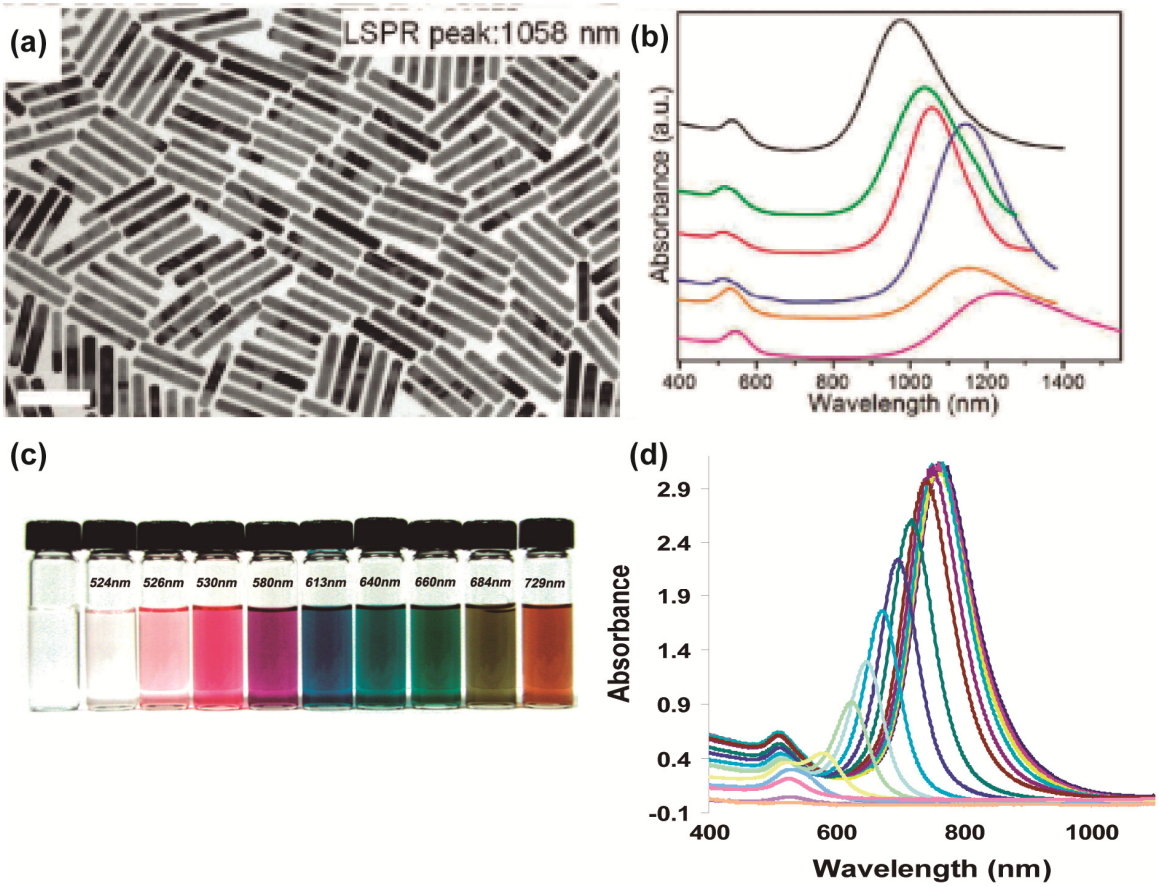

Figure 1.2. Improved synthesis and fine-tuning of gold NRs. TEM image (a) shows rods synthesized in the presence of 5-bromosalicylic acid additive and HCl with added amounts of seed and silver nitrate solution, respectively, of 0.4 mL and 48 mL. Corresponding UV-Vis absorbance spectrum (b) of rods in (a) is shown in red along with spectra of rods made under slightly different conditions.[98] Pictures (c) and UV-Vis absorbance spectra (d) of gold NRs during their gradual dissolution with $HAuCl_4$. The extent of dissolution increases from right to left in both (c) and (d).

Figure 1.2a-b. Tuning of the NR plasmon can also be achieved by post-synthetic tip-selective oxidation.[99,100] In this case, a solution of gold (III) ions complexed with CTAB serves as an oxidizing agent resulting in a controllable blue shift of the LSPR peak and a decrease of its intensity, as shown in Figure 1.2c-d.

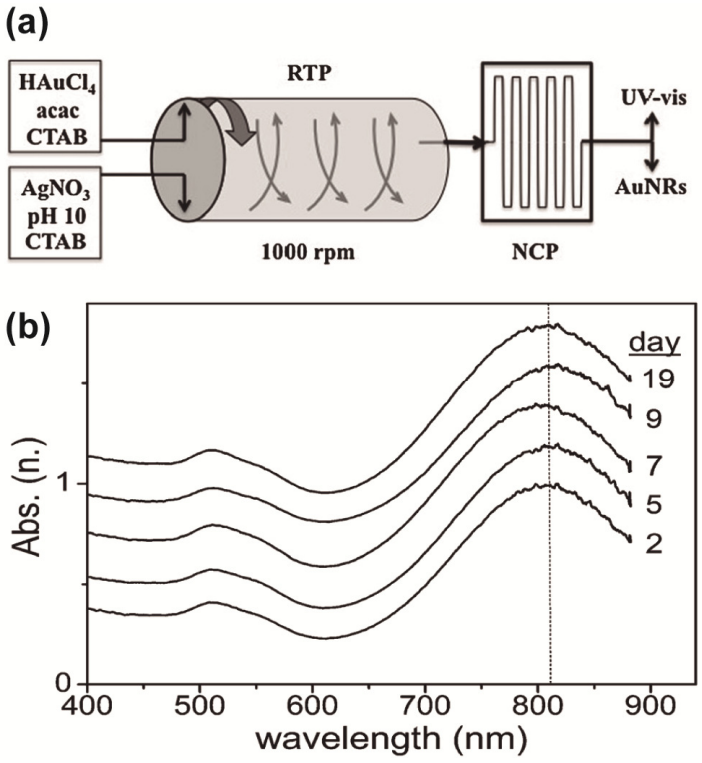

Figure 1.3. Seedless, continuous flow synthesis of gold nanords. (a) Design of fluidic system in which two stable feedstocks are fed into a rotating tube processor (RTP) followed by a narrow channel processor (NCP). (b) UV-Vis absorbance spectra of NRs produced after different times showing the stability and reproducibility of the procedure.[104]

The wet-chemical synthesis of NRs is generally carried out in small batches in standard laboratory equipment. However, there has been an interest in applying the standard silver-nitrate mediated synthesis to other environments. The synthesis of rods in a microfluidic system under continuous flow was demonstrated by Boleininger et al.[103] In such a system, it may be possible to continuously monitor the reaction conditions, such as altering the seed to growth ratio or the solution temperature.[103] More recently, a seedless approach to continuous flow synthesis of rods was developed by using a rotating tube processor (RTP) followed by a narrow

channel processor, as shown in Figure 1.3a.[104] Two separate and stable stock solutions were mixed in this experiment, leading to the reproducible synthesis of NRs with identical optical absorbance spectra for up to 19 days, as shown in Figure 1.3b. This was possible through the use of a single reducing agent system developed by Tollan and coworkers[105] which was able to reduce gold ions to the metallic form only when mixed with a separate feedstock at a higher pH.[104]

1.4.1.3. Photochemical, Ultrasonic, and Radiolytic Synthesis

Besides utilizing ascorbic acid and sodium borohydride as reducing agents, it is possible to apply a variety of other procedures, such as the electrochemical synthesis described earlier. The photochemical growth strategy is one such method which utilizes photoreduction to convert Au(III) to Au(0).[106] A gold chloride solution within a mixed CTAB-TDTAB surfactant system with silver nitrate, acetone, and hexane additives is irradiated with a 254 nm UV light for more than 24 hours. Acetone appears to drive the reduction through photochemical generation of ketyl radicals which act as the active reducing agent.[107] A good yield of rods of different aspect ratio can be obtained by changing the silver concentration, leading to LSPRs located at 600-800 nm.[106]

1.4.1.4. Crystal Structure

Gold NRs synthesized by wet chemistry methods in the presence of silver nitrate display a common crystal structure based on a single-crystal motif with no twinning faults. It has been shown that NRs grow longitudinally along the <001>

direction and have an octagonal cross-section.[90] The sides of the rods are bound by alternate {100} and {110} facets that come together at the tips in the form of {110} and {111} facets, respectively. This view has been predominant in the literature, but recent analysis by Liz-Marzán and coworkers suggests that the actual structure is likely different and includes higher-index facets on the sides of the rods, as supported by high-resolution TEM of vertically standing NRs (Figure 1.4a).[113] Although both models agree with the lateral appearance of rods (Figure 1.4b), the standing view demonstrates that they are bound by eight higher-index {250} facets with equal surface area, but different angles between them (Figure 1.4c). In addition, the <100> and <110> directions point to the corners of the rod rather than the faces as assumed previously. No difference in the tip structure was reported compared to earlier work. The implications of these structural details for the growth mechanism of rods are particularly important as discussed below.

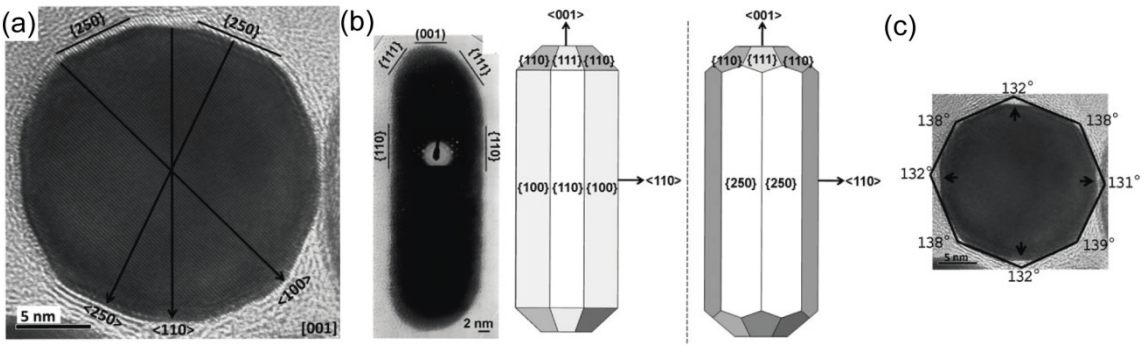

Figure 1.4. Crystal structure of gold NRs. (a) HRTEM image of a standing rod showing higer index {250} facets. (b) Old and new models for rod crystal structure, both of which are consistent with TEM image of side view of rods. (c) Angles between crystal facets measured from HRTEM.[113]

1.4.1.5. Growth Mechanism

The growth mechanism of single-crystalline gold NRs synthesized in CTAB-micellar solutions has received a large amount of attention. It has become quite evident that the presence of silver is essential for rod formation, but some disagreement exists as to the exact mechanism of its action. The synthesis of rods can be carried out in the absence of silver under very similar conditions, but this generally leads to the synthesis of pentahedrally-twinned rods (see Chapter 1.4.2). Initially, it was theorized that rod-shaped CTAB-micelles were present as soft templates for gold nanoparticle growth.[32,88,95,106] The photochemical and electrochemical procedures called for the presence of a highly hydrophobic co-surfactant TDTAB along with cyclohexane to elongate these surfactant micelles in solution. However, further photochemical[108] and seed-mediated[32,87] procedures demonstrated that these species could be removed. It is clear that the chemical nature of surfactant is extremely important, although there appears to be a limited degree of flexibility in the choice of surfactants. Exchanging CTAB for cetyltriethylammonium bromide was still found to produce rods,[114] although the growth was reported to be slower and the shape-yield was reduced significantly based on the optical absorbance spectrum (2:1 ratio of LSPR:TSPR). It is also possible to use a twin-hexadecyl tailed surfactant to synthesize rods at lower concentrations with similar results.[115] As described earlier, the use of a bulkier co-surfactant, BDAC, along with CTAB produced higher aspect ratio NRs in the seed-mediated synthesis, but also led to much lower yield and poor quality of particles.[87]

Dropping the CTAB concentration even two times leads to a large decrease in the yield of rods.[97,116]

More research has been conducted into the role of the surfactant counter-ion in the growth process. Specifically, the presence of bromide is known to be key in this synthesis. Garg and coworkers showed that gold NRs cannot be synthesized if hexadecyltrimethylammonium chloride (CTAC) or even a 1:2 ratio of CTAC:CTAB is used instead of pure CTAB.[116] However, they demonstrated that by adding an external source of sodium bromide to keep its concentration at 0.1M, it is possible to drop the CTAB concentration even below its critical micelle concentration and still form rods, although the LSPR:TSPR ratio of 1:1 suggests the procedure is not very efficient. Similarly, Si et al. showed that, in a one-pot synthesis, total bromide concentration controlled the LSPR position irrespective of its origin.[117] Although bromide cannot be substituted for chloride, the low amount of chloride present from the $HAuCl_4$ starting material is not problematic and the ionic gold is found mainly as $AuBr_4^-$ or $AuBr_2^-$ after reduction.[118] On the other hand, the presence of iodide can have a profound effect on gold NR synthesis. [119] Korgel and coworkers discovered that a micromolar amount of iodide in the growth solution is enough to completely inhibit NR growth.

Indeed, the specific binding of different species to various facets of the gold NRs during their growth has been implicated as the major structure-directing element as opposed to any particular soft-templating effects by rod-shaped micelles. Differential binding of various species to a particular set of growing facets appears

to affect the deposition rate of gold onto those facets, thereby controlling the final shape of the nanocrystal. It is clear that bromide, silver, and the CTA^+ cation have a large effect on the growth, though the exact surface-binding species have not been settled. El-Sayed and coworkers attributed the enhanced growth of {111} tip facets to the stronger binding affinity of CTAB to the {110} side facets, which have a higher surface energy due to larger interatomic distances.[87,122] Reports indicate that silver is present in the form of a soluble $AgBr_2^-$ CTA^+ complex and that this complex has a high propensity to bind to the NR surface.[118,124] However, further studies of photochemically synthesized NRs seemed to contradict these results. Detailed Extended X-ray Absorption Fine Structure (EXAFS) measurements of gold NRs were performed to determine the chemical and coordination state of silver and demonstrated that silver is present in metallic rather than ionic form in the final product.[125,126] It was also demonstrated that up to several layers of metallic silver could be present on the surface of NRs, a result consistent with previous ICP-MS analysis.[127] Since the X-ray characterization data was performed only on purified NRs, this does not rule out the importance of the $AgBr_2^-$ CTA^+ complex at some point during the synthesis.

The presence of metallic silver coating supports a different growth mechanism driven by under-potential deposition (UPD) of silver onto growing NRs. According to this hypothesis, silver is present in the growth solution as Ag(I) and cannot be reduced by ascorbic acid to its metallic form in the presence of CTAB under acidic conditions.[91] However, the deposition of silver on gold surface can

happen at lower potential and is expected to occur more readily on the {110} facets compared to the {100} facets.[128] Growth along the <110> direction would be slowed as it would require re-oxidation of silver, thus leading to the unexpected growth along the more thermodynamically stable <100> direction. It must also be noted that recent assignment of the higher-index facets to the sides of the rods, as described earlier,[113] fits well with the growth mechanism based on variable binding between side and tip facets of rods as it would imply an even larger difference in the openness and binding propensity (or silver UPD propensity) between higher-index sides and lower index tips.

The strength of binding to various gold facets may not be the only factor driving the growth of NRs. One theory posits that an enhanced electric field exists at the tips of gold rods which leads to a higher collision rate with CTAB- bound Au (I) ions and therefore enhancement of the anisotropic growth.[129] Recent work by Cortie and coworkers suggests that the main effect of silver complex binding could be in altering the surface energy of the NR sides compared to their tips which could be the driving force for anisotropic growth, as shown in Figure 1.5a.[130] Supported by a combination of cryo-TEM, modeling, and optical spectroscopy, they proposed a "popcorn" mechanism wherein growing seeds will randomly experience symmetry-breaking and then rapidly reach their final dimensions. Cryo-TEM imaging of the early stages of growth showed a low concentration of nearly fully-formed rods rather than a high concentration of very small rods, indicating that

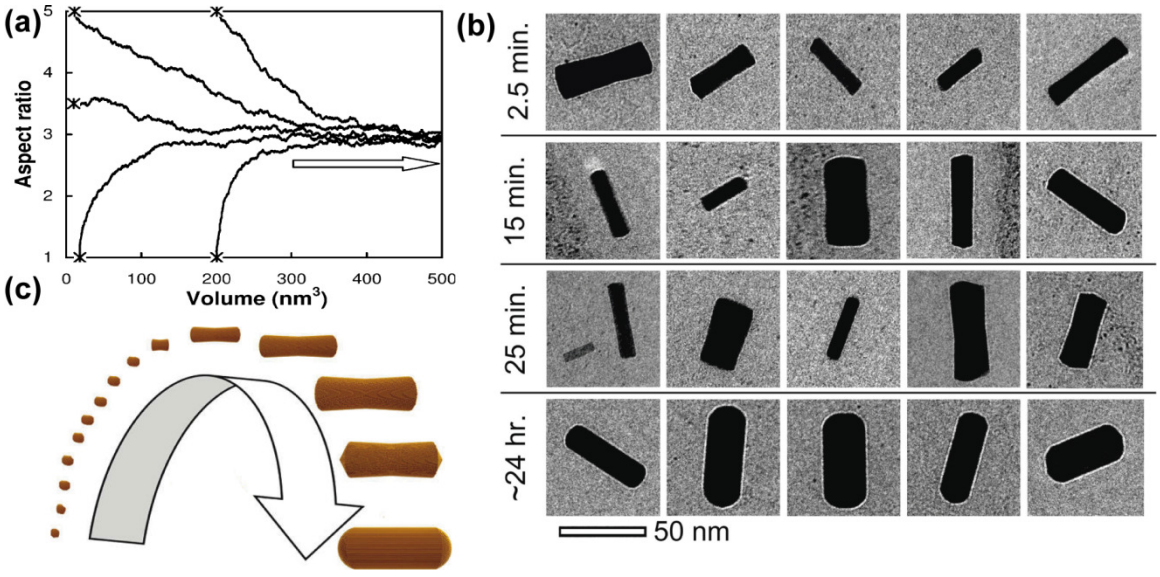

Figure 1.5. Growth of single-crystalline gold NRs. (a) Predicted growth trajectories of rods based on a particular side to end rod surface energy ratio suggesting that final aspect ratio is determined mainly by relative energies of the side and end rod facets, which can be modulated by surfactant binding/silver underpotential deposition. (b) Cryo-TEM images showing different rod morphologies and different reaction timepoints. (c) Schematic representation of rod growth including the gradual change in shape supported by cryo-TEM and UV-Vis absorbance as well as modeling.[130]

uniform growth of seeds into rods was not occurring (Figure 1.5b). Furthermore, initial rod morphology was bowtie-like and gradually reshaped into the regular quasi-cylindrical morphology (Figure 1.5c), which was supported by optical absorbance spectra and modeling. Evidence also suggests that if a growing seed does not experience symmetry-breaking prior to reaching a certain size (~5 nm), it may become incompatible for the rod growth and will instead transform into a spheroidal particle, a common impurity in these procedures,[94,130] However, the exact cause of this symmetry-breaking process and the parameters that control it are still unknown. Also, it is not clear why the growth of NRs stops at some specific

lengths, especially in the case of a non-uniform growth scenario. This may be explained by Murphy and coworkers hypothesis that rapid growth continues until metallic silver deposited through UPD completely encapsulates the rod, after which the growth rate would rapidly decrease.[127]

1.4.2. Synthesis of Pentahedrally-Twinned Nanorods

1.4.2.1. General Synthesis

It is possible to synthesize crystalline, pentahedrally-twinned gold NRs under conditions quite similar to the synthesis of single-crystalline rods described earlier with the major difference being the absence of silver ions in the growth solution. This crucial difference was capitalized upon by Murphy and coworkers who published a three-step procedure to synthesize pentahedrally-twinned gold NRs.[131] The first step is to prepare the seed particles through borohydride reduction of a citrate-containing solution of $HAuCl_4$, forming small, roughly 3.5 nm particles. Similar to previous methods, the growth solution contained CTAB and chloroauric acid reduced to Au(I) with ascorbic acid. The growth solution is different from standard seed-mediated synthesis in that the concentration of gold is two times lower, and the ascorbic acid is present in significantly higher concentration (2.2 mol equiv. with respect to gold chloride). Three such growth solutions are created and a series of sequential transfers of seed to the first growth solution, from the first to second, and from the second to the final growth solution are carried out, as shown in Figure 1.6a. The result is the synthesis of pentahedrally-twinned gold NRs with 20-

22 nm diameter and much higher aspect ratio (~20) than those prepared by silver-nitrate mediated synthesis. It is presently not possible to decrease the rod diameter much below 20 nm, although the length can be pushed to above 1 μm while maintaining nearly the same diameter by altering the reaction conditions as described later.[132]

1.4.2.2. Crystal Structure

Gold NRs synthesized in a silver-free environment possess a pentahedrally-twinned crystal structure as opposed to the single-crystalline nature of rods synthesized in the presence of silver ions. As shown in Figure 1.6c, the rods are bound by {100} or {110} facets while the tips are bound by five triangular {111} faces and five {111} twin boundaries run longitudinally along the rod.[133] The rods are shaped in the form of a pentagonal prism in which the different facets may have different tendencies to bind CTAB in solution, thus contributing to anisotropic growth as described in the previous section.

1.4.2.3. Synthetic Progress

This is currently the basis of all available methods to grow crystalline high aspect rods, but, unfortunately, it leads to a very low yield of rods, usually five percent or less,[135] with the majority of the product consisting mostly of spheroidal particles as well as a large number of platelets. As synthesized, the solution has a purple color which comes from the spherical particles. The low yield of this synthesis and the difficulty of separation of unwanted shapes are the main

limitations to this technique and several reports exist on the optimization of the original three-step procedure to improve these factors. Murphy et al. first reported that increasing the pH of the growth solution using sodium hydroxide produced rods as the major rather than minor product of the synthesis.[135] Interestingly, a later report by Wu et al. stated that addition of nitric acid to the final growth solution also led to an increase in the quality of the rods, although this was attributed to the presence of nitrate ion rather than a change in pH.[136] Other sources of nitrate were not examined though. We have had difficulty reproducing either of these techniques, but have been able to utilize part of the procedure of Wu et al. to design a procedure to completely purify rods from other impurities.[137] The first step, which was used by Wu et al. and likely explains why they show such a high concentration of rods, was to notice that high aspect-ratio rods and large platelets settle out of solution after a day or two and the top, deep purple solution consisting almost exclusively of spherical particles and low aspect ratio rods, can be carefully decanted, thereby easily removing these impurity. Commonly reported low-speed centrifugation has a similar effect,[131] but is clearly more difficult to scale up. Although the overall yield of rods is still very small, the shape-yield of rods in the precipitate is fairly high. The other major impurity is large 2D platelets, though its content can be reduced by switching from a citrate-capped seed to a CTAB-capped seed.[134] Our group has developed a separation procedure wherein the rods and platelets are first oxidized with the addition of Au(III)-CTAB solution (Figure 1.6b).[138] This oxidation occurs along the entire circumference of platelets, but only

along the tips of rods, causing the platelets to shrink faster and giving them a higher solubility. Because of that the partially dissolved platelets stay in solution longer and can be removed from the precipitated rods. The resulting isolated rods have an aspect ratio of about 7, down from the initial 20, but maintain the same diameter. The variable sedimentation rate of different sizes of rods, platelets, and spheres was later explained by Park and coworkers as a depletion-induced effect which occurs in micellar CTAB solutions.[139] The synthesis of pure pentahedrally-twinned rods can be important in further growth of rods into pure particles with controlled morphollogy.[140]

Several reports of synthesis confined to surfaces exist[142–145] and seem to show that anisotropic growth does not start until seed-particles grow to just under 20 nm in size and that rod diameter does not increase appreciably after that point.[144] The effect of varying the surfactant chain length and structure was also studied.[146] By changing the alkyl chain length in the alkyl-trimethylammonium bromide from decyl to hexadecyl, Murphy et al. demonstrated that increasing the chain length led to a higher aspect ratio. More importantly, reducing the chain length to ten carbon atoms led to complete disappearance of high aspect ratio rods. It was suggested that the growth was driven by the preference of the surfactant to bind to the sides of rods during the growth through "zipping" interactions along surfactant bilayer caused by increased van der Waals interactions between the hydrocarbon tails (Figure 1.6d).[146] Recently, it was also reported that seed-mediated growth in a surfactant mixture comprised of CTAB and

octadecyltrimethylammonium bromide (OTAB) under conditions in which gelation occurred led to the synthesis of high aspect ratio rods in yields greater than 90 percent.[132] Conditions which produced gelation, i.e. higher OTAB concentration and lower temperature, were found to be the best combination for the synthesis of rods with the highest aspect ratios of 30-50 (Figure 1.6e). Although the exact mechanism of this effect is unclear, it is consistent with the previous report by Murphy et al. in that the even longer octadecyl chain would be expected to lead to higher aspect ratio rods. Furthermore, the gelation process could enhance the "zipping" effect proposed before.[146]

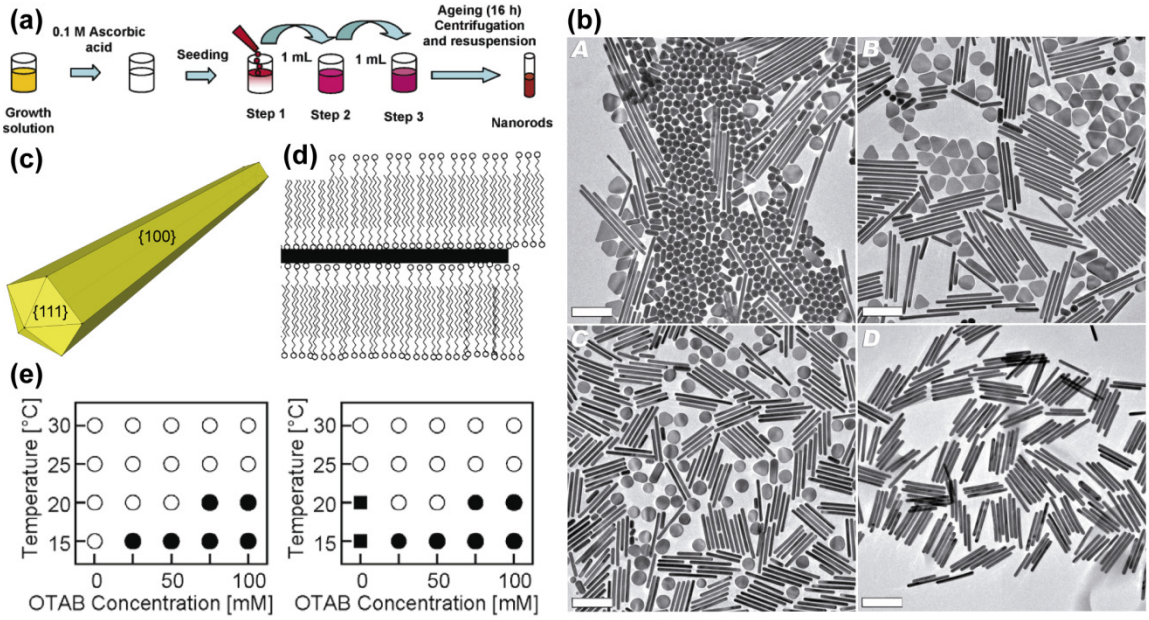

Figure 1.6. Synthesis of pentahedrally-twinned rods. (a) Three-step procedure for the growth of rods without silver nitrate. (b) TEM images of the purification of rods through dissolution and sedimentation procedure. Scale bars are 200 nm.[137] (d) Schematic of surfactant "zipping" process directing anisotropic growth.[146] (e) Graph showing the dependence on NR aspect-ratio on the gelation state of the solution containing mixtures of CTAB and octadecyltrimethylammonium bromide (OTAB). On the left, the aspect ratio of rods is depicted as normal (~25) with open

circles or high (~50) with closed circles. On the right, the solution state is depicted as liquid with open circles, gelled with closed circles, or crystallized with closed squares.[132]

1.4.3. Templated Synthesis of Gold Nanorods

So far, the discussion has been focused on the wet-chemical synthesis of crystalline rods which generally gives access to smaller rods in larger amounts. Other than crystalline growth, one could consider reduction of gold into some sort of rod-shaped template. Although rod-shaped CTAB micelles have been generally disproven to act as a template for rod growth, it is possible to fabricate harder templates out of various materials that possess rod-shaped openings. Initial applications of this technique were focused on gold reduction inside of nanoporous membranes fabricated out of polycarbonate, alumina, or other materials. Polycarbonate membranes can be ion-track etched to create uniform cylindrical pores of diameter down to 10 nm with pore density up to 10^9 pores/cm^2.[148] Porous alumina membranes can be produced in the lab through electrochemical anodization of aluminum.[149] Electrochemical deposition of gold into the pores leads to the growth of gold rods and wires. Early reports of rod synthesis using this technique came from Martin and coworkers who used both polycarbonate and alumina membranes along with electrochemical deposition of gold inside the pores.[30,31,148,150–152] Gold is electrochemically reduced inside the pores, forming NRs or NWs which can be freed by dissolution of the template.

This technique clearly has several benefits as well as limitations. A large limitation exists in the amount of material that can be synthesized at once as well as

the scalability of the technique since the rod growth is limited to a two-dimensional area of a membrane rather than taking place in a three dimensional volume as in the wet-chemical synthesis. This would make this synthetic technique very difficult to apply for real applications. While the rod diameter can be determined rather accurately based on the template, length control is more difficult and polydispersity in the sample can lead to broadening of the longitudinal plasmon.[156] In addition, gold is deposited in a polycrystalline fashion inside the pores which are not perfectly smooth, leading to an increase in roughness which can also broaden the LSPR.[156]

1.4.4. Other Synthetic Strategies

Almost all the synthetic techniques for gold NR synthesis are carried out in an aqueous environment. However, recently, there have been several reports which utilize an organic environment and produce rather different morphologies. Xia and coworkers demonstrated the formation of ultrathin gold NRs by mixture of an AuCl(oleylamine) with amorphous iron nanoparticles in chloroform and aging for one week.[165] Iron nanoparticles act as the reducing agent and lead to the creation of nanoparticles rich in defects which are slowly converted to single-crystalline rods with 2 nm diameter and average aspect ratio of 30, apparently through an etching and redeposition process. Growth of the rods occur along the <111> direction and is postulated to be directed by oleylamine. Around the same time, several other groups published the formation of ultrathin gold nanowires in organic solvent.[166–168] It appears that formation of aurophilic polymers can lead to the organization of gold

into the nanowire form, after which it is reduced into single crystalline growth along the same <111> direction. Interestingly, the choice of solvent is critical as the formation of rods rather than wires only occurred in chloroform where the aurophilic polymers do not form.

1.5. General Functionalization Strategies

For nearly all applications, the ability to properly functionalize the NR surface can determine the success or failure of the project. In general, the functionalization of gold NRs can be significantly more challenging than the functionalization of spherical particles, even via well-known gold-thiol chemistry. In particular, NRs synthesized wet-chemically in the presence of CTAB, by far the most used type of rods, present a set of unique challenges for their functionalization and further applications. The CTAB capping agent presents a surface different to that of the more "bare" surfaces of gold nanoparticles capped with citrate or similar ligands and thus specific methods have been developed for its replacement. In general, the stability of CTAB-capped rods is known to be poor under a variety of conditions including high salt content, low CTAB concentration and addition of organic solvents, making them of limited usefulness for many applications.[54,171]

It is first necessary to understand the general structure and properties of the CTAB coating on the surface of rods. Gold rods have been shown to be stabilized by a partially-interdigitated bilayer of CTAB which is similar in structure to a micelle.[172,173] El-Sayed and coworkers used FTIR to show binding of the ammonium

bromide head group to the gold surface.[172] Thermogravimetric analysis (TGA) also demonstrated the presence of CTAB molecules with different desorption properties corresponding to a weak binding outer layer and a stronger binding inner layer.[172] Characterization of this structure is generally difficult because of its noncovalent binding to the gold surface and dynamic character in solution. Gómez-Graña and coworkers carried out small angle x-ray (SAXS) and neutron (SANS) scattering experiments to measure the structure of the surfactant bilayer.[173] By using SAXS to characterize the gold core and SANS to characterize the surfactant bilayer, they were able to determine a bilayer thickness of 3.2 nm, which is less than a fully extended bilayer thickness of 4 nm and thus leads to the likelihood of partial interdigitation between the two CTAB layers.[173] This bilayer is necessary to stabilize the rods, and, as the authors note, the rods tend to aggregate if the concentration of CTAB in solution drops below the critical micelle concentration.[173] The stability of the bilayer can also be disrupted in other ways, such as the addition of organic solvents, which can be either highly problematic or can actually be used to one's advantage. For instance, a technique was developed in our lab to functionalize the NR surface with mercaptophenol.[96,174] Addition of THF solution of mercaptophenol to a 0.1 M CTAB solution of rods allows for the gradual replacement of CTAB with mercaptophenol. As the exchange proceeds, rods begin to gradually aggregate and crash out of solution. If the proper amount of THF and a large excess of mercaptophenol is used, rods will be sufficiently functionalized and can be brought back fully into organic solution through esterification with carboxyl-

containing organic polymers (Figure 1.7a).[9,11,12,14] This procedure points out a particular limitation on the functionalization of rods with small molecules: the resulting rod may simply not be soluble enough due to the large size of NR core compared to the small organic functionality. This can also lead to complete loss of solubility of rods before they can be functionalized.

The use of the classic gold-thiol bond chemistry is one common way to functionalize gold rods, though, as the previous example suggests, simple addition of any thiol may not lead to complete functionalization. For instance, direct exchange of CTAB for the commonly used thiol mercaptoundecanoic acid (MUA) generally leads to irreversible aggregation or only partial exchange.[175] The addition of an ethanolic solution of MUA to rods has been reported.[176] This is generally combined with heating to promote the direct exchange and constant sonication to keep rods from aggregating.[177] A separate procedure was developed by Wijaya and coworkers based on a round-trip phase transfer ligand exchange procedure wherein CTAB-capped rods are first transferred into a highly-concentrated dodecanethiol-acetone solution, centrifuged to remove excess thiol, and then heated in the presence of an alkyl thiol acid such as MUA until aggregation occurs, after which the rods become soluble in aqueous environment (Figure 1.7b).[178] The question of what mixture of MUA, dodecanethiol, and CTAB is present on the NR surface is difficult to assess quantitatively in this scenario, although a negative charge is present on the rods. The possibility of further "customization" of the surface via further addition of a

variety of thiolated compounds such as more acid, polyethylene glycol (PEG), or DNA could make this technique useful for a variety of biomedical applications.[178]

A normal exchange under aqueous conditions is also possible, although ligand structure must be chosen judiciously. Addition of thiol to the NR surface has been shown to preferentially occur at the NR tips, which has been attributed to a less dense CTAB bilayer at the tips compared to the sides of the rods.[179] Surface functionalization with PEG-thiols is often used to impart a high degree of stability and biocompatibility and can be carried out simply by adding thiol-terminated PEG to centrifuged rods.[54,180–183] Purification usually follows the standard procedure of multiple rounds of centrifugation and removal of the supernatant. Such rods are highly stable in aqueous and even some organic solutions. Attaching a thiolated PEG linker to an antibody or other molecules is often the simplest way of covalent connection to gold NRs surface as it reduces the chances of aggregation or loss of solubility. For instance, a bifunctional molecule such as a thiol-PEG-acid can be used.[54,184,185] Similarly, one could expect that relatively large, neutral, hydrophilic molecules with a thiol moiety could be used in a similar way, although even with PEG, it is unknown how much CTAB is left on the gold NR surface.[48] Given that the surface-binding density of PEG-thiols is relatively low due to their large size, it is possible to conduct further exchange with different thiols that might otherwise not be amenable to direct exchange.[175] Exchange with cationic molecules is also usually less problematic than exchange with anionic molecules as the charge character is more similar to the native CTAB coating. Indeed, we have recently demonstrated

the complete exchange of CTAB with its thiolated analogue called MTAB, which is a low molecular weight thiol containing a permanent positive charge in the form of a

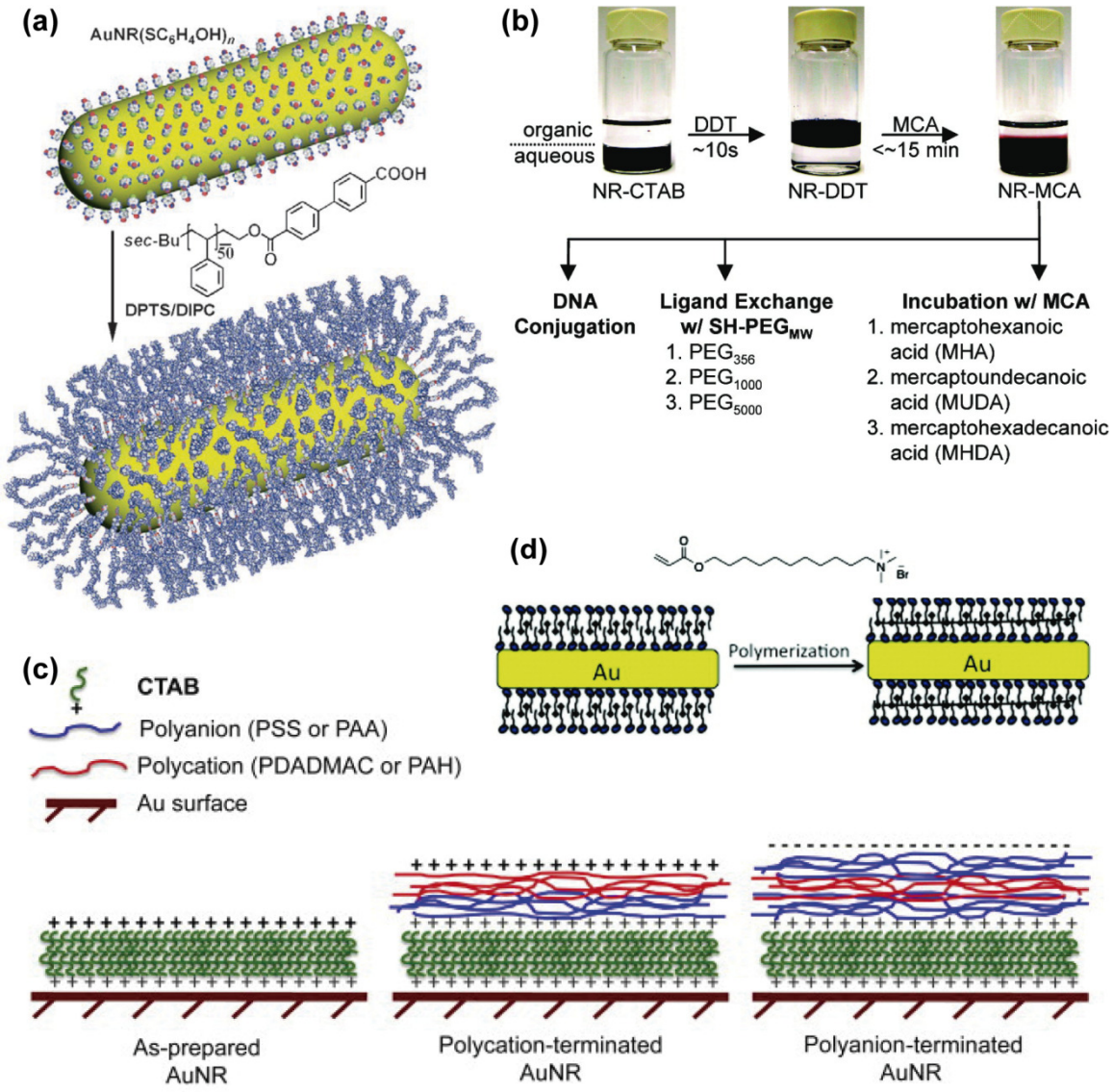

Figure 1.7. Various methods for gold NR functionalization. (a) Schematic representation of the reaction of mercaptophenol-coated rods with carboxyl-terminated polystyrene leading to highly organic-soluble rods.[96] (b) Ligand exchange of gold NRs with various alkyl-thiol acids, PEG-thiols, and DNA utilizing round-trip phase transfer.[178] (c) Schematic representation of polyelectrolyte coated rods. Consecutive layers of polyanion and polycation are strongly adsorbed to the rod surface, leading to highly stable complexes.[192] (d) Representation of the

in situ polymerization of gold rods exchanged with a vinyl carboxylate-modified cationic surfactant.[201]

quaternary ammonium group.[48] Partial exchange with hydrophobic polymer-thiols is also possible through controlled addition of ethanolic or THF polymer solutions.[186]

Attachment through a single gold-thiol linkage is not the only mechanism to achieve covalent functionalization of NRs. Disulfides represent one alternative as they are often easier to handle and allow for the attachment of larger biomolecules to rods.[180] Cyclic disulfides such as thioctic acid can also be used and display strong binding to gold while being relatively easy to link to the molecule of choice.[184] Alternatively, in-situ dithiocarbamate synthesis can transform an amine group of a molecule into a bidentate dithiocarbamate group through the use of carbon disulfide at controlled pH, a robust binding motif which may have superior chemisorptive properties compared to regular thiols.[187,188] Polymers containing multiple thiol groups can sometimes be utilized,[189,190] however, this may often lead to partial or complete aggregation of rods due to cross-linking. With any such techniques, proving that all of the surface-bound CTAB has been removed is very difficult and could have implications for further applications.[48]

An alternative method to the covalent functionalization of NRs was developed by Murphy coworkers, which utilizes layer-by-layer (LBL) deposition of polyelectrolytes directly onto the CTAB bilayer surrounding rods (Figure 1.7c).[191,192] In this technique, alternate layers of anionic and cationic polyelectrolytes are

deposited onto the surface of the rods through electrostatic interactions. First, a negatively-charged polymer such as polyacrylic acid or polystyrene sulfonate is mixed with positively-charged CTAB-capped rods, leading to its deposition on the rods and switching the net charge on the rod to a negative value. This can be followed by a layer of cationic polymer such as poly(diallyldimethylammonium chloride) or poly(allylamine hydrochloride) and the cycle can be repeated multiple times, similar to standard layer-by-layer deposition techniques.[193–195] Biological polyelectrolytes such as chitosan or glycosaminoglycan were also used for that purpose.[196–200] Rods coated in this manner can be purified by centrifugation or dialysis and are soluble under high salt conditions, in biological media, and even in polar organic solvents.[191,201,202] Functional groups introduced by this technique can include carboxylic acid and amine and further reactions can be carried out to include new functionality, for example, an azide group for "click" chemistry.[203] Electrostatic adsorption of proteins directly onto CTAB-capped rods or LBL-modified rods has also been demonstrated.[69,196,204] In addition, polyacrylate coating can be produced by reverse-micelle polymerization of acrylate monomers coating the surface of rods.[205]

A surfactant exchange can be used to partially displace CTAB with amphiphilic molecules such as phospholipids[206–209] or a modified cationic surfactant.[201] For instance, exchange with a cationic, polymerizable surfactant has been used to render rods high stable after *in situ* polymerization within the bilayer (Figure 1.7d).[201] The exchange is usually carried out by first reducing the

concentration of CTAB in solution through centrifugation or extractions and then introducing an excess of alternate surfactant. In particular, both cationic phospholipids such as commercially available transfection agents,[207] as well as net neutral phospholipids such as phosphatidylcholine (PC) can be used for that purpose.[206,208] ^{1}H-NMR analysis has shown that PC penetrates into both layers of the CTAB bilayer around the NR and that the total CTAB content in the PC-modified rods was below 10 percent.[208]

1.6. Thesis Outline

Chapter 2 describes the synthesis of gold NRs using hydroquinone which provides benefits in the overall yield of gold conversion as well allows for the synthesis of rods with LSPR peak as high as 1250 nm. Chapter 3 shows the synthesis of gold mesorods and nanowires with hydroquinone as a reducing agent and details the synthesis of nanoparticles with a novel starfruit-like morphology and their SERS applications. In Chapter 4, the functionalization of gold NRs with an ammonium bromide-terminated thiol is described and detailed experiments are shown which prove the complete replacement of toxic CTAB on the NR surface. Chapter 5 then shows that not only are MTAB NRs nontoxic and can be taken up into cancer cell in unprecedented numbers, MTAB nanowires and mesorods can also be taken up into cells in large quantities. Finally, an overview of this work and future direction will be given.

1.7. References

(1) Daniel, M.-C.; Astruc, D. *Chem. Rev.* **2004**, *104*, 293–346.

(2) Critchley, K.; Khanal, B. P.; Górzny, M. Ł.; Vigderman, L.; Evans, S. D.; Zubarev, E. R.; Kotov, N. A. *Adv. Mater.* **2010**, *22*, 2338–42.

(3) Faraday, M. *Phil. Trans. R. Soc. Lond.* **1857**, *147*, 145–181.

(4) Turkevich, J.; Stevenson, P. C.; Hillier, J. *Discuss. Faraday Soc.* **1951**, *11*, 55–75.

(5) Frens, G. *Nat. Phys. Sci.* **1973**, *241*, 20–22.

(6) Jadzinsky, P. D.; Calero, G.; Ackerson, C. J.; Bushnell, D. A.; Kornberg, R. D. *Science* **2007**, *318*, 430–433.

(7) Hong, R.; Han, G.; Fernández, J. M.; Kim, B. jin; Forbes, N. S.; Rotello, V. M. *J. Am. Chem. Soc.* **2006**, *128*, 1078–1079.

(8) Brust, M.; Walker, M.; Bethell, D.; Schiffrin, D. J.; Whyman, R. *J.Chem.Soc.Chem.Comm.* **1994**, 801–802.

(9) Zubarev, E. R.; Xu, J.; Sayyad, A.; Gibson, J. D. *J. Am. Chem. Soc.* **2006**, *128*, 4958–4959.

(10) Shan, J.; Tenhu, H. *Chemical Communications* **2007**, 4580–4598.

(11) Genson, K. L.; Holzmueller, J.; Jiang, C.; Xu, J.; Gibson, J. D.; Zubarev, E. R.; Tsukruk, V. V. *Langmuir* **2006**, *22*, 7011–7015.

(12) Zubarev, E. R.; Xu, J.; Sayyad, A.; Gibson, J. D. *J. Am. Chem. Soc.* **2006**, *128*, 15098–15099.

(13) Senyuk, B.; Evans, J. S.; Ackerman, P. J.; Lee, T.; Manna, P.; Vigderman, L.; Zubarev, E. R.; van de Lagemaat, J.; Smalyukh, I. I. *Nano Lett.* **2012**, *12*, 955–63.

(14) Gibson, J. D.; Khanal, B. P.; Zubarev, E. R. *J. Am. Chem. Soc.* **2007**, *129*, 11653–11661.

(15) Grzelczak, M.; Pérez-Juste, J.; Mulvaney, P.; Liz-Marzán, L. M.; Perez-Juste, J.; Liz-Marzan, L. M. *Chem. Soc. Rev.* **2008**, *37*, 1783–1791.

(16) Kim, C. K.; Ghosh, P.; Pagliuca, C.; Zhu, Z. J.; Menichetti, S.; Rotello, V. M. *Journal of the American Chemical Society* **2009**, *131*, 1360–1361.

(17) Agasti, S. S.; Chompoosor, A.; You, C. C.; Ghosh, P.; Kim, C. K.; Rotello, V. M. *Journal of the American Chemical Society* **2009**, *131*, 5728–5729.

(18) Templeton, A. C.; Hostetler, M. J.; Warmoth, E. K.; Chen, S.; Hartshorn, C. M.; Krishnamurthy, V. M.; Forbes, M. D. E.; Murray, R. W. *J. Am. Chem. Soc.* **1998**, *120*, 4845–4849.

(19) Stratakis, M.; Garcia, H. *Chem. Rev.* **2012**, *112*, 4469–4506.

(20) Vigderman, L.; Zubarev, E. R. *Adv. Drug Deliv. Rev.* **2012**, 10.1016/j.addr.2012.05.004.

(21) Pingarrón, J. M.; Yáñez-Sedeño, P.; González-Cortés, A. *Electrochim. Acta* **2008**, *53*, 5848–5866.

(22) Guo, S.; Wang, E. *Anal. Chim. Acta* **2007**, *598*, 181–192.

(23) Murphy, C. J.; Gole, A. M.; Stone, J. W.; Sisco, P. N.; Alkilany, A. M.; Goldsmith, E. C.; Baxter, S. C. *Acc. Chem. Res.* **2008**, *41*, 1721–1730.

(24) Rosi, N. L.; Mirkin, C. A. *Chem. Rev.* **2005**, *105*, 1547–1562.

(25) Bönnemann, H.; Richards, R. M. *Eur. J. Inorg. Chem.* **2001**, *2001*, 2455–2480.

(26) Tao, A. R.; Habas, S.; Yang, P. *Small* **2008**, *4*, 310–325.

(27) Kamat, P. V. *J. Phys. Chem. B* **2002**, *106*, 7729–7744.

(28) Daniel, M. C.; Astruc, D. *Chemical Reviews* **2003**, *104*, 293–346.

(29) Hu, M.; Chen, J.; Li, Z.-Y.; Au, L.; Hartland, G. V.; Li, X.; Marquez, M.; Xia, Y. *Chem. Soc. Rev.* **2006**, *35*, 1084–1094.

(30) Foss, C. A.; Hornyak, G. L.; Stockert, J. A.; Martin, C. R. *J. Phys. Chem.* **1994**, *98*, 2963–2971.

(31) Foss, C. A.; Hornyak, G. L.; Stockert, J. A.; Martin, C. R. *J. Phys. Chem.* **1992**, *96*, 7497–7499.

(32) Jana, N. R.; Gearheart, L.; Murphy, C. J. *Adv. Mater.* **2001**, *13*, 1389–1393.

(33) Huang, X.; Neretina, S.; El-Sayed, M. A. *Adv. Mater.* **2009**, *21*, 4880–4910.

(34) Murphy, C. J.; Sau, T. K.; Gole, A. M.; Orendorff, C. J.; Gao, J.; Gou, L.; Hunyadi, S. E.; Li, T. *J. Phys. Chem. B* **2005**, *109*, 13857–13870.

(35) Kumar, J.; Thomas, K. G. *J. Phys. Chem. Lett.* **2011**, *2*, 610–615.

(36) Slaughter, L. S.; Chang, W.-S.; Swanglap, P.; Tcherniak, A.; Khanal, B. P.; Zubarev, E. R.; Link, S. *J. Phys. Chem. C* **2010**, *114*, 4934–4938.

(37) Solis, D.; Chang, W.-S.; Khanal, B. P.; Bao, K.; Nordlander, P.; Zubarev, E. R.; Link, S. *Nano Lett.* **2010**, *10*, 3482–5.

(38) Wild, B.; Cao, L.; Sun, Y.; Khanal, B. P.; Zubarev, E. R.; Gray, S. K.; Scherer, N. F.; Pelton, M. *ACS Nano* **2012**, *6*, 472–82.

(39) Link, S.; Mohamed, M. B.; El-Sayed, M. A. *J. Phys. Chem. B* **1999**, *103*, 3073–3077.

(40) Prescott, S. W.; Mulvaney, P. *J. Appl. Phys.* **2006**, *99*, 123504.

(41) Grzelczak, M.; Sánchez-Iglesias, A.; Rodríguez-González, B.; Alvarez-Puebla, R.; Pérez-Juste, J.; Liz-Marzán, L. M. *Adv. Funct. Mater.* **2008**, *18*, 3780–3786.

(42) Kennedy, L. C.; Bickford, L. R.; Lewinski, N. A.; Coughlin, A. J.; Hu, Y.; Day, E. S.; West, J. L.; Drezek, R. A. *Small* **2011**, *7*, 169–183.

(43) Khlebtsov, N.; Dykman, L. *Chem. Soc. Rev.* **2011**, *40*, 1647–1671.

(44) Huang, X.; Jain, P. K.; El-Sayed, I. H.; El-Sayed, M. A. *Laser Med.Sci.* **2008**, *23*, 217–228.

(45) Xia, Y.; Li, W.; Cobley, C. M.; Chen, J.; Xia, X.; Zhang, Q.; Yang, M.; Cho, E. C.; Brown, P. K. *Accounts of Chemical Research* **2011**, *44*, 914–924.

(46) Alkilany, A. M.; Thompson, L. B.; Boulos, S. P.; Sisco, P. N.; Murphy, C. J. *Adv. Drug Deliv. Rev.* **2012**, *64*, 190–199.

(47) Chen, J.; Wiley, B.; Li, Z. Y.; Campbell, D.; Saeki, F.; Cang, H.; Au, L.; Lee, J.; Li, X.; Xia, Y. *Advanced Materials* **2005**, *17*, 2255–2261.

(48) Vigderman, L.; Manna, P.; Zubarev, E. R. *Angew. Chem. E. Int. Ed.* **2012**, *51*, 636–641.

(49) Wang, H.; Huff, T. B.; Zweifel, D. A.; He, W.; Low, P. S.; Wei, A.; Cheng, J. X. *Proc. Natl. Acad. Sci.* **2005**, *102*, 15752–15756.

(50) Durr, N. J.; Larson, T.; Smith, D. K.; Korgel, B. A.; Sokolov, K.; Ben-Yakar, A. *Nano Lett.* **2007**, *7*, 941–5.

(51) Alkilany, A. M.; Nagaria, P. K.; Hexel, C. R.; Shaw, T. J.; Murphy, C. J.; Wyatt, M. D. *Small* **2009**, *5*, 701–708.

(52) Fay, F.; Scott, C. J. *Immunotherapy* **2011**, *3*, 381–394.

(53) Jaracz, S.; Chen, J.; Kuznetsova, L. V.; Ojima, I. *Bioorganic & Medicinal Chemistry* **2005**, *13*, 5043–5054.

(54) Betty, C. R.-K.; Rostro-Kohanloo, B. C.; Bickford, L. R.; Payne, C. M.; Day, E. S.; Anderson, L. J. E.; Zhong, M.; Lee, S.; Mayer, K. M.; Zal, T.; Adam, L.; Dinney, C. P. N.; Drezek, R. A.; West, J. L.; Hafner, J. H. *Nanotechnology* **2009**, *20*, 434005.

(55) Zhu, Y.; Kuang, H.; Xu, L.; Ma, W.; Peng, C.; Hua, Y.; Wang, L.; Xu, C. *J. Mater. Chem.* **2012**, *22*, 2387.

(56) Wang, L.; Zhu, Y.; Xu, L.; Chen, W.; Kuang, H.; Liu, L.; Agarwal, A.; Xu, C.; Kotov, N. a *Angew. Chem. E. Int. Ed.* **2010**, *49*, 5472–5.

(57) Huang, H.; Qu, C.; Liu, X.; Huang, S.; Xu, Z.; Zhu, Y.; Chu, P. K. *Chem. Commun.* **2011**, *47*, 6897–9.

(58) Sim, H. R.; Wark, A. W.; Lee, H. J. *Analyst* **2010**, *135*, 2528–32.

(59) Truong, P. L.; Cao, C.; Park, S.; Kim, M.; Sim, S. J. *Lab Chip* **2011**, *11*, 2591–7.

(60) Vigderman, L.; Khanal, B. P.; Zubarev, E. R. *Adv. Mater.* **2012**, *24*, 4811–4841.

(61) Lu, G.; Hou, L.; Zhang, T.; Li, W.; Liu, J. *J. Phys. Chem. C* **2011**, *115*, 22877–22885.

(62) Mayer, K. M.; Lee, S.; Liao, H.; Rostro, B. C.; Fuentes, A.; Scully, P. T.; Nehl, C. L.; Hafner, J. H. *ACS Nano* **2008**, *2*, 687–692.

(63) Marinakos, S. M.; Chen, S.; Chilkoti, A. *Anal. Chem.* **2007**, *79*, 5278–83.

(64) Nusz, G. J.; Marinakos, S. M.; Curry, A. C.; Dahlin, A.; Höök, F.; Wax, A.; Chilkoti, A. *Anal. Chem.* **2008**, *80*, 984–9.

(65) Wanga, J.; Zhanga, P.; Lia, C. M.; Lia, Y. F.; Huang, C. Z.; Wang, J.; Zhang, P.; Li, C. M.; Li, Y. F. *Biosens. Bioelectron.* **2012**, *34*, 197–201.

(66) Wang, C.; Chen, Y.; Wang, T.; Ma, Z. *Chem. Mater.* **2007**, *19*, 5809–5811.

(67) Parab, H. J.; Jung, C.; Lee, J.-H.; Park, H. G. *Biosens. Bioelectron.* **2010**, *26*, 667–73.

(68) Fu, X.; Chen, L.; Li, J.; Lin, M.; You, H.; Wang, W. *Biosens. Bioelectron.* **2012**, *34*, 227–31.

(69) Zhu, Y.; Qu, C.; Kuang, H.; Xu, L.; Liu, L.; Hua, Y.; Wang, L.; Xu, C. *Biosens. Bioelectron.* **2011**, *26*, 4387–92.

(70) Sönnichsen, C.; Franzl, T.; Wilk, T.; von Plessen, G.; Feldmann, J. *Phys. Rev. Lett.* **2002**, *88*, 1–4.

(71) Liu, X.; Dai, Q.; Austin, L.; Coutts, J.; Knowles, G.; Zou, J.; Chen, H.; Huo, Q. *J. Am. Chem. Soc.* **2008**, *130*, 2780–2782.

(72) Fan, M.; Andrade, G. F. S.; Brolo, A. G. *Anal. Chim. Acta* **2011**, *693*, 7–25.

(73) Dougan, J. A.; Faulds, K. *Analyst* **2012**, *137*, 545–54.

(74) Bailo, E.; Deckert, V. *Chem. Soc. Rev.* **2008**, *37*, 921–30.

(75) Qian, X.-M. M.; Nie, S. M. *Chem. Soc. Rev.* **2008**, *37*, 912–920.

(76) Tian, Z. Q.; Ren, B.; Wu, D. Y. *J. Phys. Chem. B* **2002**, *106*, 9463–9483.

(77) Campion, A.; Kambhampati, P. *Chem. Soc. Rev.* **1998**, *27*, 241–250.

(78) Kneipp, J.; Kneipp, H.; Kneipp, K. *Chem. Soc. Rev.* **2008**, *37*, 1052–1060.

(79) Kneipp, K.; Kneipp, H.; Kneipp, J. *Acc. Chem. Res.* **2006**, *39*, 443–450.

(80) Lee, C. H.; Tian, L.; Singamaneni, S. *ACS Appl. Mater. Interfaces* **2010**, *2*, 3429–35.

(81) Liao, Q.; Mu, C.; Xu, D.-S.; Ai, X.-C.; Yao, J.-N.; Zhang, J.-P. *Langmuir* **2009**, *25*, 4708–4714.

(82) Doherty, M. D.; Murphy, A.; McPhillips, J.; Pollard, R. J.; Dawson, P. *J. Phys. Chem. C* **2010**, *114*, 19913–19919.

(83) Alvarez-Puebla, R. a; Agarwal, A.; Manna, P.; Khanal, B. P.; Aldeanueva-Potel, P.; Carbó-Argibay, E.; Pazos-Pérez, N.; Vigderman, L.; Zubarev, E. R.; Kotov, N. a; Liz-Marzán, L. M. *Proc. Natl. Acad. Sci.* **2011**, *108*, 8157–8161.

(84) Lee, J.; Mubeen, S.; Ji, X.; Stucky, G. D.; Moskovits, M. *Nano letters* **2012**, *12*, 5014–5019.

(85) Knight, M. W.; Sobhani, H.; Nordlander, P.; Halas, N. J. *Science* **2011**, *332*, 702–4.

(86) Warren, S. C.; Walker, D. a; Grzybowski, B. a *Langmuir* **2012**, *28*, 9093–9102.

(87) Nikoobakht, B.; El-Sayed, M. A. *Chem. Mater.* **2003**, *15*, 1957–1962.

(88) Chang, S.-S.; Lee, C.-L.; Wang, C. R. C. *J. Phys. Chem. B* **1997**, *101*, 6661–6664.

(89) Chang, S.-S.; Shih, C.-W.; Chen, C.-D.; Lai, W.-C.; Wang, C. R. C. *Langmuir* **1999**, *15*, 701–709.

(90) Wang, Z. L.; Mohammed, M. B.; Link, S.; El-Sayed, M. A. *Surf. Sci.* **1999**, *283*, 368–L814.

(91) Pal, T.; (nee Das), S. D.; Jana, N. R.; Pradhan, N.; Mandal, R.; Pal, A.; Beezer, A. E.; Mitchell, J. C. *Langmuir* **1998**, *14*, 4724–4730.

(92) Jiang, X. C.; Brioude, A.; Pileni, M. P. *Colloids Surf. A* **2006**, *277*, 201–206.

(93) Zweifel, D. A.; Wei, A. *Chem. Mater.* **2005**, *17*, 4256–4261.

(94) Hubert, F.; Testard, F.; Rizza, G.; Spalla, O. *Langmuir* **2010**, *26*, 6887–6891.

(95) Jana, N. R. *Small* **2005**, *1*, 875–82.

(96) Khanal, B. P.; Zubarev, E. R. *Angew. Chem. E. Int. Ed.* **2007**, *46*, 2195–2198.

(97) Sau, T. K.; Murphy, C. J. *Langmuir* **2004**, *20*, 6414–6420.

(98) Ye, X.; Jin, L.; Caglayan, H.; Chen, J.; Xing, G.; Zheng, C.; Doan-Nguyen, V.; Kang, Y.; Engheta, N.; Kagan, C. R.; Murray, C. B. *ACS Nano* **2012**, *6*, 2804–2817.

(99) Jana, N. R.; Gearheart, L.; Obare, S. O.; Murphy, C. J. *Langmuir* **2002**, *18*, 922–927.

(100) Zou, R.; Guo, X.; Yang, J.; Li, D.; Peng, F.; Zhang, L.; Wang, H.; Yu, H. *CrystEngComm* **2009**, *11*, 2797–2803.

(101) Samal, A. K.; Sreeprasad, T. S.; Pradeep, T. *J. Nanopart. Res.* **2009**, *12*, 1777–1786.

(102) Zijlstra, P.; Bullen, C.; Chon, J. W. M.; Gu, M. *J. Phys. Chem. B* **2006**, *110*, 19315–19318.

(103) Boleininger, J.; Kurz, A.; Reuss, V.; Sonnichsen, C. *Phys. Chem. Chem. Phys.* **2006**, *8*, 3824.

(104) Bullen, C.; Latter, M. J.; D'Alonzo, N. J.; Willis, G. J.; Raston, C. L. *Chem. Commun.* **2011**, *47*, 4123–4125.

(105) Tollan, C. M.; Echeberria, J.; Marcilla, R.; Pomposo, J. A.; Mecerreyes, D. *J. Nanopart. Res.* **2008**, *11*, 1241–1245.

(106) Kim, F.; Song, J. H.; Yang, P. *J. Am. Chem. Soc.* **2002**, *124*, 14316–14317.

(107) Nishioka, K.; Niidome, Y.; Yamada, S. *Langmuir* **2007**, *23*, 10353–10356.

(108) Niidome, Y.; Nishioka, K.; Kawasaki, H.; Yamada, S. *Chem. Commun.* **2003**, *18*, 2376–2377.

(109) Miranda, O. R.; Dollahon, N. R.; Ahmadi, T. S. *Cryst. Growth Des.* **2006**, *6*, 2747–2753.

(110) Okitsu, K.; Sharyo, K.; Nishimura, R. *Langmuir* **2009**, *25*, 7786–7790.

(111) Abidi, W.; Selvakannan, P. R.; Guillet, Y.; Lampre, I.; Beaunier, P.; Pansu, B.; Palpant, B.; Remita, H. *J. Phys. Chem. C* **2010**, *114*, 14794–14803.

(112) Biswal, J.; Ramnani, S. P.; Tewari, R.; Dey, G. K.; Sabharwal, S. *Radiat. Phys. Chem.* **2010**, *79*, 441–445.

(113) Carbó-Argibay, E.; Rodríguez-González, B.; Gómez-Graña, S.; Guerrero-Martínez, A.; Pastoriza-Santos, I.; Pérez-Juste, J.; Liz-Marzán, L. M. *Angew. Chem. E. Int. Ed.* **2010**, *49*, 9397–400.

(114) Kou, X.; Zhang, S.; Tsung, C.-K.; Yeung, M. H.; Shi, Q.; Stucky, G. D.; Sun, L.; Wang, J.; Yan, C. *J. Phys. Chem. B* **2006**, *110*, 16377–16383.

(115) Kuwahara, Y.; Yoshimori, K.; Tomita, K.; Sakai, M.; Sawada, T.; Niidome, Y.; Yamada, S.; Shosenji, H. *Chem. Lett.* **2007**, *36*, 1230–1231.

(116) Garg, N.; Scholl, C.; Mohanty, A.; Jin, R. *Langmuir* **2010**, *26*, 10271–10276.

(117) Si, S.; Leduc, C.; Delville, M.-H.; Lounis, B. *Chemphyschem* **2012**, *13*, 193–202.

(118) Niidome, Y.; Nakamura, Y.; Honda, K.; Akiyama, Y.; Nishioka, K.; Kawasaki, H.; Nakashima, N. *Chem. Commun.* **2009**, 1754–1756.

(119) Smith, D. K.; Miller, N. R.; Korgel, B. a *Langmuir* **2009**, *25*, 9518–9524.

(120) Smith, D. K.; Korgel, B. a *Langmuir* **2008**, *24*, 644–649.

(121) Rayavarapu, R. G. R. G.; Ungureanu, C.; Krystek, P.; van Leeuwen, T. G. T. G.; Manohar, S. *Langmuir* **2010**, *26*, 5050–5055.

(122) Wang, Z.; Gao, R.; Nikoobakht, B.; El-Sayed, M. A. *J. Phys. Chem. B* **2000**, *104*, 5417–5420.

(123) Gole, A.; Murphy, C. J. *Chem. Mater.* **2004**, *16*, 3633–3640.

(124) Hubert, F.; Testard, F.; Spalla, O. *Langmuir* **2008**, *24*, 9219–9222.

(125) Giannici, F.; Placido, T.; Curri, M. L.; Striccoli, M.; Agostiano, A.; Comparelli, R. *Dalton Trans.* **2009**, *46*, 10367–74.

(126) Placido, T.; Comparelli, R.; Giannici, F.; Cozzoli, P. D.; Capitani, G.; Striccoli, M.; Agostiano, A.; Curri, M. L. *Chem. Mater.* **2009**, *21*, 4192–4202.

(127) Orendorff, C. J.; Murphy, C. J. *J. Phys. Chem. B* **2006**, *110*, 3990–3994.

(128) Liu, M.; Guyot-Sionnest, P. *J. Phys. Chem. B* **2005**, *109*, 22192–200.

(129) Pérez-Juste, J.; Liz-Marzán, L. M.; Carnie, S.; Chan, D. Y. C.; Mulvaney, P. *Adv. Funct. Mater.* **2004**, *14*, 571–579.

(130) Edgar, J. A.; McDonagh, A. M.; Cortie, M. B. *ACS Nano* **2012**, *6*, 1116–1125.

(131) Jana, N. R.; Gearheart, L.; Murphy, C. J. *J. Phys. Chem. B* **2001**, *105*, 4065–4067.

(132) Takenaka, Y.; Kitahata, H. *Chem. Phys. Lett.* **2009**, *467*, 327–330.

(133) Johnson, C. J.; Dujardin, E.; Davis, S. A.; Murphy, C. J.; Mann, S. *J. Mater. Chem.* **2002**, *12*, 1765–1770.

(134) Wu, H.-Y. H. Y.; Huang, W. L. W.-L.; Huang, M. H. M. H. *Cryst. Growth Des.* **2007**, *7*, 831–835.

(135) Busbee, B. D. D.; Obare, S. O. O.; Murphy, C. J. J. *Adv. Mater.* **2003**, *15*, 414–416.

(136) Wu, H.-Y.; Chu, H.-C.; Kuo, T.-J.; Kuo, C.-L.; Huang, M. H. *Chem. Mater.* **2005**, *17*, 6447–6451.

(137) Khanal, B. P.; Zubarev, E. R. *J. Am. Chem. Soc.* **2008**, *130*, 12634–12635.

(138) Rodríguez-Fernández, J.; Pérez-Juste, J.; Mulvaney, P.; Liz-Marzán, L. M. *J. Phys. Chem. B* **2005**, *109*, 14257–14261.

(139) Park, K.; Koerner, H.; Vaia, R. a *Nano Lett.* **2010**, *10*, 1433–9.

(140) Vigderman, L.; Zubarev, E. R. *Langmuir* **2012**, *28*, 9034–9040.

(141) Schlesinger, H. I.; Brown, H. C.; Finholt, A. E.; Gilbreath, J. R.; Hoekstra, H. R.; Hyde, E. K. *J. Am. Chem. Soc.* **1953**, *75*, 215–219.

(142) Taub, N.; Krichevski, O.; Markovich, G. *J. Phys. Chem. B* **2003**, *107*, 11579–11582.

(143) Wei, Z.; Mieszawska, A. J.; Zamborini, F. P. *Langmuir* **2004**, *20*, 4322–4326.

(144) Liao, H.; Hafner, J. H. *J. Phys. Chem. B* **2004**, *108*, 19276–19280.

(145) Kannan, P.; Sampath, S.; John, S. A. *J. Phys. Chem. C* **2010**, *114*, 21114–21122.

(146) Gao, J.; Bender, C. M.; Murphy, C. J. *Langmuir* **2003**, *19*, 9065–9070.

(147) Bai, X.; Gao, Y.; Liu, H.-G.; Zheng, L. *J. Phys. Chem. C* **2009**, *113*, 17730–17736.

(148) Martin, C. R. *Chem. Mater.* **1996**, *20*, 1739–1746.

(149) Wade, T. L.; Wegrowe, J. *Eur. Phys. J. Appl. Phys.* **2005**, *29*, 3–22.

(150) Cepak, V. M.; Martin, C. R. *J. Phys. Chem. B* **1998**, *102*, 9985–9990.

(151) Hulteen, J. C.; Martin, C. R. *J. Mater. Chem.* **1997**, *7*, 1075–1087.

(152) Tierney, M. J.; Martin, C. R. *J. Phys. Chem.* **1989**, *93*, 2878–2880.

(153) Wurtz, G. A.; Pollard, R.; Hendren, W.; Wiederrecht, G. P.; Gosztola, D. J.; Podolskiy, V. A.; Zayats, A. V. *Nat. Nanotechnol.* **2011**, *6*, 107–11.

(154) Hornyak, G. L.; Patrissi, C. J.; Martin, C. R. *J. Phys. Chem. B* **1997**, *101*, 1548–1555.

(155) van der Zande, B. M. I.; Böhmer, M. R.; Fokkink, L. G. J.; Schönenberger, C.; Zande, B. M. I. V. D.; Bo, M. R.; Scho, C. *J. Phys. Chem. B* **1997**, *101*, 852–854.

(156) van der Zande, B. M. I.; Böhmer, M. R.; Fokkink, L. G. J.; Schönenberger, C. *Langmuir* **2000**, *16*, 451–458.

(157) Banholzer, M. J.; Li, S.; Ketter, J. B.; Rozkiewicz, D. I.; Schatz, G. C.; Mirkin, C. A. *J. Phys. Chem. C* **2008**, *112*, 15729–15734.

(158) Qin, L.; Park, S.; Huang, L.; Mirkin, C. A. *Science* **2005**, *309*, 113–5.

(159) Pan, S. L.; Zeng, D. D.; Zhang, H. L.; Li, H. L. *Appl. Phys. A* **2000**, *70*, 637–640.

(160) Dickson, W.; Evans, P. R.; Wurtz, G. a; Hendren, W.; Atkinson, R.; Pollard, R. J.; Zayats, a V. *J. Microsc.* **2008**, *229*, 415–20.

(161) Li, Z.; Kübel, C.; Pârvulescu, V. I.; Richards, R. *ACS Nano* **2008**, *2*, 1205–12.

(162) Xie, Y.; Quinlivan, S.; Asefa, T. *J. Phys. Chem. C* **2008**, *112*, 9996–10003.

(163) Gao, C.; Zhang, Q.; Lu, Z.; Yin, Y. *J. Am. Chem. Soc.* **2011**, *133*, 19706–19709.

(164) Gao, C.; Lu, Z.; Yin, Y. *Langmuir* **2011**, *27*, 12201–12208.

(165) Li, Z.; Tao, J.; Lu, X.; Zhu, Y.; Xia, Y. *Nano Lett.* **2008**, *8*, 3052–5.

(166) Lu, X.; Yavuz, M.; Tuan, H. *J. Am. Chem. Soc.* **2008**, *130*, 8900–8901.

(167) Wang, C.; Hu, Y.; Lieber, C. M.; Sun, S. *J. Am. Chem. Soc.* **2008**, *130*, 8902–8903.

(168) Huo, Z.; Tsung, C.; Huang, W.; Zhang, X.; Yang, P. *Nano Lett.* **2008**, *8*, 2041–2044.

(169) Seo, D.; Park, J. H.; Jung, J.; Park, S. M.; Ryu, S.; Kwak, J.; Song, H. *J. Phys. Chem. C* **2009**, *113*, 3449–3454.

(170) Ryu, H. J.; Sanchez, L.; Keul, H. A.; Raj, A.; Bockstaller, M. R. *Angew. Chem. E. Int. Ed.* **2008**, *47*, 7639–43.

(171) Leonov, A. P.; Zheng, J.; Clogston, J. D.; Stern, S. T.; Patri, A. K.; Wei, A. *ACS Nano* **2008**, *2*, 2481–2488.

(172) Nikoobakht, B.; El-Sayed, M. A. *Langmuir* **2001**, *17*, 6368–6374.

(173) Gómez-Graña, S.; Hubert, F.; Testard, F.; Guerrero-Martínez, A.; Grillo, I.; Liz-Marzán, L. M.; Spalla, O. *Langmuir* **2012**, *28*, 1453–1459.

(174) Khanal, B. P.; Zubarev, E. R. *Angew. Chem. E. Int. Ed.* **2009**, *48*, 6888–6891.

(175) Thierry, B.; Ng, J.; Krieg, T.; Griesser, H. J. *Chem. Commun.* **2009**, *1*, 1724–6.

(176) Gentili, D.; Ori, G.; Comes Franchini, M.; Comes, F. M. *Chem. Commun.* **2009**, *39*, 5874–6.

(177) Yu, C.; Nakshatri, H.; Irudayaraj, J. *Nano Lett.* **2007**, *7*, 2300–6.

(178) Wijaya, A.; Hamad-Schifferli, K. *Langmuir* **2008**, *24*, 9966–9969.

(179) Caswell, K. K.; Wilson, J. N.; Bunz, U. H. F.; Murphy, C. J. *J. Am. Chem. Soc.* **2003**, *125*, 13914–13915.

(180) Liao, H.; Hafner, J. H. *Chem. Mater.* **2005**, *17*, 4636–4641.

(181) Li, C.; Wu, C.; Zheng, J.; Lai, J.; Zhang, C.; Zhao, Y. *Langmuir* **2010**, *26*, 9130–9135.

(182) Bogliotti, N.; Oberleitner, B.; Di-Cicco, A.; Schmidt, F.; Florent, J.-C.; Semetey, V. *J. Colloid Interface Sci.* **2011**, *357*, 75–81.

(183) Dickerson, E. B.; Dreaden, E. C.; Huang, X.; El-Sayed, I. H.; Chu, H.; Pushpanketh, S.; McDonald, J. F.; El-Sayed, M. A. *Cancer lett.* **2008**, *269*, 57–66.

(184) Chanda, N.; Shukla, R.; Katti, K. V.; Kannan, R. *Nano Lett.* **2009**, *9*, 1798–1805.

(185) Bartczak, D.; Kanaras, A. G. *Langmuir* **2011**, *27*, 10119–10123.

(186) Nie, Z.; Fava, D.; Kumacheva, E.; Zou, S.; Walker, G. C.; Rubinstein, M. *Nat. Mater.* **2007**, *6*, 609–614.

(187) Huff, T. B.; Hansen, M. N.; Zhao, Y.; Cheng, J. X.; Wei, A. *Langmuir* **2007**, *23*, 1596–1599.

(188) Zhao, Y.; Pérez-Segarra, W.; Shi, Q.; Wei, A. *J. Am. Chem. Soc.* **2005**, *127*, 7328–7329.

(189) Choi, R.; Yang, J.; Choi, J.; Lim, E.-K.; Kim, E.; Suh, J.-S.; Huh, Y.-M.; Haam, S. *Langmuir* **2010**, *26*, 17520–17527.

(190) Nandanan, E.; Jana, N. R.; Ying, J. Y. *Adv. Mater.* **2008**, *20*, 2068–2073.

(191) Gole, A.; Murphy, C. J. *Chem. Mater.* **2005**, *17*, 1325–1330.

(192) Wilson, C. G.; Sisco, P. N.; Gadala-Maria, F. a; Murphy, C. J.; Goldsmith, E. C. *Biomaterials* **2009**, *30*, 5639–48.

(193) Chen, W.; McCarthy, T. J. *Macromolecules* **1997**, *30*, 78–86.

(194) Huang, H.-C. C.; Barua, S.; Kay, D. B.; Rege, K. *ACS Nano* **2009**, *3*, 2941–2952.

(195) Qiu, Y.; Liu, Y.; Wang, L.; Xu, L.; Bai, R.; Ji, Y.; Wu, X.; Zhao, Y.; Li, Y.; Chen, C. *Biomaterials* **2010**, *31*, 7606–19.

(196) Peng, C.-A.; Wang, C.-H. *Cancers* **2011**, *3*, 227–240.

(197) Matteini, P.; Ratto, F.; Rossi, F.; Pini, R. *Proc. SPIE* **2010**, *7574*, 75740U–75740U–4.

(198) Ratto, F.; Matteini, P.; Rossi, F.; Menabuoni, L.; Tiwari, N.; Kulkarni, S. K.; Pini, R. *Nanomed. Nanotechnol.* **2009**, *5*, 143–151.

(199) Guo, R.; Zhang, L.; Qian, H.; Li, R.; Jiang, X.; Liu, B. *Langmuir* **2010**, *26*, 5428–5434.

(200) Wilson, C. G.; Sisco, P. N.; Goldsmith, E. C.; Murphy, C. J. *J. Mater. Chem.* **2009**, *19*, 6332–6340.

(201) Alkilany, A. M.; Nagaria, P. K.; Wyatt, M. D.; Murphy, C. J. *Langmuir* **2010**, *26*, 9328–9333.

(202) Alkilany, A. M.; Thompson, L. B.; Murphy, C. J. *ACS Appl. Mater. Interfaces* **2010**, *2*, 3417–21.

(203) Gole, A.; Murphy, C. J. *Langmuir* **2008**, *24*, 266–272.

(204) Huang, X.; El-Sayed, I. H.; Qian, W.; El-Sayed, M. A. *J. Am. Chem. Soc.* **2006**, *128*, 2115–2120.

(205) Basiruddin, S. K.; Saha, A.; Pradhan, N.; Jana, N. R. *Langmuir* **2010**, *26*, 7475–7481.

(206) Takahashi, H.; Niidome, Y.; Niidome, T.; Kaneko, K.; Kawasaki, H.; Yamada, S. *Langmuir* **2006**, *22*, 2–5.

(207) Lee, S. E.; Sasaki, D. Y.; Perroud, T. D.; Yoo, D.; Patel, K. D.; Lee, L. P. *J. Am. Chem. Soc.* **2009**, *131*, 14066–14074.

(208) Orendorff, C. J.; Alam, T. M.; Sasaki, D. Y.; Bunker, B. C.; Voigt, J. A. *ACS Nano* **2009**, *3*, 971–983.

(209) Nakashima, H.; Furukawa, K.; Kashimura, Y.; Torimitsu, K. *Langmuir* **2008**, *24*, 5654–5658.

Chapter 2

High-Yield Synthesis of Gold Nanorods Using Hydroquinone as a Reducing Agent

2.1. Introduction

Most of the applications of gold NRs hinge on their unique shape-dependent optical and electronic properties[2,4,6,14–16] so their efficient and reliable synthesis with a broad range of dimensions is highly desirable. The most widely used procedure for the synthesis of gold NRs is the seed-mediated method developed by Murphy[17,18] and El-Sayed, as described in Chapter 1.4.1.[19] In this procedure, an amount of seed solution, produced by the rapid reduction of gold ions with sodium borohydride is added to an Au(III)-CTAB solution reduced to Au(I) with ascorbic acid in the presence of silver nitrate.[19] This procedure is particularly sensitive to small changes in the experimental protocol as discussed in the literature.[6] For

instance, changing the surfactant to anything other than CTAB generally cannot be done with a few exceptions.[19–22] The ascorbic acid concentration used in the growth solution can also have a great impact on the NR growth and generally must fall within a small window around 1.1 times the Au(III) molar concentration in order to produce high quality gold NRs.[23] Murphy and coworkers performed a detailed ICP-MS analysis of gold NRs prepared by classical seed-mediated synthesis[19] and determined that only ~15% of gold ions are converted to metallic gold.[23] This extremely low yield makes this procedure particularly wasteful considering the cost of the starting materials. On the other hand, utilizing less ascorbic acid leads to very little NR growth, while using too much results in the formation of spherical particles, which are difficult to separate from the desired product. In addition, the reliability and reproducibility of the NR synthesis may be limited by this large sensitivity to ascorbic acid concentration. However, there have been few reports of using a different reducing agent for gold NR growth. Bullen and coworkers utilized acetylacetone in an increased pH growth solution leading to simultaneous nucleation and growth in a continuous flow synthesis of gold NRs.[24] Ye and coworkers noted that the salicylic acid derivatives could reduce Au(III) to Au(I) ions, but ascorbic acid was still required for the reduction to metallic gold. Acetone has also been used in the photochemical growth of nanorods,[25–28] although the mechanism of this procedure is significantly different from the more popular seed-mediated synthesis.

Many of the interesting optical properties of gold NRs depend on the position of their LSPR peak, which is largely governed by their aspect ratio.[29] However, one of the limitations of the standard seed-mediated procedure is related to the maximum LSPR peak position that can be realistically obtained. Typically, only NRs with a maximum LSPR of no more than 850 nm and aspect ratio of 4.5 – 5 can be reliably prepared with a high degree of purity.[19] El-Sayed and coworkers described the synthesis of gold NRs with LSPR above 1000 nm through the use of a mixed CTAB/BDAC (benzyldimethylhexadecylammonium chloride) surfactant system, but this was accompanied by a large fraction of spherical particles and very poor quality of the NRs.[19,30] Similarly, it is possible to use a silver-free seed-mediated procedure for the synthesis of high aspect ratio gold NRs, but this technique produces a very high level of spherical and platelet impurities[6,17,31] which must be further purified and is difficult to scale up.[32,33] More recently, Zhu and coworkers used the addition of HCl to drive the formation of higher aspect ratio NRs with LSPR above 1000 nm,[34] while Ye and coworkers used HCl and aromatic additives,[35] but both of these procedures maintain the use of ascorbic acid and suffer from extremely low yield of gold conversion and decreasing NR quality. In addition, it is possible to modulate the LSPR through the formation of altered rod morphologies such as dumbbells[36–38] and dogbones,[37] leading to a red-shift up to 1050 nm.[38] Finally, post-synthetic modification of NRs is also possible by reshaping,[39] dissolution,[40,41] and overgrowth with gold[42–45] or other metals.[46–49] However, these techniques only result in a blue-shift of the LSPR peak.

In this chapter, we describe the use of a novel reducing agent, hydroquinone, to replace ascorbic acid in the seed-mediated growth of gold nanorods to address the long-standing limitations of this technique, namely, poor yield of gold conversion and LSPR peaks no higher than 850 nm. While hydroquinone has been used in the synthesis of silver[50,51] and gold nanoparticles[52,53] as well as for the reduction of silver onto gold nanorods,[48] its use in the synthesis of gold NRs has not been demonstrated to date. When added to the growth solution at 10 – 20 times the concentration of gold, it leads to the slow growth of NRs of tunable dimensions. The rods are reproducibly synthesized in high quality and the excess of reducing agent allows for a near quantitative (~100 %) isolated yield of metallic rods as opposed to much lower level of conversion in classical techniques (~15%).[19,23] By modifying the hydroquinone, silver, gold, and seed concentration in the growth solution, it is possible to produce gold NRs with LSPR up to 1250 nm with a distinctive asymmetrical tip structure. These rods show a unique LSPR relaxation process that can be halted by thiol functionalization.

2.2. Nanorod Synthesis and Morphology

Gold nanorods were synthesized by replacing the traditional ascorbic acid reducing agent with hydroquinone. However, while using hydroquinone at the same concentrations as ascorbic acid does lead to reduction of Au (III) to Au(I), as indicated by the disappearance of color, no nanoparticle growth is observed with the introduction of seed solution under these conditions. Increasing the

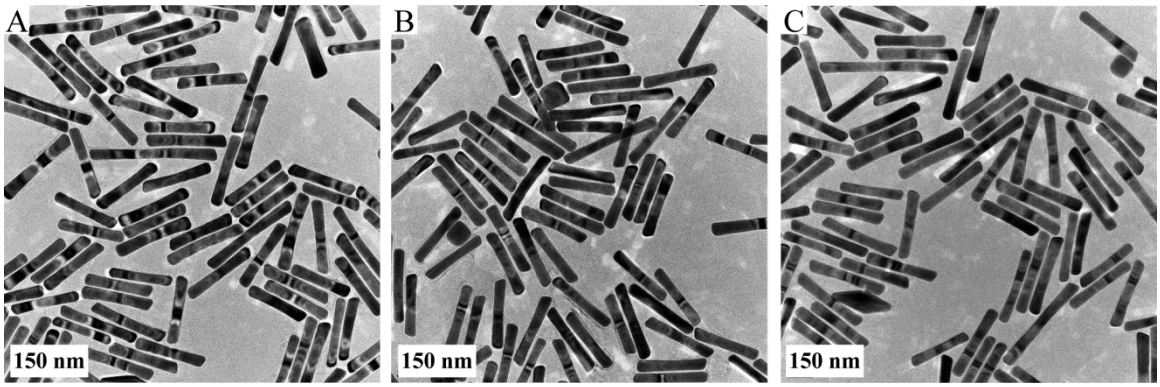

Figure 2.1. Representative TEM images of gold NRs synthesized with hydroquinone (a). Typical cubic and bipyramidal impurities are shown in (b) and (c), respectively.

hydroquinone concentration from 1.1 to 10 times with respect to gold concentration led to a slow growth of NRs with red-brown color. Combined with increases in both the silver nitrate and seed nanoparticles concentration, NRs with an aspect ratio of 6-8 were produced, as seen in the representative TEM images shown in Figure 2.1. Interestingly, these gold NRs have a unique morphology with a small pinching at the rod center and anisotropic tips that extend farther on one side of the rod, as seen in the TEM image in Figure 2.2a. High-resolution TEM imaging shown in Figure 2.2b and c confirms the single-crystalline structure of the NRs, equivalent to NRs made by the standard procedure. The high shape-wise yield of gold NRs versus other morphologies can be clearly seen in the TEM image and is also evident when examining the UV-Vis spectrum of gold NRs, shown in Figure 2.3a. Recently, we put forward an estimate of gold NR shape-yield based on the ratio of the longitudinal-to-transverse surface plasmon resonance (TSPR) peak. For NRs of aspect ratio 3.5-4, we estimated empirically that an LSPR:TSPR ratio of 10 or higher is indicative of low spherical impurity.[6] Although this estimate may not apply to these higher aspect

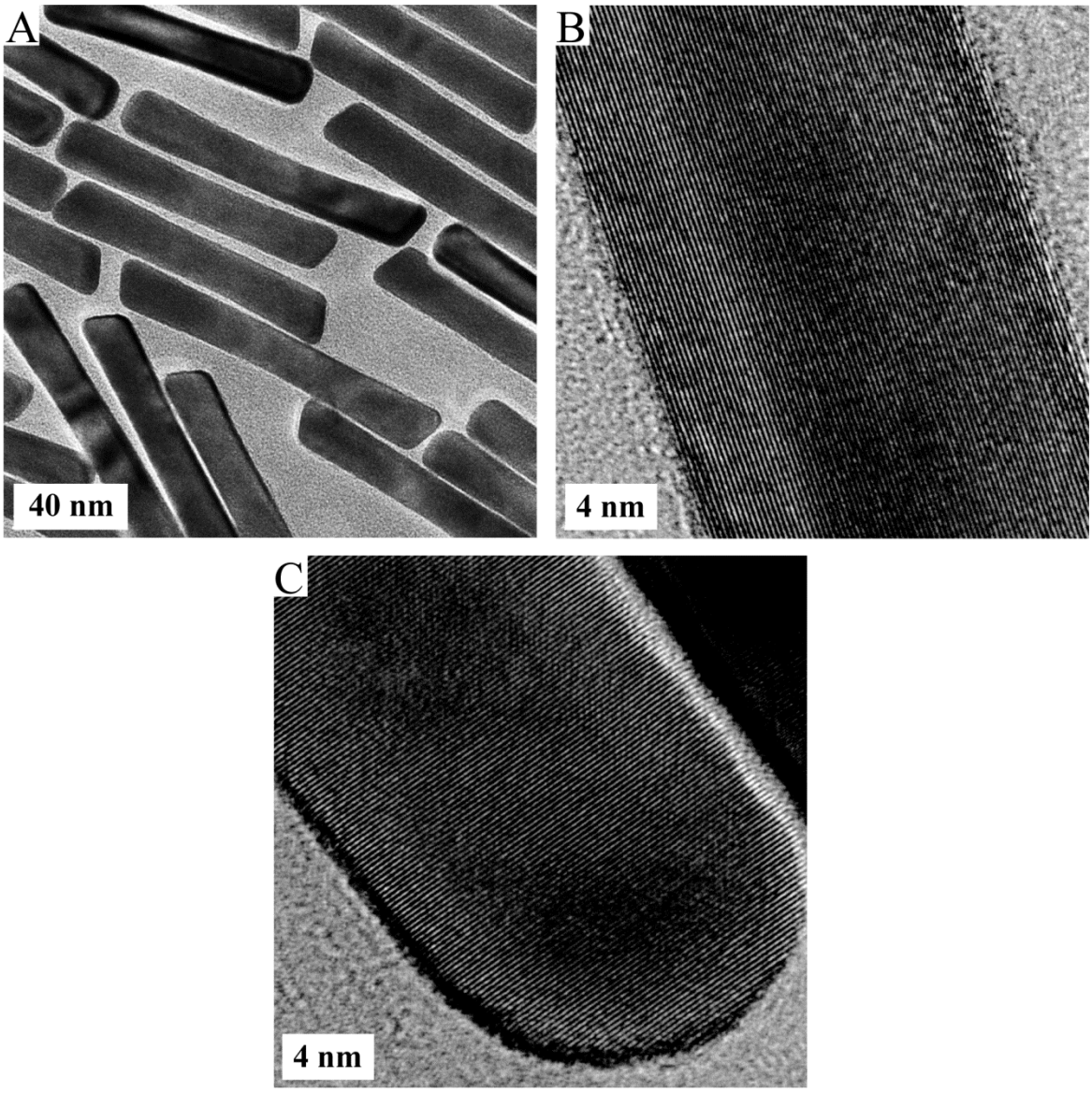

Figure 2.2. Medium (a) and high-magnification (b-c) TEM images of NRs synthesized with hydroquinone.

ratio rods, the high intensity of the LSPR compared to the TSPR band (ratio of ~11) strongly suggests a low level of spherical particles. This ratio is better than that in the standard synthesis, in which case it is less than 4.[19] Certainly, this is a large improvement compared to the mixed-surfactant synthesis of high aspect ratio NRs which produce a very impure product.[19] Small peaks are visible at around 600 and

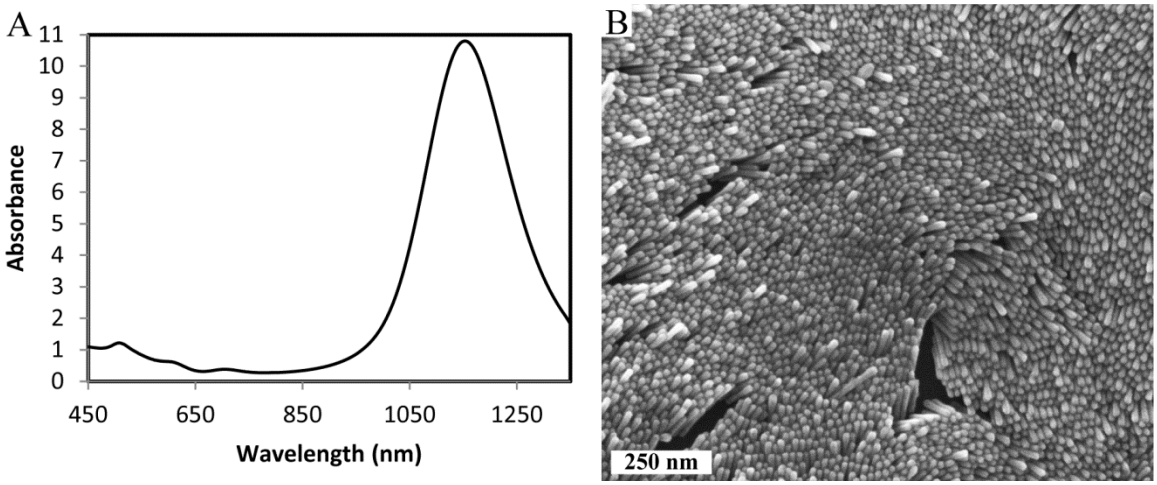

Figure 2.3. UV-Vis spectrum of NRs (a) as well SEM image of vertically-standing NRs (b).

700 nm which may correspond to cube-like and bipyramidal impurities, as seen in Figure 2.1b and c, respectively. This unique tip structure led us to question whether the nanostructures could actually be flat with a belt-like morphology. To elucidate their three-dimensional structure, the rods were dried onto a silicon substrate and imaged by SEM, resulting in vertically standing assemblies of up to 6 μm in lateral size, shown in Figure 2.3b. From this image, it is clear that the particles do have a rod-like morphology with a circular cross-section rather than a belt-like morphology with a rectangular cross-section.

2.3. Analysis of Nanorod Growth

Even though the hydroquinone reducing agent is present in large excess quantity, the growth occurred much slower than in the standard procedure, taking up to 12 hours compared to the usual 30 minutes. This slow growth makes it much

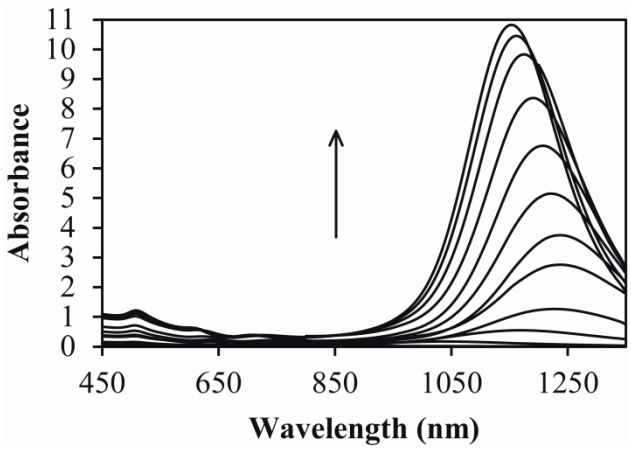

Figure 2.4. Evolution of the UV-Vis absorbance spectrum of gold NRs during their growth. Spectra are shown after each hour of growth time and increase in intensity up to the 12 hour point.

simpler to track NR growth by UV-Vis absorbance spectroscopy as well as by TEM. Figure 2.4 shows the evolution of the absorbance spectrum of the rods over time. The LSPR maximum starts at approximately 1000 nm and redshifts and intensifies over the course of several hours, shifting to as far as 1230 nm after 6 hours. After this point, it blueshifts down to 1150 nm while continuing to intensify until the growth is complete after 12 hours. It must be noted that the absorbance intensity of the solution was far greater than that seen from a normal rod synthesis and after 4 hours it was necessary to dilute the solution 10-fold prior to UV-Vis measurements and multiply the resulting spectrum by 10 to obtain the true result. The final LSPR absorbance intensity climbed to above 10 compared to 1-1.5 for a typical ascorbic acid mediated synthesis, indicating the much higher yield of Au(III)-to-Au(0) conversion in this procedure. The use of hydroquinone addresses one of the largest limitations of the standard synthesis, in which ascorbic acid must be used in a molar

excess of about 10% compared to the gold concentration.[23] Using less than a 10% excess offers a very little NR growth while using more leads to the formation of large amounts of spherical particles, possibly due to an increased reduction rate and random nucleation events in solution. However, as hydroquinone is a significantly weaker reducing agent than ascorbic acid, it can be present in large excess which should allow for the slow, controlled growth of NRs until all gold has been consumed. We utilized ICP-OES analysis to confirm whether this was actually occurring. Specifically, gold NRs were purified by three rounds of centrifugation to remove any possible unreacted gold, dissolved with aqua regia, followed by measuring the concentration of gold using ICP-OES. There was no statistical difference comparing this value (0.496±0.010 mM) to the concentration of gold ions in the initial growth solution as also determined by ICP (0.496±0.006 mM), confirming the quantitative isolated yield of this procedure.

While tracking the growth of gold NRs is most often accomplished through UV-Vis analysis, TEM can be invaluable in understanding their growth mechanism. However, few such reports exist due to several inherent difficulties with this technique. One major problem is that NRs will generally continue to grow and change their morphology as the TEM sample is being prepared. Wei and coworkers noted that simply centrifuging the growth solution does not halt rod growth and developed a technique that used sodium sulfide to arrest the growth.[36] However, this procedure leads to a significant red shift of the LSPR, which the authors attribute to a change in the dielectric constant of the surface due to sulfide

adsorption. In addition, they cannot exclude the possibility of morphological change due to the reducing ability of sodium sulfide. More recently, Edgar and coworkers used cryo-TEM to image rods in-situ, thereby eliminating these questions by rapidly freezing the growth solution and halting the rod growth.[54] They discovered the presence of a bowtie morphology with non-rounded tips[54] as opposed to the highly pronounced dumbbell-like morphology shown by Wei et al.[36] However, cryo-TEM is particularly difficult to carry out and is not amenable to viewing large amounts of nanoparticles. Thus, we sought a different method to stop NR growth while maintaining their UV-Vis spectrum and, presumably, morphology, which can be analyzed by traditional TEM. We hypothesized that a water-soluble thiol could halt NR growth while maintaining their solubility and without affecting their morphology. We recently published a report on the synthesis of a cationic thiol, 16-mercaptohexadecyltrimethyl-ammonium bromide (MTAB), which can covalently functionalize the surface of gold NRs[55] that seemed like an excellent candidate. We have also found similar results with the C11 version of this molecule, 11-mercaptoundecyltrimethylammonium bromide (MUTAB), which is simpler to synthesize, is more water-soluble, and can

Table 2.1 Efficacy of halting AuNR growth via MUTAB addition as determined by UV-Vis spectroscopy

Time of MUTAB addition (hr)	3	4	5	6	7
Initial LSPR Wavelength (nm)	1166	1226.5	1222.5	1208	1188
LSPR after 2 days (nm)	1174	1225.5	1223	1203	1180
LSPR shift (nm)	8	-1	0.5	-5	-8

even be found from commercial sources. Addition of MUTAB to a solution of growing NRs at various points of time was indeed found to halt the growth. A comparison of the UV-Vis spectra during the growth and after the treatment with MUTAB followed by aging for two days, demonstrated a small shift in the LSPR peak position. There was a small red shift for early growth points, a small blue shift for later growth points, and a minimal change around the midpoint when the LSPR peak has reached its maximum, as seen in Table 2.1. The directions of LSPR shifts match the pattern observed when the growth continues normally. This finding indicates that there is a finite period of time after the MUTAB addition during which the growth continues before the thiol can coat the surface of gold NRs. It is possible

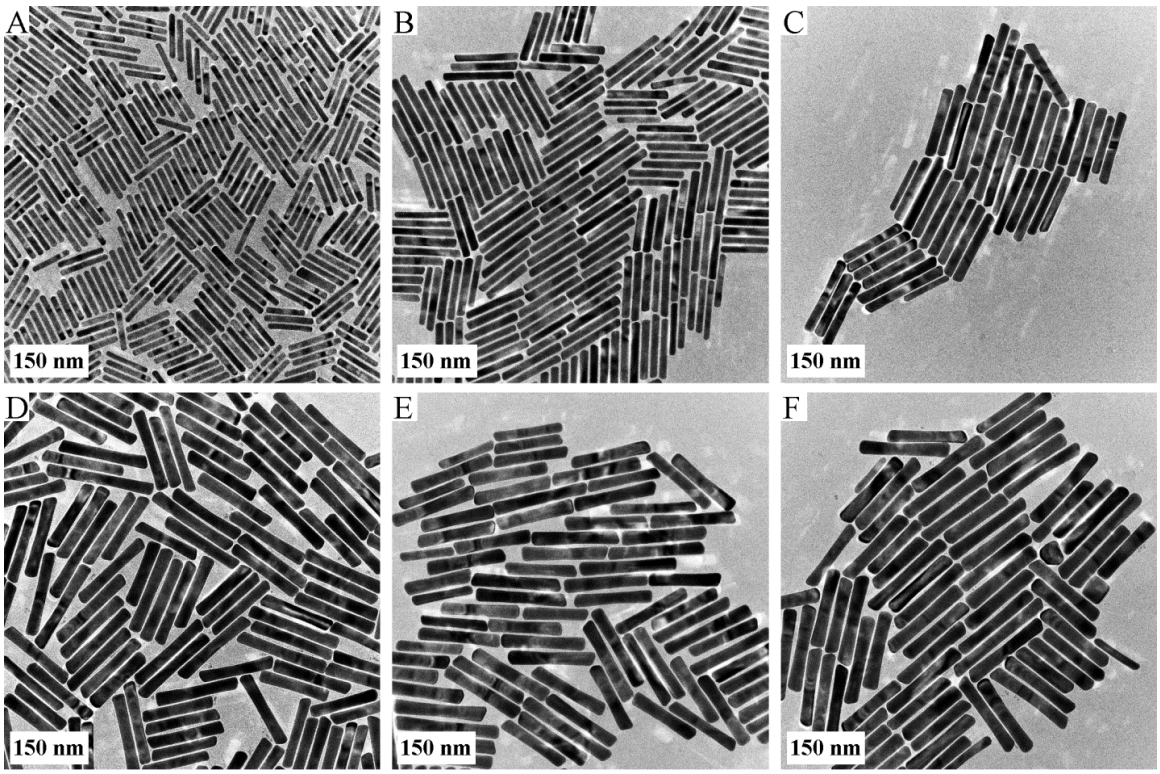

Figure 2.5. TEM images of HQ-grown gold NRs after 3 (A), 5 (B), 7 (C), 9 (D), 11 (E), and 12 (F) hours of growth obtained by halting growth with MUTAB.

that the thiol may bind to the nanorods tips faster than the sides, but the limited change in the optical properties suggests that it is an efficient method to quickly stop the growth.

In order to monitor the growth of gold NRs by TEM, aliquots were removed from the growth solution every hour, their absorbance spectra were measured, and they were incubated with MUTAB for 2 days to ensure that a maximum surface coverage had occurred. TEM images of these rods after 3, 5, 7, 9, 11 and 12 hours of growth are shown in Figure 2.5. Figure 2.6 details the change in NR dimensions extracted from the TEM images. Specifically, the change in length (Figure 2.6a), waist and tip diameter (Figure 2.6b), and total volume, estimated by assuming a cylindrical structure with diameter averaged between the waist and tips

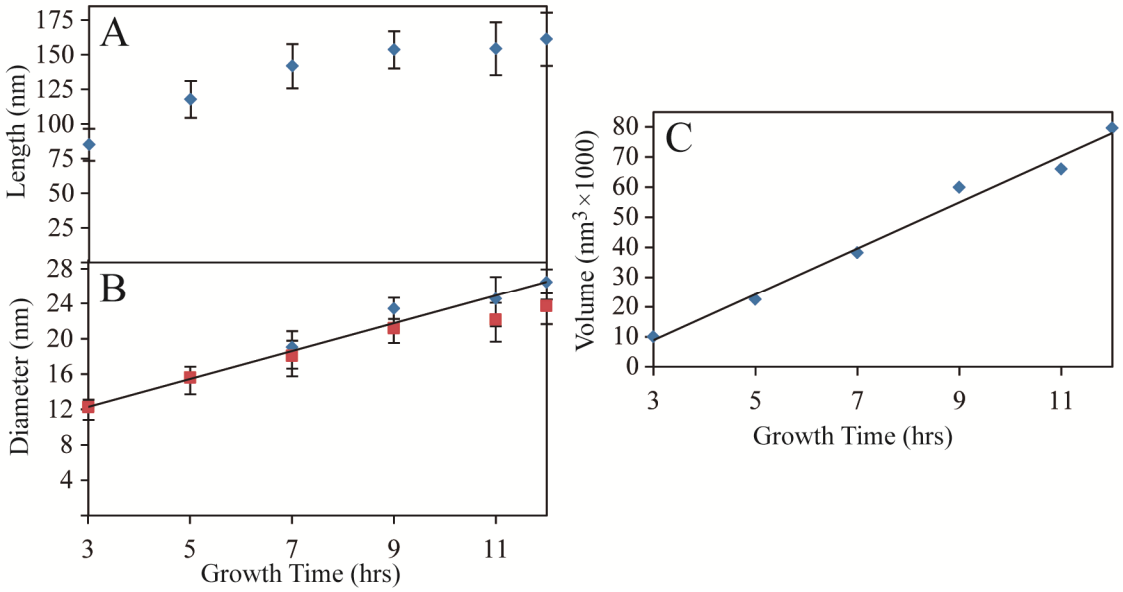

Figure 2.6. Graphs showing the increase in (a) length, (b) diameter, and (c) volume of gold NRs with time as measured from TEM images at the 3, 5, 7, 9, and 11 hour time points. Both tip (blue) and waist (red) diameters are shown in (b). Volume in (c) was estimated by assuming a cylindrical shape with diameter averaged between the waist and tips.

(Figure 2.6c) are plotted against the growth time. A summary of this information is provided in Table 2.2. After 3 hours, the NRs display the standard cylindrical morphology with the aspect ratio and LSPR peak close to the final values. However, at this point the rods have grown to only about 15% of their final size based on the estimated volume. The linear increase in volume from that point shown in Figure 2.6a demonstrates that the reduction to metallic gold occurred at a roughly constant rate, assuming that no new nucleation events are taking place in solution. This steady growth in size is in contrast to the "popcorn" model of ascorbic acid-mediated nanorods growth proposed by Edgar and coworkers.[54] This model states that rather than following the traditional assumption that all seed particles grow evenly from the start of the reaction to the end, the seed particles actually lie quiescent for variable amounts of time and then rapidly grow to their final size.[54] This model was supported by the presence of both small and nearly fully-grown gold NRs starting from the very beginning of the reaction up until nearly the end, which is clearly not evident in our procedure. reduced growth rate, most seeds that

Table 2.2. Summary of different measures of gold NR growth

Time (hrs)	LSPR peak	Length (nm)	σ_{length} (nm)	Waist Diameter (nm)	σ_{waist} (nm)	Tip Diameter (nm)	Aspect Ratio	Volume (nm^3)
3	1163	85.0	11.7	12.3	1.1	12.3	6.9	10000
5	1233	117.8	13.3	15.6	1.6	15.6	7.6	22400
7	1223	141.7	16.0	18.0	2.0	19.0	7.9	38200
9	1191	153.5	13.5	21.2	1.4	23.4	7.2	60000
11	1162	154.3	19.1	22.2	2.2	24.5	7.0	66000
12	1151	161.1	19.2	23.7	1.8	26.5	6.6	79700

The shape-evolution of hydroquinone-grown gold NRs is also unique. Edgar and coworkers outlined the growth of ascorbic acid-mediated nanorods as passing through several stages: from bowtie to conically-capped bowtie to conically-capped cylinder, and finally to hemispherically-capped cylinder.[54] Switching to hydroquinone as a reducing agent leads to a significantly different growth dynamics. The earliest morphology visible is the standard hemispherically-capped cylindrical structure. At the five hour point, the tip morphology begins to sharpen and becomes more anisotropic, similar to the conically-capped cylindrical structure, but with a point that is skewed off-center. This type of structure can be visible on either one or both tips, and tips may be skewed in either the same or opposite directions on a single rod (see Fig. 2.2a). At the seven hour point, a more pronounced bowtie structure becomes apparent, with an average waist depth, defined as the difference between the waist and tip diameters, of about 1 nm. At the nine hour point, the sharpness of the tip edges increases while the waist depth reaches 2.2 nm. The waist depth continues to increase to a maximum of 2.8 nm as growth is complete at the 12 hour time point.

Correlating these morphological changes to the optical properties of the nanorods is a significant challenge. Typically, the LSPR wavelength of rods is seen as dependent on their aspect ratio. It has been shown empirically that the LSPR peak wavelength (λ_{max}) depends linearly on the aspect ratio (AR) of the rods, for instance: $\lambda_{max} = 95AR + 420$.[4] Such an equation is best applied to normal, cylindrically-shaped NRs and deviations in rod shape, for instance, to dog-bone,

dumbbell, and bowtie structures can lead to significant shifts in the LSPR when compared to values predicted by this simple formula. It has been reported that small differences in tip structure can have a major effect on the LSPR peak,[38,56] and that its position is much more sensitive to changes in the waist diameter compared to that of the tips.[36,37] Indeed, we previously demonstrated that the formation of gold dog-bones by rapid reduction of gold onto nanorods was not accompanied by any change in the LSPR position or intensity.[57] In the case of hydroquinone-grown NRs, applying the Equation 1 using an aspect ratio based on the waist diameter does not accurately predict the actual LSPR. For instance, this approximation predicts a peak at 1050 nm for the fully-grown rods, nearly 100 nm below the experimental value of 1150 nm. Further complications include the significant change in size, the large final length of the rods at greater than 150 nm, and the changing tip morphology.

2.4. Nanorod Morphological Stability

Next, we examined the morphological stability of our NRs as a function of time. The rod structure resembles the conically-capped bowtie intermediate growth structure seen by Edgar and coworkers which they described as thermodynamically unstable.[54] Conversion of this structure to a standard cylindrical structure should lead to a blue-shift in the LSPR peak.[54] Indeed,

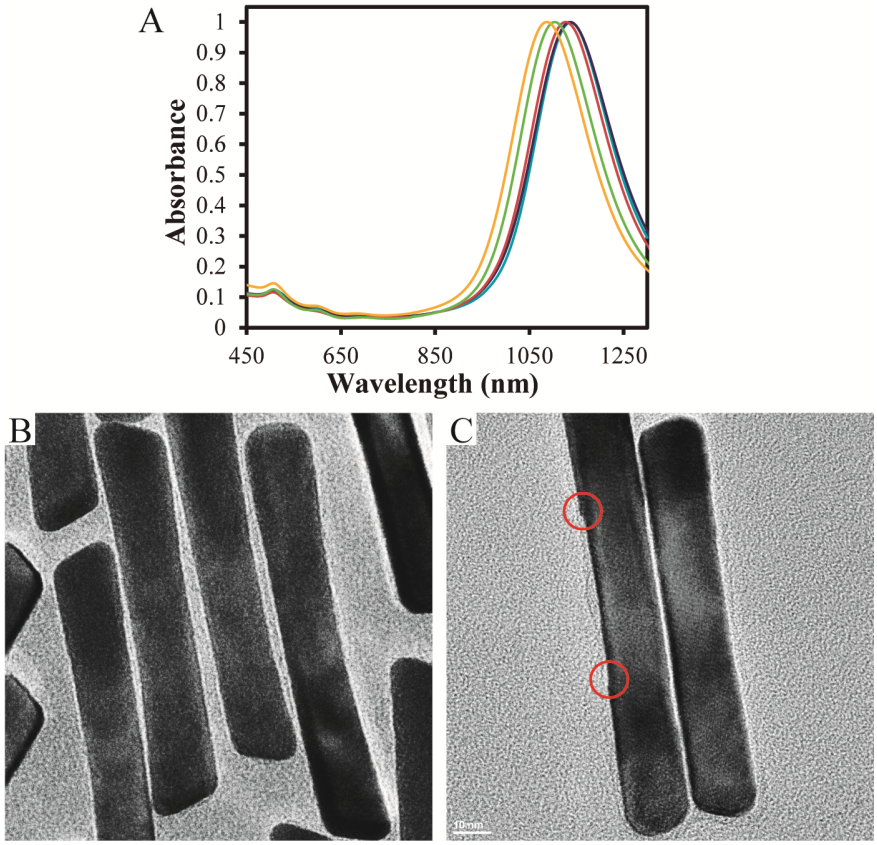

Figure 2.7. UV-Vis absorbance spectra of gold NRs aged for 2 months under different conditions are shown in (a). Spectra are shown of the original nanorods prior to aging (light blue) and nanorods aged in the growth solution (yellow), after one round of centrifugation (green), after PEG-thiol functionalization (red), and after MUTAB functionalization (dark blue). TEM images of nanorods (b) prior to aging and (c) after aging in growth solution are also shown. The presence of step-like morphological changes is highlighted in (c).

Table 2.3. Summary of the effects of aging for 2 months under different conditions in terms of the magnitude of the blue-shift in LSPR as well as change in NR aspect ratio.

Treatment	None	Centrifuged	PEG-thiol	MUTAB
Shift (nm)	50	35	15	0
Aspect Ratio	6.75	7.04	7.15	7.23

this blue-shift is apparent in the UV-Vis absorbance spectra of a batch of gold NRs aged for two months under different conditions, as shown in Figure 2.7a. Table 2.3 shows a summary of these changes. Gold NRs aged in the growth solution with a high CTAB concentration experienced the greatest blue shift in the LSPR of about 50 nm while one round of centrifugation caused the shift to decrease to 35 nm. Next, based on our experience with halting rod growth, we hypothesized that MUTAB or another thiol such as PEG-thiol could be effective at controlling this gradual shift. Indeed, addition of either thiol was clearly effective at stopping this blue shift, though to different degrees. PEG-thiol was able to reduce it to only 15 nm while MUTAB stopped the shift almost entirely. From this data, it does appear that the morphology of the rods may not be thermodynamically stable and that there is some reshaping occurring over time, although the rate of this change is not very rapid. The addition of water-soluble thiols was found to be the best way to control the changes in NR optical properties. The superiority of MUTAB compared to PEG-thiol in arresting the plasmon shift may be due to the enhanced NR surface coverage of MUTAB compared to the much bulkier PEG-thiol ligand. Indeed, we recently demonstrated that a similar cationic thiol MTAB can pack onto the NR surface with a grafting density approaching that of neutral alkanethiols on flat gold substrates[55] and expect that MUTAB would behave similarly. In order to further understand the morphological changes associated with the LSPR blue-shifting, we used TEM to directly image the NR structure. Figure 2.7 shows high magnification images of representative NRs immediately after the synthesis (b) and after aging in the growth

solution (c) in which the morphological changes are apparent. First, the sides of the rods show stepped features which may be due to the gradual elimination of the bowtie structure with time. This appears similar to the blue-shift seen by Wei and coworkers for gold NRs centrifuged during their growth.[36] Indeed, reconstruction of the side facets of gold NRs is a well-known phenomen,[58] most often seen under heating conditions.[39,59,60] There is also some reshaping of the tips, but this effect is not as pronounced as we expected. The anisotropic tip shape is still evident, but the sharpness of the tip is slightly decreased. Measurements of the NRs in the TEM images before and after the aging demonstrated a decreasing aspect ratio for samples with increasing blue shift due to a slight increase in diameter and a decrease in length, as shown in Table 2.3 (standard deviation in aspect ratio was constant at about 0.8). This suggests that the change in the aspect ratio due to conversion of NRs from bowtie to cylindrical morphology may be driving the observed gradual LSPR blue shift.

2.5. Tunability of Nanorod Synthesis

Next, we explored the tunability of the procedure by varying different parameters in the synthesis of gold NRs and measuring the effect on their optical properties, as shown in Figure 2.8. It is important to note that all spectra in Figure 2.8 have been obtained after a 10-fold dilution to bring their absorbance into spectrometer range. Figure 2.8a shows the effect of varying the concentration of hydroquinone (HQ) while keeping all other variables constant. Using less HQ leads

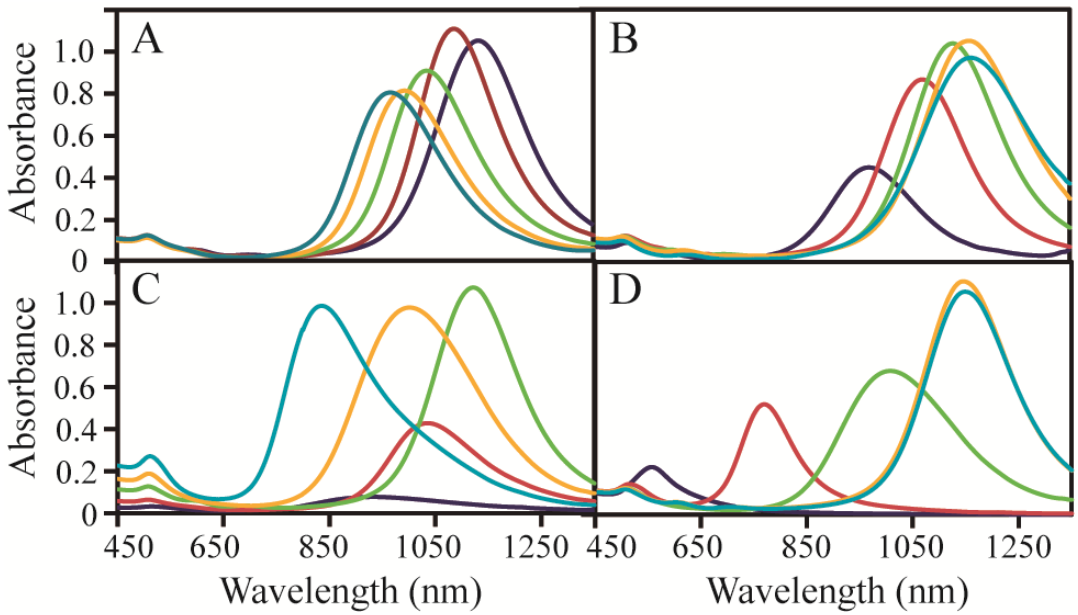

Figure 2.8. Effect on nanorod UV-Vis spectra of varying different different synthetic parameters including: (a) hydroquinone concentration at 5, 7, 9, 11, and 13 mM; (b) seed concentration at 1.9, 5.6, 10, 20, and 30 times the standard concentration; (c) gold concentration at 0.1, 0.25, 0.5, 0.75, and 1 mM; and (d) silver concentration at 0.05, 0.15, 0.25, 0.35, and 0.40 mM. Spectra are color-coded from lowest to highest concentration: dark blue, red, green, orange, and light blue.

to a higher LSPR wavelength with a generally higher LSPR intensity. Using 5 mM HQ, or 10-fold excess with respect to gold chloride concentration gave the most red-shifted LSPR at about 1130 nm while the largest concentration tested, 13 mM, gave an LSPR at about 970 nm. In addition, two small peaks at about 600 nm and 700 nm become more pronounced towards the higher concentration of HQ, possibly corresponding to slightly increased amounts of cubic and pyramidal morphologies. The amount of reducing agent also has a large effect on the total NR growth time; while at 5 mM HQ the growth usually takes around 12 hours, at double the HQ concentration the growth is complete within 3-4 hours. This data supports the idea

that a slower growth rate leads directly to higher aspect ratio NRs. Below 5 mM HQ, we observed incomplete growth and with HQ at the standard reducing agent level (0.55 mM), no growth is visible at all. The use of the reducing agent in large excess provides significant benefits to the procedure compared to the standard seed-mediated synthesis[19] in which ascorbic acid (AA) can only be present in approximately 10% molar excess. First, as described earlier, the total yield of rods is nearly quantitative. Second, controlling the reducing agent concentration is now a viable strategy for tuning NR optical properties. This is in stark contrast to ascorbic acid, given the narrow concentration range in which it must be used in order to synthesize high quality rods. Finally, the ease and reproducibility of the synthesis is significantly increased. In the standard synthesis, the effect of small variations in the amount of AA or gold chloride can lead to drastically different results or even complete failure of the synthesis. On the other hand, the use of HQ in 10 times molar excess means that minor variations in concentration do not have a critical effect on the growth of nanorods. We have found that the procedure is very reliable and simple to carry out.

One area that contributes to variability in NR synthesis is the preparation of seed particles. Figure 2.8b shows the effect of varying the amount of seed solution, expressed as its multiples used in the standard synthesis. As the amount of seed is increased 10-fold with respect to the standard protocol,[19] the LSPR peak undergoes a 60 nm red shift from 970 nm to 1130 nm and more than doubles in intensity. Further doubling of the seed amount redshifts the LSPR peak by 30 nm and its

tripling leads to only another 10 nm shift. Thus, increasing the seed concentration leads to a consistent, although nonlinear, red shift of the LSPR peak, which offers an additional way to control NR optical properties. One possible explanation for this effect is that the increased seed concentration and thus increased number of NRs in solution causes the supply of Au(III) ions to be exhausted quicker, allowing less time for the LSPR blue-shift which occurs towards the end of NR growth, as shown in Figure 2.4.

Next the effect of Au(I) ions concentration in the growth solution was measured by varying it from 0.1 mM to 1.0 mM and measuring the UV-Vis spectra of the resulting NR solution, shown in Figure 2.8c. In this case, the amount of HQ was scaled along with the gold concentration to remove the effect of the Au(I)-to-HQ ratio on the reaction. Nikoobakht et al. showed that a maximum LSPR peak position was reached at an intermediate gold concentration, 1 mM, and dropped off at concentrations above and below that value.[19] Our method displays a similar trend, although the LSPR maximum appears at 0.5 mM and the sensitivity of LSPR position to the gold concentration appears to be much greater. This suggests that the gold concentration is already near its ideal concentration for obtaining the highest possible value of LSPR peak. At higher gold concentrations, it is likely that the increased NR growth rate leads to less selectivity for anisotropic growth and thus a lower aspect ratio. At lower gold concentrations, NR growth is halted before they reach their maximum length.

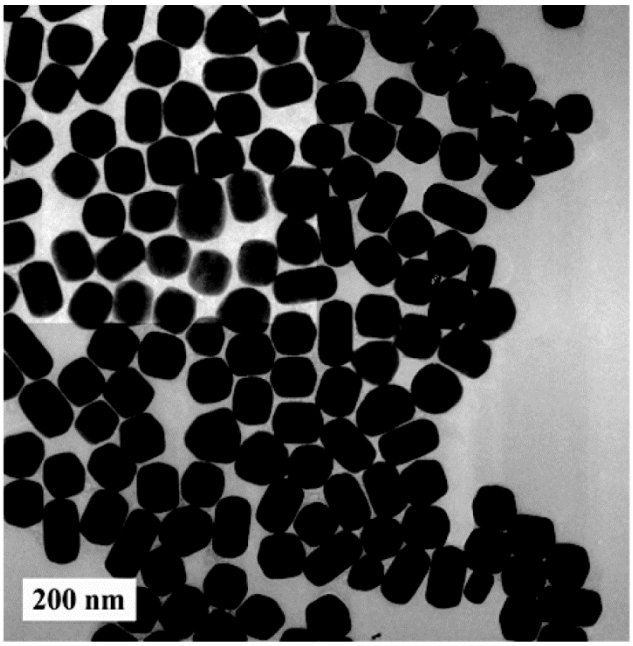

Figure 2.9. TEM image of short nanorods and octahedrons produced from the synthesis with 0.05 mM silver nitrate.

Finally, we studied the effect of silver nitrate concentration on gold NRs growth, as shown in Figure 2.8d. Similar to the AA-mediated synthesis, the presence of silver is necessary for the rod formation. At the lowest silver nitrate concentration (0.05 mM) particles with a plasmon resonance peak at 560 nm are formed. TEM demonstrates that these particles are actually very low aspect ratio NRs and octahedrons rather than spheres, as seen in Figure 2.9. Increasing the silver concentration to 0.15 mM leads to the formation of gold NRs with LSPR peak at 770 nm, and further increase continues to *red-shift* the LSPR until it hits a maximum of about 1150 nm at 0.35 mM silver nitrate. Little change in the peak position is evident when the silver concentration reaches 0.40 mM, the maximum concentration above which silver begins to precipitate from solution. The effect of silver in this HQ-mediated growth is distinctly different from that in the standard

AA-mediated synthesis. In the latter case, the maximum LSPR peak of about 850 nm is achieved at 0.12 mM silver,[19] which is about 3 times lower than in our synthesis. Most importantly, higher silver concentration in the standard procedure leads to a *blue shift* of the LSPR as well as a large decrease in rod quality. However, by using hydroquinone, it is possible to extend the range of silver concentrations which can be used up to the saturation point. One model of growth provided by Edgar and coworkers states that the final NR aspect ratio is determined by the ratio S of the surface energy of the sides to the surface energy of the caps determined by solution conditions such as silver and surfactant concentration.[54] They predicted that the value of S varies between 0.65 and 0.35 in standard growth solutions, corresponding to final nanorods aspect ratios between 2 and 5, respectively.[54] In this new technique, the ability to use higher concentrations of silver nitrate may extend the accessible values of S, thus increasing access to higher aspect ratio morphologies. This ability may be related to the higher seed concentration in solution as well as the increased total gold conversion, both of which lead to a much higher gold nanoparticle surface area exposed to solution with which a higher concentration of silver could interact.

Overall, a great deal of control over gold NRs optical properties can be achieved by varying the hydroquinone, seed, gold, and silver concentrations in the growth solution. Through this technique, nanorods with LSPR peaks ranging from 770 to 1160 nm were synthesized. Furthermore, the slow growth of the rods during this procedure means that it is possible to track and freeze the growth at any

particular point, as was done for the TEM analysis of gold NRs. Nanorods with LSPR up to 1230 nm are attainable through this procedure. On the other hand, the gradual shift in LSPR originating from the morphological changes in the rods is undesirable, especially if the preparation of gold NRs with an exact LSPR value is required. As noted earlier, the addition of MUTAB is the most reliable way to stop this drift while PEG-thiol can slow it down significantly.

2.6. Conclusions

We have demonstrated a highly versatile and efficient synthesis of gold nanorods by utilizing hydroquinone as a reducing agent. This new method produces high aspect ratio gold NRs with a unique bowtie structure containing anisotropic tips with a longitudinal surface plasmon resonance of higher than 1200 nm. The rods are synthesized in a pure state without any appreciable amount of other shapes, while offering a nearly quantitative yield of gold ions conversion. This could become especially important considering that the ever-increasing price of gold presents a significant challenge to real-world applications of gold NRs. The use of hydroquinone instead of ascorbic acid also lessens the sensitivity of nanorod synthesis to reagents concentration thereby increasing the reliability of this technique. In addition, we have shown that it is possible to fine-tune nanorod optical properties by varying synthetic parameters including the concentration of hydroquinone, seed particles, gold ions, and silver nitrate.

2.7. Experimental Methods

2.7.1. Materials and Characterization

Silver nitrate (99%), S-(11-Bromoundecyl) thioacetate (95%), and sodium borohydride (≥96%) were purchased from Sigma-Aldrich. Hydrogen tetrachloroaurate trihydrate (ACS reagent) and CTAB (99%) were purchased from Acros Organics. Hydroquinone (99%) and thiolated polyethylene glycol (MW=2000 g/mol) were received from Alfa Aesar and Nanocs, respectively. All chemicals were used without further purification and all solutions, other than those of gold and CTAB, were prepared fresh daily. Scanning electron microscopy (SEM) was performed on an FEI Quanta 400 instrument. Transmission electron microscope (TEM) images were collected on a JEOL 2010, while high-resolution TEM images were collected on a JEM 2100F instrument. UV-vis-NIR absorbance (UV-Vis) spectra were obtained on a Cary 3000 UV–vis-NIR spectrophotometer. ICP-OES analysis was performed on a PerkinElmer Optima 4300 DV.

2.7.2. Nanorod Synthesis

Gold seed was prepared as described elsewhere[19] with minor modification. A solution of 0.01M sodium borohydride dissolved in 0.01M sodium hydroxide was freshly prepared. To an $HAuCl_4$ solution (10 mL, 0.5 mM) in 0.1M CTAB was added 460 μL of the sodium borohydride aqueous solution under rapid stirring, leading to a change in color from greenish to light brown. Next, silver nitrate (70 μL, 0.1 M)

solution was added to an $HAuCl_4$ solution (10 mL, 0.5 mM) in 0.1M CTAB, followed by addition of hydroquinone aqueous solution (500 μL, 0.1 M) and hand-stirred until the resulting mixture became clear. Next, 160 μL of seed solution was added, mixed thoroughly, and the growth solution was allowed to age overnight.

2.7.3. UV-Vis and TEM Analysis

A 20 mL batch of gold NRs solution was synthesized and samples were taken simultaneously for UV-Vis and TEM analysis every hour. Samples for TEM were prepared by withdrawing 1 mL of growth solution, adding 11-mercaptoundecyltrimethyl-ammonium bromide (MUTAB – see Supporting Information for detailed synthetic procedure) solution (500 μL, 92 mM), and diluting up to 3 mL total volume with DI water. After incubating for two days, gold NRs were purified by centrifugation at 13,000 rpm, re-dispersed in water and cast onto TEM grids. After the 4 hour mark, 0.1 mL of the growth solution was diluted to 1 mL to bring their absorbance into UV-Vis spectrometer range.

2.7.4. Synthesis of MUTAB

Synthesis of 11-bromo-1-undecanethiol. To a stirred solution of S-(11-Bromoundecyl) thioacetate (1g, 3.23 mmol) in 20 mL of methanol, 8 mL of acetyl chloride was added drop-wise and the reaction mixture was kept at 50 °C for 4 hours. After the reaction was complete, 200 mL of methylene chloride was added to the reaction mixture and excess acetyl chloride and HCl were removed by multiple extractions with DI water. The mixture was dried over sodium sulfate. Methylene

chloride was evaporated under reduced pressure to obtain 650 mg of 3 as colorless oil (75 % isolated yield). ^{1}H NMR ($CDCl_3$, 400 MHz): δ 1.3 (15H, m), 1.6 (m, 2H), 1.85 (m, 2H), 2.5 (q, 2H), 3.4 (t, 2H).

Synthesis of MUTAB. 1-bromoundecanethiol (600 mg, 2.25 mmol) was dissolved in 3 mL ethyl acetate and placed under argon with magnetic stirring. To this, 3 mL of the ethanolic trimethylamine solution (~13 mmol) was added and the reaction mixture was stirred for 4 days, after which time a white precipitate had formed. The solid was isolated by centrifugation and purified several times by addition of hexane followed by centrifugation and was dried under vacuum to yield 587 mg of a white solid (1.8 mmol, 80%). ^{1}H NMR ($CDCl_3$, 400 MHz): δ 1.3 (m, 15H), 1.6 (p, 2H), 1.75 (m, 2H), 2.5 (q, 2H), 3.4 (s, 9H), 3.6 (m, 2H).

2.8. References

(1) Huang, X.; Jain, P. K.; El-Sayed, I. H.; El-Sayed, M. A. *Laser Med.Sci.* **2008**, 23, 217–228.

(2) Hu, M.; Chen, J.; Li, Z.-Y.; Au, L.; Hartland, G. V; Li, X.; Marquez, M.; Xia, Y. *Chem. Soc. Rev.* **2006**, 35, 1084–1094.

(3) Kennedy, L. C.; Bickford, L. R.; Lewinski, N. A.; Coughlin, A. J.; Hu, Y.; Day, E. S.; West, J. L.; Drezek, R. A. *Small* **2011**, 7, 169–183.

(4) Huang, X.; Neretina, S.; El-Sayed, M. A. *Adv. Mater.* **2009**, 21, 4880–4910.

(5) Alkilany, A. M.; Thompson, L. B.; Boulos, S. P.; Sisco, P. N.; Murphy, C. J. *Adv. Drug Deliv. Rev.* **2012**, 64, 190–199.

(6) Vigderman, L.; Khanal, B. P.; Zubarev, E. R. *Adv. Mater.* **2012**, 24, 4811–4841.

(7) Kneipp, J.; Kneipp, H.; Kneipp, K. *Chem. Soc. Rev.* **2008**, 37, 1052–1060.

(8) Tian, Z. Q.; Ren, B.; Wu, D. Y. *J. Phys. Chem. B* **2002**, 106, 9463–9483.

(9) Qian, X.-M. M.; Nie, S. M. *Chem. Soc. Rev.* **2008**, 37, 912–920.

(10) Homola, J.; Yee, S.; Gauglitz, G. *Sensor. Actuat. B Chem.* **1999**, 54, 3–15.

(11) Lee, J.; Mubeen, S.; Ji, X.; Stucky, G. D.; Moskovits, M. *Nano letters* **2012**, 12, 5014–5019.

(12) Knight, M. W.; Sobhani, H.; Nordlander, P.; Halas, N. J. *Science* **2011**, 332, 702–4.

(13) Warren, S. C.; Walker, D. a; Grzybowski, B. a *Langmuir* **2012**, 28, 9093–9102.

(14) Daniel, M.-C.; Astruc, D. *Chem. Rev.* **2004**, 104, 293–346.

(15) Murphy, C. J.; Sau, T. K.; Gole, A. M.; Orendorff, C. J.; Gao, J.; Gou, L.; Hunyadi, S. E.; Li, T. *J. Phys. Chem. B* **2005**, 109, 13857–13870.

(16) Jain, P. K.; Huang, X.; El-Sayed, I. H.; El-Sayed, M. A. *Acc. Chem. Res.* **2008**, 41, 1578–1586.

(17) Jana, N. R.; Gearheart, L.; Murphy, C. J. *J. Phys. Chem. B* **2001**, 105, 4065–4067.

(18) Sau, T. K.; Murphy, C. J. *Langmuir* **2004**, 20, 6414–6420.

(19) Nikoobakht, B.; El-Sayed, M. A. *Chem. Mater.* **2003**, 15, 1957–1962.

(20) Kou, X.; Zhang, S.; Tsung, C.-K.; Yeung, M. H.; Shi, Q.; Stucky, G. D.; Sun, L.; Wang, J.; Yan, C. *J. Phys. Chem. B* **2006**, 110, 16377–16383.

(21) Kuwahara, Y.; Yoshimori, K.; Tomita, K.; Sakai, M.; Sawada, T.; Niidome, Y.; Yamada, S.; Shosenji, H. *Chem. Lett.* **2007**, 36, 1230–1231.

(22) Guerrero-Martínez, A.; Pérez-Juste, J.; Carbó-Argibay, E.; Tardajos, G.; Liz-Marzán, L. M. *Angew. Chem. E. Int. Ed.* **2009**, 48, 9484–9488.

(23) Orendorff, C. J.; Murphy, C. J. *J. Phys. Chem. B* **2006**, 110, 3990–3994.

(24) Bullen, C.; Latter, M. J.; D'Alonzo, N. J.; Willis, G. J.; Raston, C. L. *Chem. Commun.* **2011**, 47, 4123–4125.

(25) Kim, F.; Song, J. H.; Yang, P. *J. Am. Chem. Soc.* **2002**, 124, 14316–14317.

(26) Nishioka, K.; Niidome, Y.; Yamada, S. *Langmuir* **2007**, 23, 10353–10356.

(27) Niidome, Y.; Nishioka, K.; Kawasaki, H.; Yamada, S. *Chem. Commun.* **2003**, 18, 2376–2377.

(28) Abidi, W.; Selvakannan, P. R.; Guillet, Y.; Lampre, I.; Beaunier, P.; Pansu, B.; Palpant, B.; Remita, H. *J. Phys. Chem. C* **2010**, 114, 14794–14803.

(29) Link, S.; Mohamed, M. B.; El-Sayed, M. A. *J. Phys. Chem. B* **1999**, 103, 3073–3077.

(30) Tsutsui, Y.; Hayakawa, T.; Kawamura, G.; Nogami, M. *Nanotechnology* **2011**, 22, 275203.

(31) Wu, H.-Y. H. Y.; Huang, W. L. W.-L.; Huang, M. H. M. H. *Cryst. Growth Des.* **2007**, 7, 831–835.

(32) Busbee, B. D. D.; Obare, S. O. O.; Murphy, C. J. J. *Adv. Mater.* **2003**, 15, 414–416.

(33) Khanal, B. P.; Zubarev, E. R. *J. Am. Chem. Soc.* **2008**, 130, 12634–12635.

(34) Zhu, J.; Yong, K.-T.; Roy, I.; Hu, R.; Ding, H.; Zhao, L.; Swihart, M. T.; He, G. S.; Cui, Y.; Prasad, P. N. *Nanotechnology* **2010**, 21, 285106.

(35) Ye, X.; Jin, L.; Caglayan, H.; Chen, J.; Xing, G.; Zheng, C.; Doan-Nguyen, V.; Kang, Y.; Engheta, N.; Kagan, C. R.; Murray, C. B. *ACS Nano* **2012**, 6, 2804–2817.

(36) Zweifel, D. A.; Wei, A. *Chem. Mater.* **2005**, 17, 4256–4261.

(37) Xu, X.; Cortie, M. B. B. *Adv. Funct. Mater.* **2006**, 16, 2170–2176.

(38) Grzelczak, M.; Sánchez-Iglesias, A.; Rodríguez-González, B.; Alvarez-Puebla, R.; Pérez-Juste, J.; Liz-Marzán, L. M. *Adv. Funct. Mater.* **2008**, 18, 3780–3786.

(39) Ng, K. C.; Cheng, W. *Nanotechnology* **2012**, 23, 105602.

(40) Jana, N. R.; Gearheart, L.; Obare, S. O.; Murphy, C. J. *Langmuir* **2002**, 18, 922–927.

(41) Zou, R.; Guo, X.; Yang, J.; Li, D.; Peng, F.; Zhang, L.; Wang, H.; Yu, H. *CrystEngComm* **2009**, 11, 2797–2803.

(42) Kou, X.; Zhang, S.; Yang, Z.; Tsung, C.-K.; Stucky, G. D.; Sun, L.; Wang, J.; Yan, C. *J. Am. Chem. Soc.* **2007**, 129, 6402–6404.

(43) Ni, W.; Kou, X.; Yang, Z.; Wang, J. *ACS Nano* **2008**, 2, 677–686.

(44) Xiang, Y.; Wu, X.; Liu, D.; Feng, L.; Zhang, K.; Chu, W.; Zhou, W.; Xie, S. *J. Phys. Chem. C* **2008**, 112, 3203–3208.

(45) Sohn, K.; Kim, F.; Pradel, K. C.; Wu, J.; Peng, Y.; Zhou, F.; Huang, J. *ACS Nano* **2009**, 3, 2191–2198.

(46) Park, K.; Vaia, R. A. *Adv. Mater.* **2008**, 20, 3882–3886.

(47) Okuno, Y.; Nishioka, K.; Kiya, A.; Nakashima, N.; Ishibashi, A.; Niidome, Y. *Nanoscale* **2010**, 2, 1489–1493.

(48) Sánchez-Iglesias, A.; Carbó-Argibay, E.; Glaria, A.; Rodríguez-González, B.; Pérez-Juste, J.; Pastoriza-Santos, I.; Liz-Marzán, L. M. *Chem. Eur. J.* **2010**, 16, 5558–5563.

(49) Rodríguez-González, B.; Attouchi, F.; Cardinal, M. F.; Myroshnychenko, V.; Stéphan, O.; García de Abajo, F. J.; Liz-Marzán, L. M.; Kociak, M. *Langmuir* **2012**, 28, 9063–9070.

(50) Pérez, M. A.; Moiraghi, R.; Coronado, E. A.; Macagno, V. A. *Cryst. Growth Des.* **2008**, 8, 1377–1383.

(51) Gentry, S. T.; Fredericks, S. J.; Krchnavek, R. *Langmuir* **2009**, 25, 2613–2621.

(52) Mechler, A.; Torriero, A. A. J.; Nafady, A.; Lee, C.-Y.; Bond, A. M.; O'Mullane, A. P.; Bhargava, S. K. *Colloids Surf. A* **2010**, 370, 35–41.

(53) Li, J.; Wu, J.; Zhang, X.; Liu, Y.; Zhou, D.; Sun, H.; Zhang, H.; Yang, B. *J. Phys. Chem. C* **2011**, 115, 3630–3637.

(54) Edgar, J. A.; McDonagh, A. M.; Cortie, M. B. *ACS Nano* **2012**, 6, 1116–1125.

(55) Vigderman, L.; Manna, P.; Zubarev, E. R. *Angew. Chem. E. Int. Ed.* **2012**, 51, 636–641.

(56) Prescott, S. W.; Mulvaney, P. *J. Appl. Phys.* **2006**, 99, 123504.

(57) Khanal, B. P.; Zubarev, E. R. *Angew. Chem. E. Int. Ed.* **2009**, 48, 6888–6891.

(58) Wang, Z.; Gao, R.; Nikoobakht, B.; El-Sayed, M. A. *J. Phys. Chem. B* **2000**, 104, 5417–5420.

(59) Petrova, H.; Perez Juste, J.; Pastoriza-Santos, I.; Hartland, G. V; Liz-Marzán, L. M.; Mulvaney, P. *Phys. Chem. Chem. Phys.* **2006**, 8, 814–821.

(60) Mohamed, M. B.; Ismail, K. Z.; Link, S.; El-Sayed, M. A. *J. Phys. Chem. B* **1998**, 102, 9370–9374.

Chapter 3

Nanorod Overgrowth: Synthesis of Smooth and Branched Nanostructures

3.1. Introduction

3.1.1. Nanorods as Seeds

In Chapter 2, we have discussed the synthesis of smooth gold NRs through a seed-mediated procedure based on gold reduction onto preformed gold nanoparticles with size under 3 nm. We noted that the synthesis of the seed is a crucial step for producing NRs with high shape-yield but highly reproducible seed synthesis can be quite difficult. In fact, it is not yet clear what causes the induction of anisotropic growth from an isotropic seed. Furthermore, although using this seed can be highly effective for NR growth, it is limited in producing other, more complex morphologies with high purity. Thus, it would be highly beneficial if a new type of

seed nanoparticle can be used to access a wider degree of nanoparticle morphologies. It is important to note that the ability to conduct controlled overgrowth of gold nanoparticles in CTAB solution is a significant advantage that is not generally true for other methods of Au NP synthesis. For instance, it is not possible with the thiol-capped NP created by the Brust procedure and quite difficult for citrate-capped NPs (see Chapter 1.1). This can be explained by the ability of CTAB to stabilize the Au(I) intermediate which is then catalytically reduced exclusively at the gold nanoparticle surface, most likely through a disproportionation reaction.[1] This suggests that an Au(I)-CTAB solution, produced by reduction of Au(III) with a weak reducing agent such as ascorbic acid or hydroquinone, can provide a flexible solution to design different nanoparticle architectures by the controlled deposition of gold onto various seed types.

Our experience with the high-yield synthesis of gold NRs of both the single-crystalline and pentahedrally-twinned varieties suggested that they could serve as excellent seeds for further gold overgrowth. Single-crystalline rods have a high shape-yield and relatively low degree of polydispersity which should be a good basis for further growth. Indeed, overgrowth of these NRs under various conditions has been reported to produce a variety of morphologies including dog-bone, dumbbell, octahedral or simply reduced aspect-ratio rods.[2–5] Along these lines, we conducted the overgrowth of gold NR seeds under acidic conditions to synthesize octahedral nanoparticles with very high shape-yield, as shown in Figure 3.1. However, as useful as this technique can be, any further growth can function only to decrease the

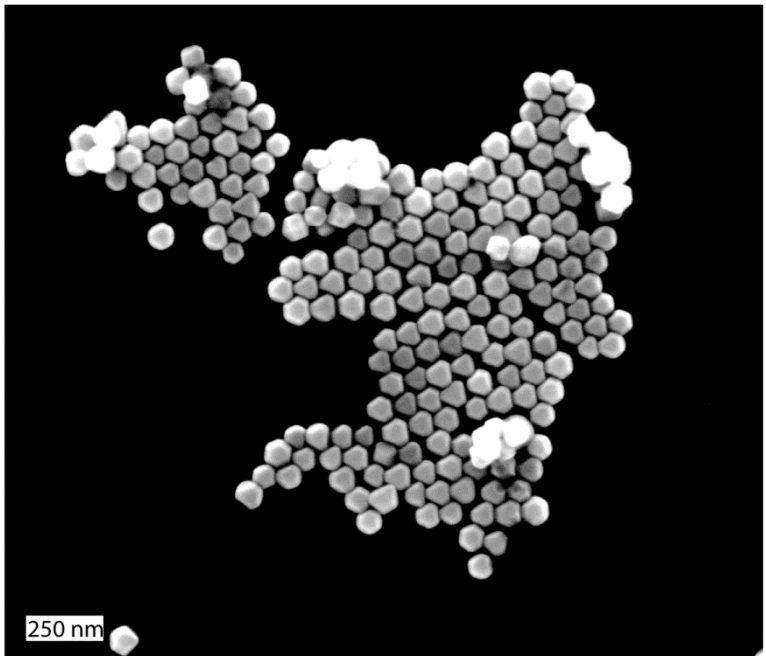

Figure 3.1. SEM image of gold truncated octahedron made from overgrowth of single-crystalline NRs.

NP aspect ratio, eventually leading to zero dimensional structures. There are no reports of growth leading to higher aspect-ratio structures using single-crystalline gold NRs as a seed. For this reason, we switched from the single-crystalline to pentahedrally-twinned NRs (PNRs) as seeds for the further growth of larger anisotropic structures such as gold nanowires and mesorods. In fact, the synthesis of pentahedrally-twinned gold nanowires has been demonstrated, but it is limited by the large amount of impurities which are produced due to its dependence on the traditional three-step NR synthesis (see Chapter 1.4.2).[6] Previous work in our group by Bishnu Khanal described the basis of using PNRs as the seed for further

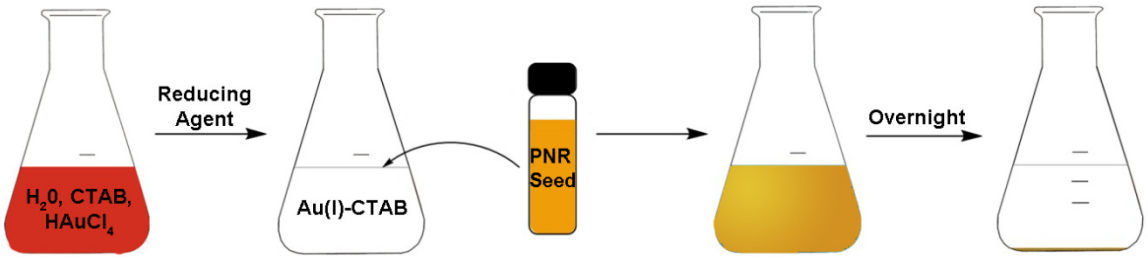

Figure 3.2. General synthetic scheme for growth of anisotropic particles via PNR seed addition to and Au(I)-CTAB growth solution. Growth continues for several hours and the product is isolated after sedimentation.

anisotropic growth as shown schematically in Figure 3.2. Addition of a Au(I)-CTAB growth solution, produced by ascorbic acid reduction of gold, to a PNR solution leads to the growth of gold mesorod structures. By reducing the pH of the growth solution to 1, tip growth becomes much more favored compared to side growth, leading to the formation of gold nanowires with length above 10 μm.

3.1.2. Branched Gold Nanoparticles

Branched gold nanoparticles have received a great amount of interest for their unusual optical and plasmonic properties.[7–10] Specifically, the unique shape of these gold nanoparticles, otherwise known as star-shaped nanoparticles or nanostars, leads to strong absorptions in the near-IR regime[7,11] and to extremely high electric field intensities at their tips, which, in turn, can result in very high activity in surface-enhanced Raman spectroscopy (SERS),[12–16] to the point where zeptomol analyte detection is possible.[17] Sensitive SERS detection shows great promise as an analytical platform, especially in biological systems.[18–22] A number of techniques can be used to synthesize nanostars in aqueous solutions with a variety

of surface capping agents and gold reducing agents using both seed-mediated[8,11,15,23–26] as well as one-pot syntheses.[27–29]

Although there have been many reported methods of nanostar syntheses, almost all of them form zero-dimensional structures which have a spherical core with different numbers of branches coming from the center. As described previously, one-dimensional, anisotropic gold nanoparticles such as gold NRs and gold nanowires have received a great deal of attention for their possible electronic,[33–35] catalytic,[36] and biomedical applications.[12,37–40] Combining these properties with the unique capabilities of star-shaped particles could be beneficial, but almost no examples of one-dimensional structures with a star-shape cross-section have been reported. Most recently, Wu and coworkers reported the synthesis of penta-branched gold nanoparticles from pentagonally-twinned bipyramids.[25] However, the synthesis of more extended one-dimensional star-shaped particles such as NRs or nanowires has not been demonstrated.

This chapter will describe a new methodology to synthesize smooth gold nanowires (NW) as well as NRs, mesorods (MRs), and NWs with a well-defined pentagonal star cross-section. This is achieved by applying the silver-mediated overgrowth conditions reported earlier[25] but changing the seed particles from spheres to PNRs and nanowires. The enhanced SERS activity of the starfruit structure will also be discussed.

3.2. Synthesis of Gold Mesorods

The synthesis of highly pure PNRs was described in detail by our group[41] and is detailed in Chapter 1.4.2.3. This procedure involves a dissolution-based purification procedure that removes nearly all morphological impurities from a non-silver assisted gold NR synthesis. Figure 3.3 shows TEM of the purified NRs and

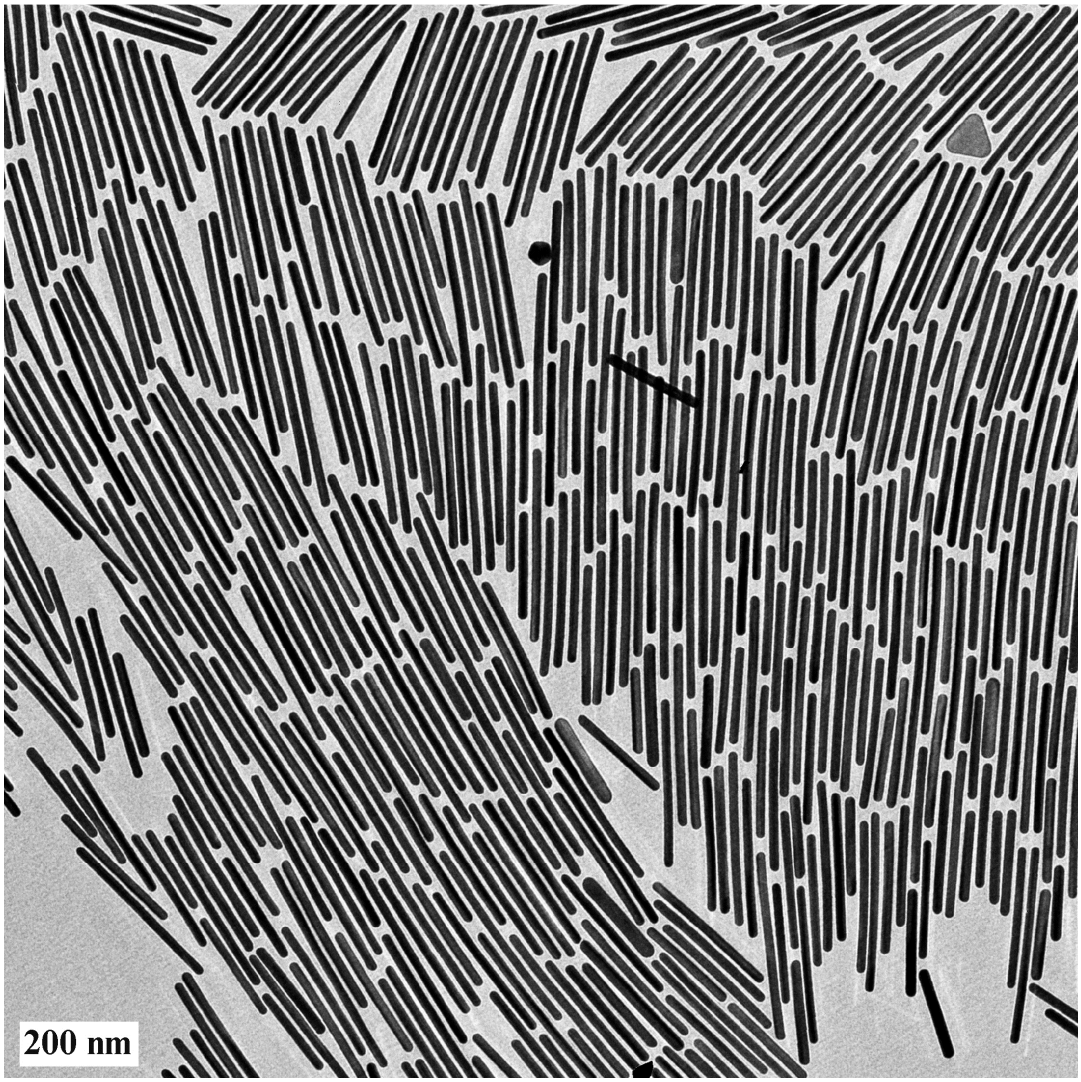

Figure 3.3. TEM image of pentahedrally-twinned gold NRs (PNRs) used as seed particles.

demonstrates the extremely high purity of these nanoparticles which makes them highly desirable for use as *one-dimensional seed particles* in a further overgrowth step.[5,42–45] They have a length and width of about 300 nm and 20 nm, respectively, corresponding to an aspect ratio of 15 and contain the pentahedrally-twinned structure which should make them amenable to further anisotropic overgrowth. The main impurity which is usually present is faceted platelets, as can be seen in Figure 3.3. In practice, complete removal of these platelets may take multiple rounds of dissolution/precipitation such that having a small degree of platelet impurity may be acceptable, although further growth will lead to the presence of larger platelets along with the desired product. Introduction of PNR seeds into an Au(I)-CTAB-AA growth solution without acid addition leads to the formation of gold MRs of length up to 1-1.2 μm and diameter up to 300 nm. As expected, these MRs can be produced in high purity, but as seen in the SEM image in Figure 3.4a, the

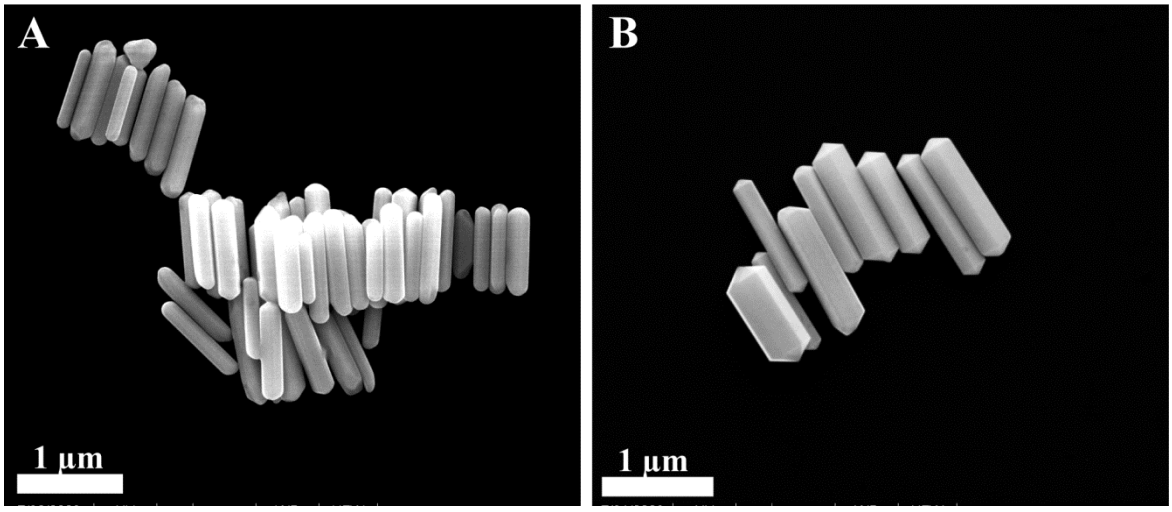

Figure 3.4. SEM images of gold MRs produced through the overgrowth of PNRs (a) and MRs which have been further overgrown to enhance their morphology (b).

larger sized rods have rather non-uniform tips and sides that appear more round than could be expected from a crystalline object at this scale. We hypothesized that it could be possible to refine this morphology further by submitting them to a further growth step under the standard growth conditions. Indeed, this procedure produced larger MRs with significantly enhanced facets and sharp, prismatic tips, as shown in Figure 3.4b. Although several of the MRs appear to have a "perfect" crystalline morphology, there is a concomitant increase in their size polydispersity, which is similar to previous results obtained in our lab for the growth of MRs with length greater than 1 μm or higher. This result demonstrates the power of the CTAB-mediated growth procedure which can be conducted any number of times as long as the surface of the particle remains CTAB-capped. This allowed for the separate synthesis and purification of the PNR seed, followed by MR growth, and finally overgrowth to fine-tune the particle morphology.

3.3. Synthesis of Gold Nanowires

The previous growth of gold MRs was conducted using the standard growth conditions developed in our lab, i.e. Au(I) in CTAB produced by reduction with ascorbic acid. However, Chapter 2 demonstrated that changing the reducing agent to hydroquinone (HQ) can have a large effect on gold nanoparticle synthesis. Specifically, it was found that HQ functioned as a weaker reducing agent than ascorbic acid and produced a higher yield as well as higher-aspect ratio NRs. We speculated that using a HQ-based growth solution in the overgrowth of PNRs could

lead to interesting results. However, switching to HQ in the previously-developed NW synthesis led to the absence of any growth, even when HQ was used in 40 times molar excess quantities or higher as compared to the gold concentration. This is not surprising, though, since the original NW procedure utilizes low pH to reduce the growth rate such that one-dimensional growth was favored; carrying out the reaction without acid addition leads only to the formation of the MR morphology described earlier. HQ reduction is also pH dependent and since it is a significantly weaker reducing agent than AA, it is not surprising that low pH conditions lead to complete halting of growth. Thus, it was clear that the acid addition step would have to be removed.

Interestingly, growth of PNRs under high HQ concentration without the addition of acid led not to MRs but to NWs, as seen in Figure 3.5a. The higher-magnification SEM images of these wires seen in Figure 3.5b show a morphology which is significantly different from that previously seen in our lab under similar conditions (same PNR seed and gold concentration). Those wires were 8 – 10 μm in length and 45 – 50 nm in diameter and had a more rounded tip and side morphology. The HQ wires, on the other hand, have a slightly smaller length of 6 – 8 μm along with a much larger diameter of 140 nm and have a significantly more faceted morphology. It is important to note that, although NW width tends to be quite monodisperse, their length polydispersity is typically quite high, making accurate size determination difficult. Still, based on these dimensions, it appears that more than 5 times as much gold was converted using this excess amount of HQ

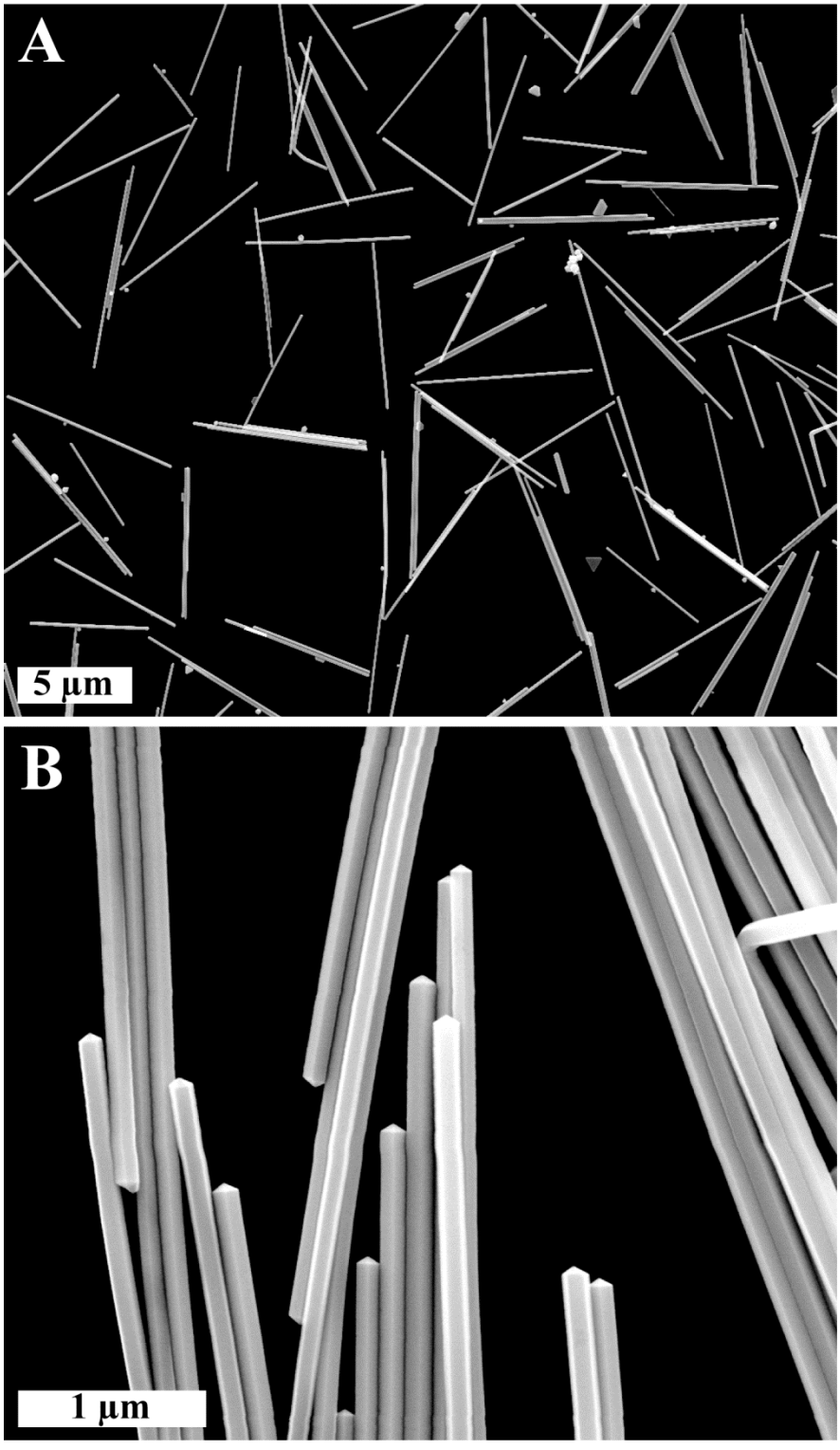

Figure 3.5. SEM images of gold nanowires synthesized with HQ concentration of 40 times the gold concentration at lower (a) and higher (b) magnification.

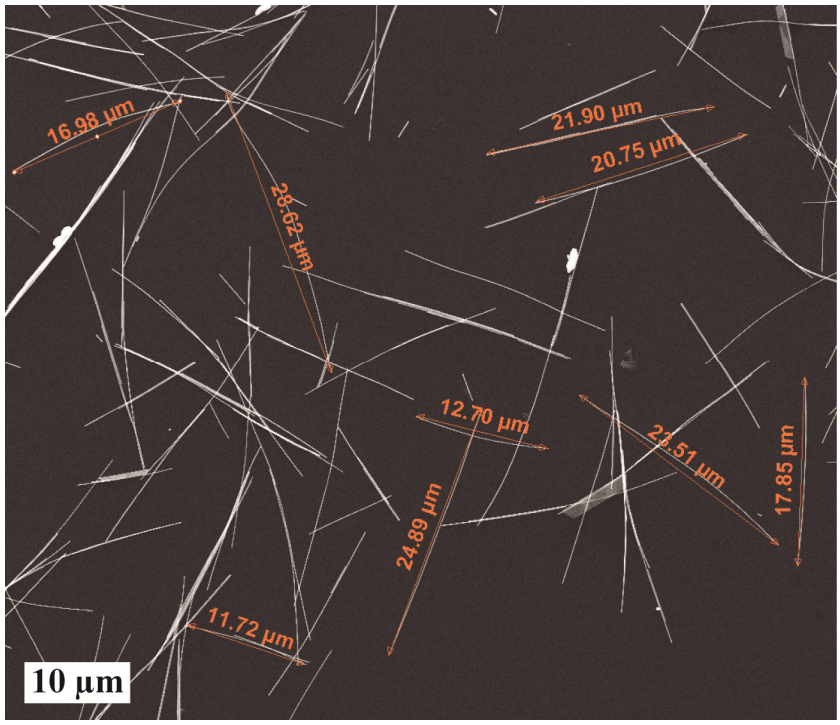

Figure 3.6. SEM image of long NWs synthesized using less PNR seed.

compared to the AA procedure. In order to see if the length of the wires could be increased and the diameter decreased, the amount of HQ reducing agent added was reduced from ten times to 4 times the gold concentration. As expected, these NWs grew to nearly double the length (10-15 µm) with a concomitant decrease in diameter to 85 nm. Further decrease of the HQ concentration to 3 times the gold concentration produced NWs with roughly the same length but decreased diameter of 60 nm. Although this suggests that the amount of gold utilized decreases with decreasing HQ concentration, it would be necessary to measure the gold content directly through ICP-OES or ICP-MS to prove this. There is a clear trend that moving to lower reducing agent concentrations produces wires with decreased diameter and increased length, up to a point. Reducing the concentration to below 3 times the

gold concentration precluded any growth from occurring, at least within a couple of days. The next strategy to increase the length of the NWs was to increase the proportion of gold to PNR seed. By reducing the amount of PNR seed used by a factor of 4, NWs of maximum length 20 – 30 μm and diameter of 85 nm were produced, as shown in Figure 3.6. Similarly, it is possible to create shorter wires by reducing the volume of growth solution or increasing the amount of PNR seed used.

In general, the ascorbic acid and HQ mediated procedures for NW synthesis produce comparable results in terms of quality and length of the wires produced. However, there are some differences in terms of the diameter of wires that can be produced. It does appear that using AA at low pH tends to give somewhat thinner wires than those made with HQ at comparable lengths. However, using HQ provides a greater degree of flexibility in terms of tuning the width by varying the HQ concentration over a larger range. In addition, thicker wires had a more-perfectly faceted morphology that could lead to improved properties such as conductivity.[46] It is expected that further optimization of reaction conditions including PNR seed, HQ, and gold concentrations as well as the reaction pH could bring access to an even greater tunability of NW dimensions.

3.4. Synthesis of Starfruit Nanorods

As mentioned earlier, the controlled synthesis of branched or star-shaped particles is highly desirable, but nearly all examples of such structures are zero-dimensional objects. We aimed to synthesize extended, anisotropic, branched

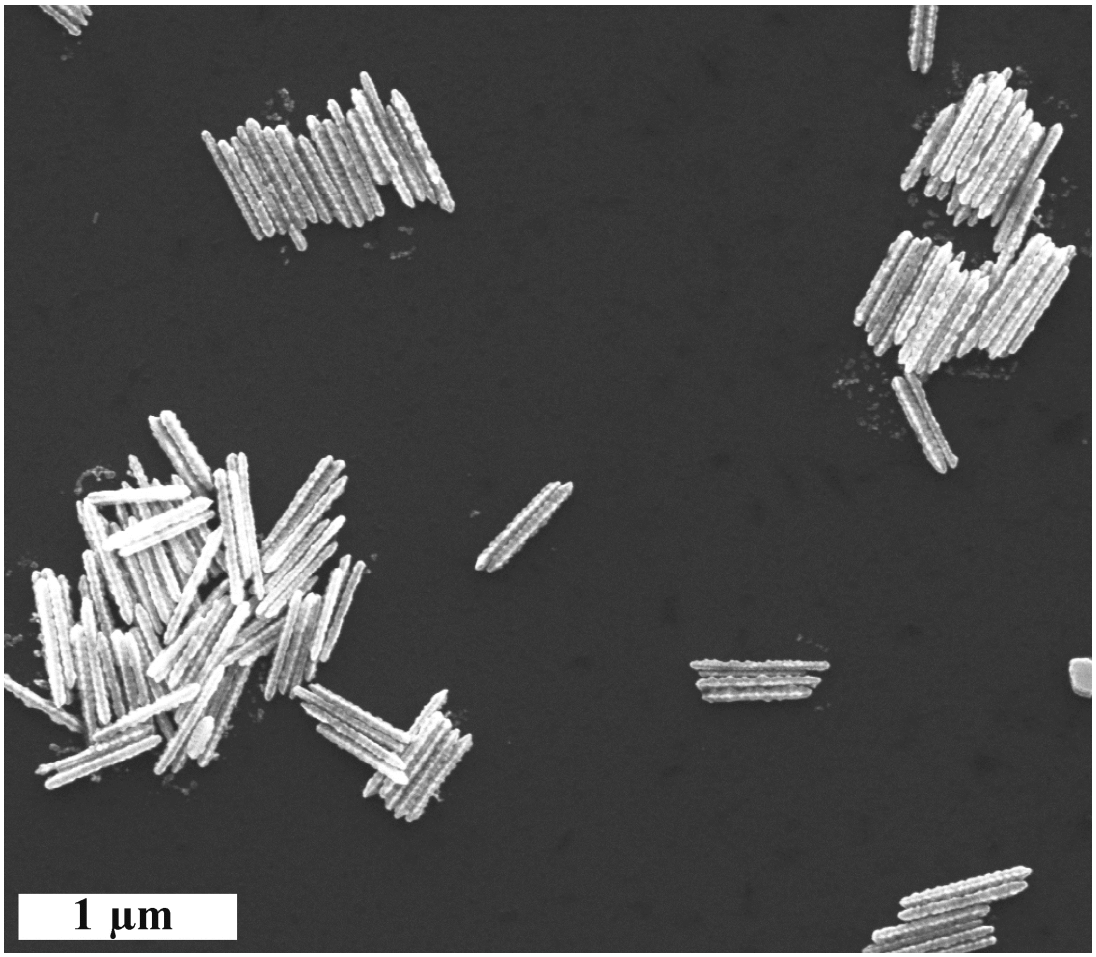

Figure 3.7. Representative SEM image of starfruit NRs with aspect ratio 10. The uniformity of the sample in terms of size and shape is clearly evident.

structures by modifying the traditional PNR seed-mediated growth procedure. Concurrently with Wu and coworkers, we determined that the addition of silver is the key step in inducing branching during the growth of pentahedrally-twinned structures such as PNRs.[25] By following the same procedure as shown in Figure 3.2 but with the addition of 0.3 mM silver nitrate into the growth solution, we were able to synthesize highly-pure, anisotropic structure with a unique starfruit-like morphology. When only a small amount of growth solution was used, the result was the formation of the starfruit-shaped NRs shown in Figure 3.7. This overgrowth

step results in a significant increase in length to about 550 nm and an increase in width to 55 nm leading to an aspect ratio of 10, which is still quite high, but lower than the starting seed NRs by about a factor of 2. This growth was accompanied by an increase in roughness due to the evolution of the starfruit morphology. The uniformity in shape and size of these structures has clearly been conserved from the starting PNR seeds.

3.5. Synthesis of Starfruit Mesorods

With this amount of overgrowth it is still difficult to clearly see the penta-branched structure which is evolving. Increasing the volume of the growth solution leads to the formation of MR structures with length approaching 1 μm and the diameter around 300 nm, which appear to show an ordered penta-branched structure as seen in Figure 3.8. Most of these structures display sharp needle-like tips at the ends of the rods, but also have a core segment which contains roughened pentagonal branches. The low-magnification SEM images of these starfruit MRs (SMRs) shown in Figure 3.8a demonstrate the high yield and uniformity of this overgrowth procedure which leads to rod-like structures with starfruit morphology. Two factors are important in order to achieve this result. First, the PNR seeds have been purified to an extremely high level leading to a uniform seed solution with almost no other shape impurities, as discussed previously. If impurities such as platelets or spherical particles are present in the seed due to incomplete purification

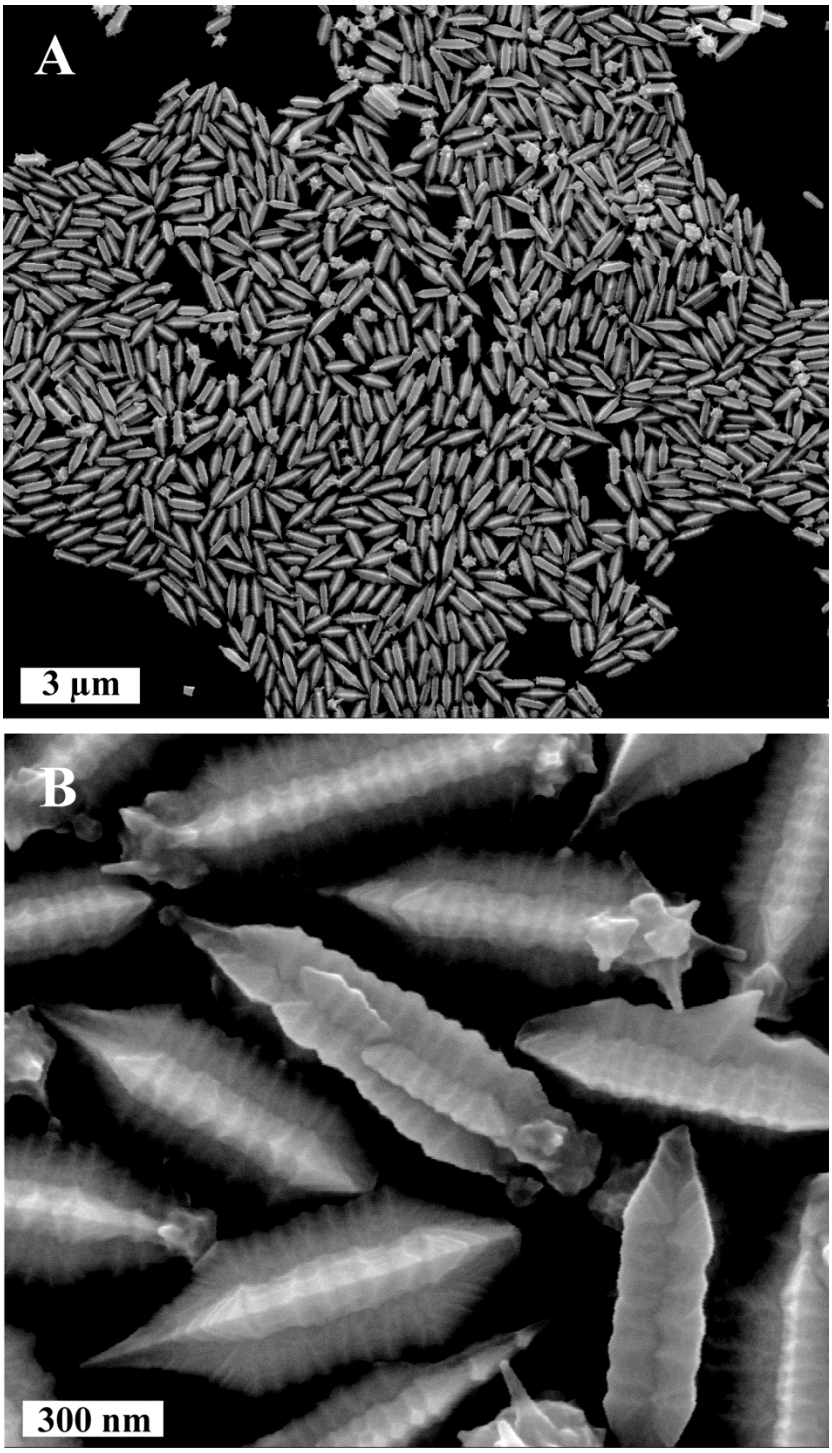

Figure 3.8. SEM images of starfruit MRs. The low magnification image (a) demonstrates the purity and monodispersity of the sample. The roughened, branched structure of the MRs is visible in the high magnification image (b).

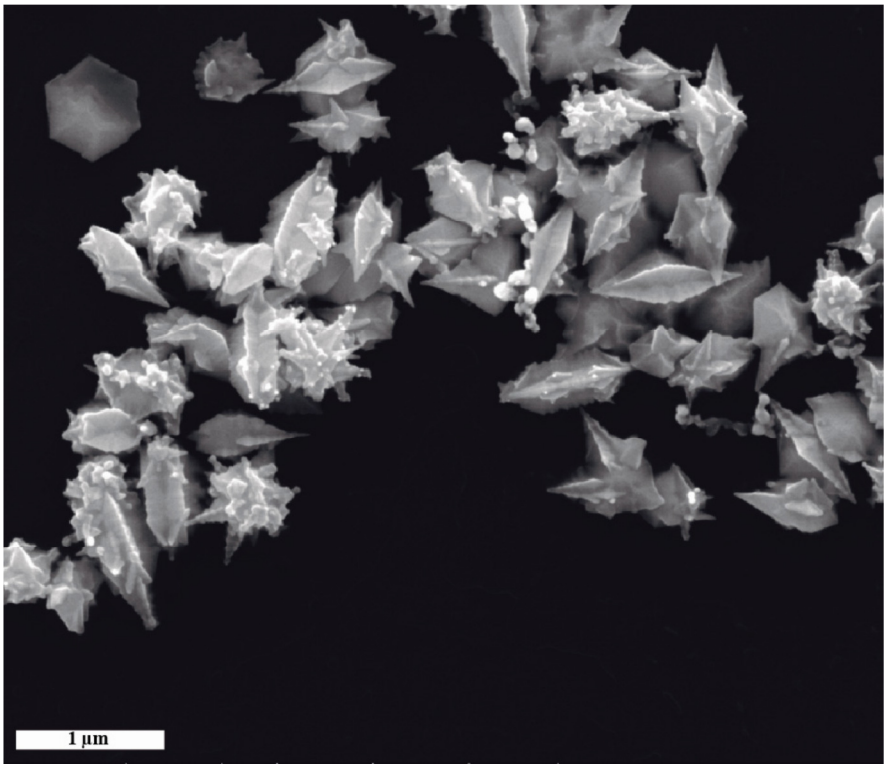

Figure 3.9. SEM image of MRs synthesized in the presence of impurities including platelets, spheres, and short rods.

of the PNRs, they are carried through directly into the products leading to the presence of various non-uniform shapes as seen in Figure 3.9. Second, the Au(I)-CTAB growth conditions minimize unwanted nucleation in solution, resulting in growth only of the added seed particles. Due to their size, the SMRs tend to settle out of solution within one to two hours and can be brought back into solution indefinitely as long as the concentration of CTAB remains sufficiently high (well above cmc). SMRs can also be redispersed into pure water to reduce the concentration of CTAB in solution. Under these conditions, the rate of SMR precipitation is lower but it may lead to irreversible aggregation if the particles are stored in this way. It is difficult to confirm the penta-branched starfruit morphology

of the SMRs from particles lying flat on a substrate. Therefore, it was necessary to achieve a standing orientation to better see the cross-section of the particles. By casting a concentrated solution of the SMRs directly onto a non-uniform aluminum stub, it was possible to find areas with multiple SMRs standing on their tips as seen in Figure 3.10. The SMRs five-point star-like cross-section is clearly visible in these high-resolution SEM images which also reveal a higher degree of order than is expected from previous images. The roughness along the tips which initially appears to be random is revealed to be the result of periodic ridges which create the impression of a stack of stars culminating in a uniform star-shaped "arrow head." In addition, the surface of the SMRs appears not to be perfectly smooth or faceted, instead showing a consistent high roughness along the entire structure. These images also demonstrate the presence of a variety of tip structures. Many contain a broken-off tip while others exhibit random spiky overgrowths. The amount of these spiky tips can be increased greatly by simply increasing the amount of reducing agent during the overgrowth process.

The previous report demonstrated that silver was the key element in the synthesis of the starfruit morphology[25] and its importance has been noted in other nanostar syntheses.[24,26] By varying both the cation and anion added to the synthesis, it was confirmed that the silver cation is the crucial structure-directing agent. The effect of the added anion was explored by changing the type of the silver salt to sulfate, triflate, or acetate rather than nitrate. There was no difference in morphology as evidenced by the SEM micrographs in

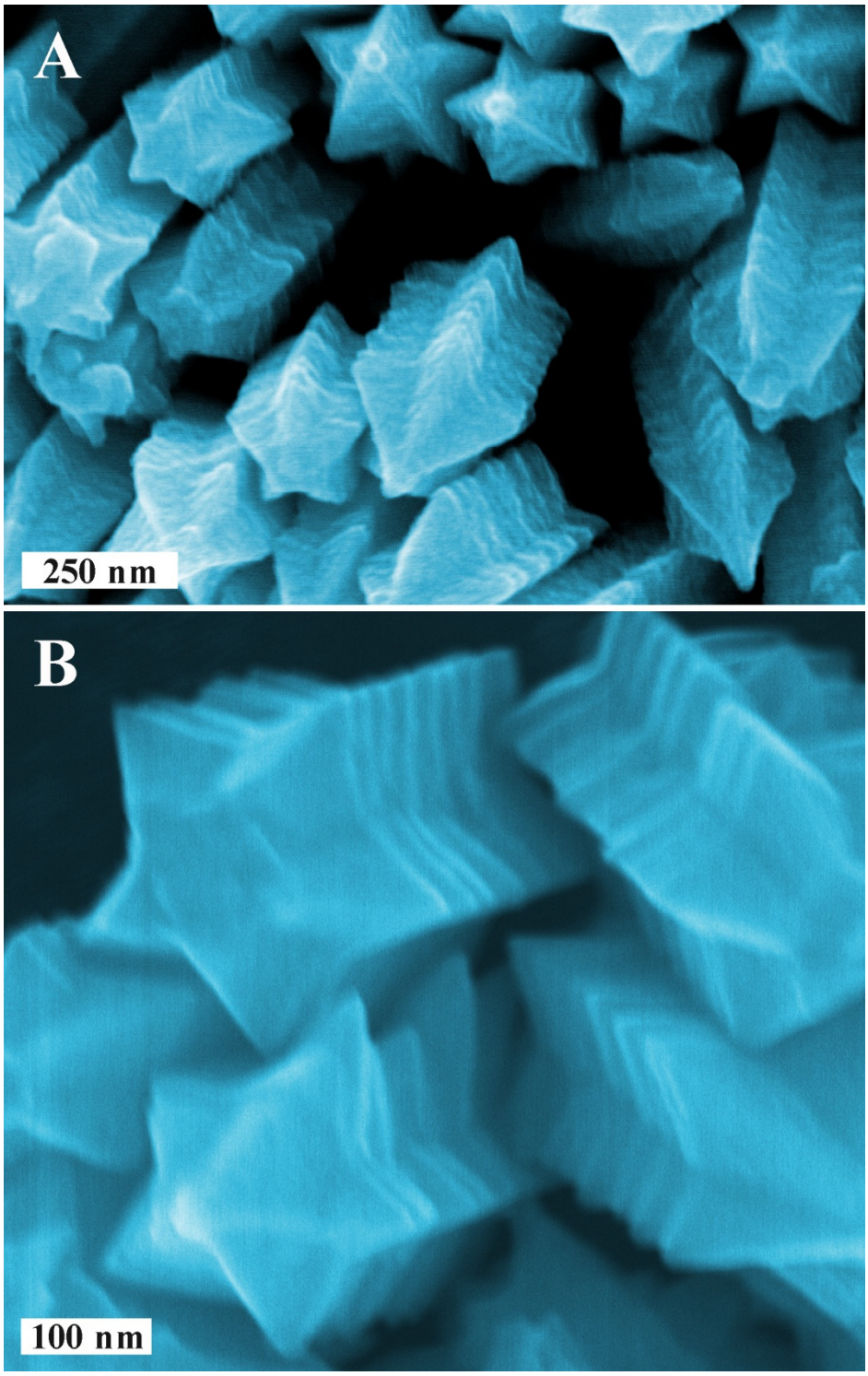

Figure 3.10. Low magnification (a) and high magnification (b) SEM images of standing starfruit MRs showing their periodic five-point star cross-section.

Figure 3.11, indicating that the counter-ion is not playing an important role in this synthesis. In addition, determination of the silver content of the starfruit MRs by ICP-OES showed that no silver was present in the final particles, indicating its role as a structure-directing agent rather than leading to the formation of bimetallic particles. To study the effect of the cation, various metal salts beside silver were tested including iron sulfate, copper sulfate, nickel sulfate, as well as mercury acetate and the effects of these additives were analyzed by SEM (Figure 3.12). The

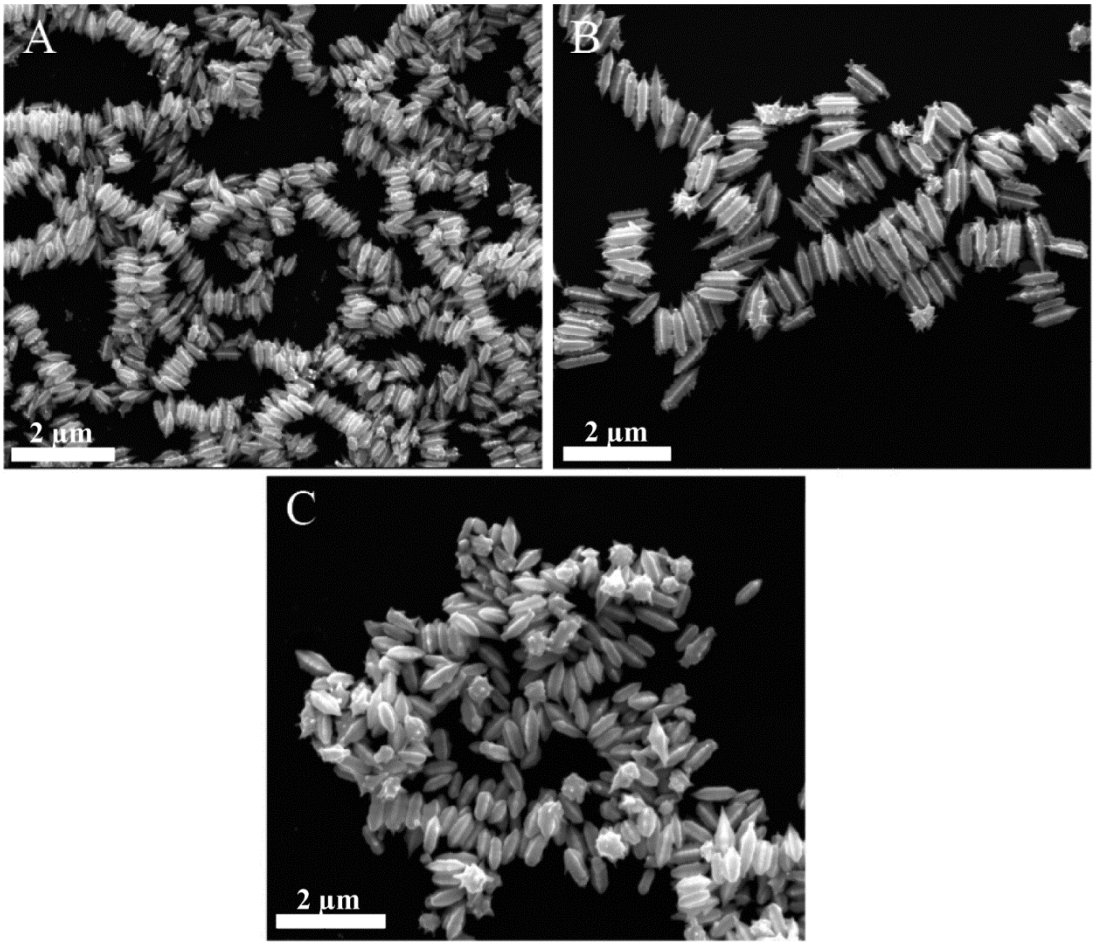

Figure 3.11. SEM images of starfruit MRs synthesized with other silver salts including silver triflate (a), silver acetate (b), and silver sulfate (c).

starfruit morphology is clearly not present in any of these cases, resulting in generally much smoother particles. In the case of nickel and mercury, the appearance is similar to the case of the standard MR synthesis described previously. Iron sulfate addition leads to highly rounded morphology which displays very little faceting, but still maintains a distinct rod-like shape. Copper sulfate addition leads

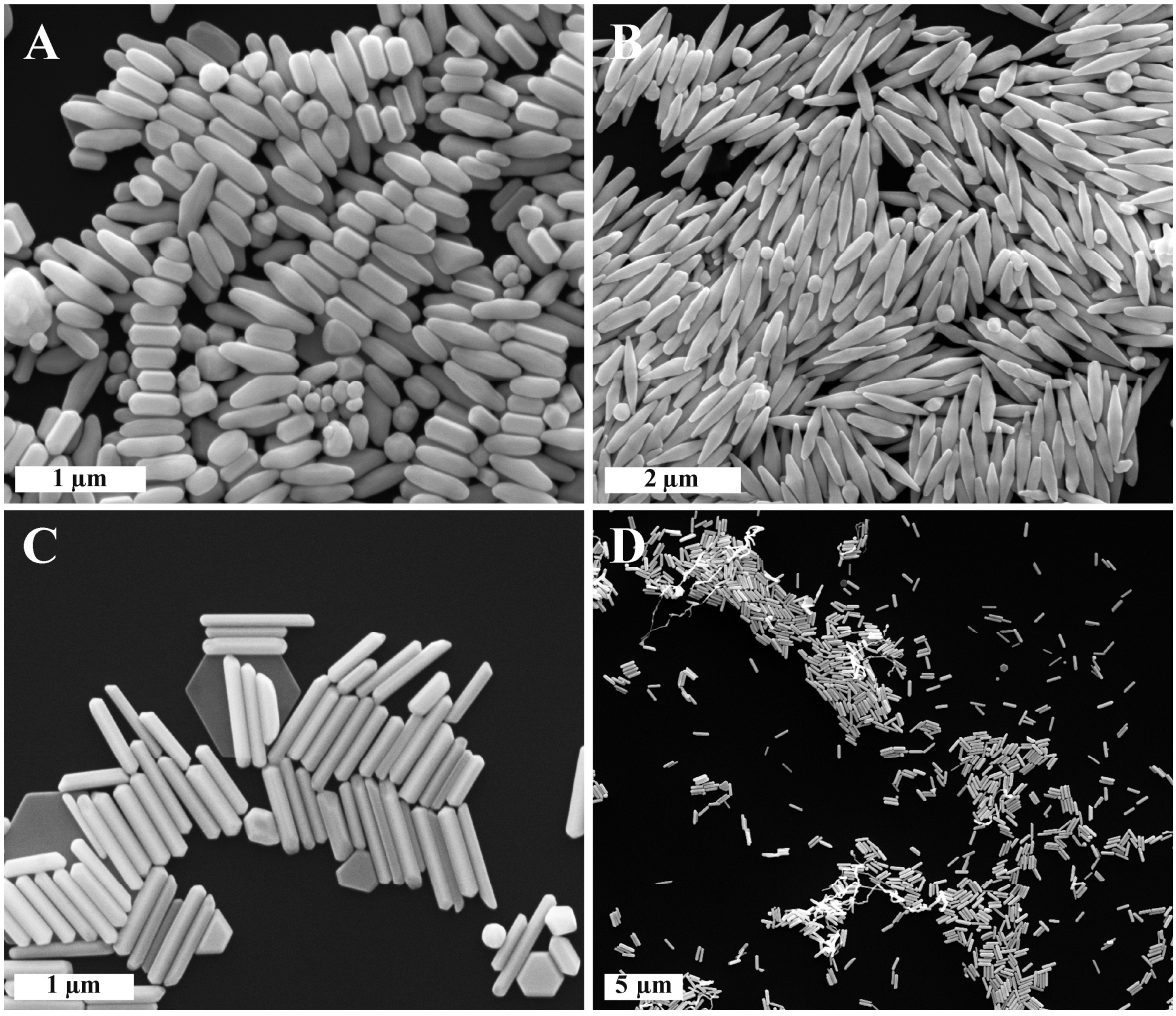

Figure 3.12. SEM micrographs of rods overgrowth in the presence of iron(II) sulfate (a), copper(II) sulfate (b), nickel(II) sulfate (c), and mercury(II) acetate (d). No starfruit morphology is evident. Scale bars are 1 µm, 3 µm, 1 µm, and 10 µm for (a), (b), (c), and (d) respectively.

to a similar rounded morphology, but the overall shape is more reminiscent of a smoothed bipyramid than a rod. Further research is necessary to understand the reason for these changes, but it is clear that silver is unique in affecting gold nanoparticle overgrowth in this procedure even though copper and mercury should be reduced by ascorbic acid to the +1 oxidation state similar to that of silver. It may be that the specific ability of silver to undergo underpotential deposition onto or the particular binding affinity of the silver-CTAB complex to the gold surface leads to its unique structure-directing capability in this synthesis.[47] Next, the effect of the amount of silver on the starfruit MR overgrowth was investigated by varying the concentration of silver nitrate in the growth solution from 5.9 μM to 590 μM. Above

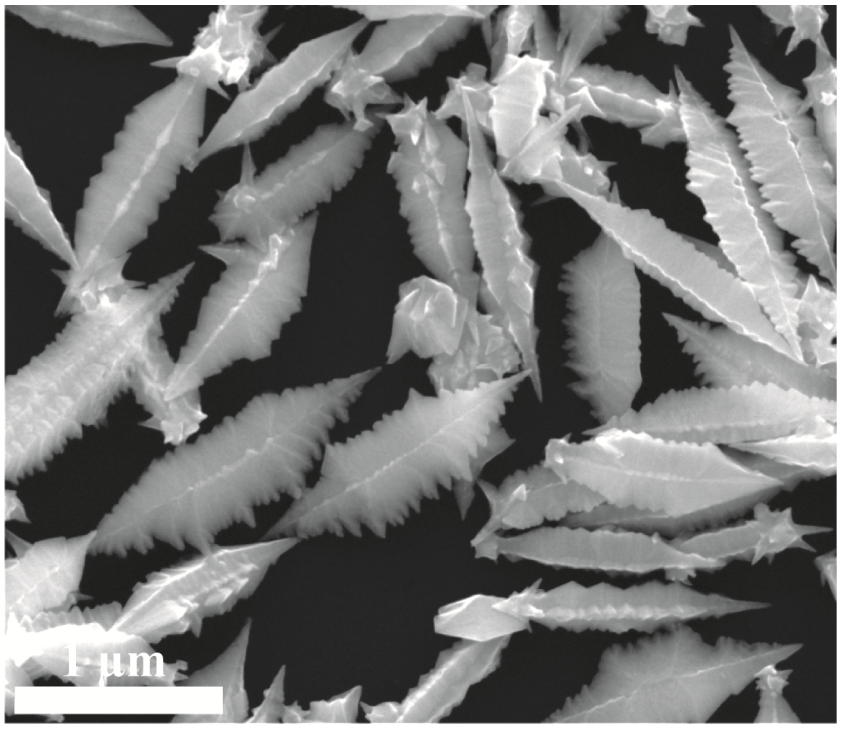

Figure 3.13. SEM images of plate-like particles synthesized at low silver concentration.

the silver concentration of about 59 μM, the starfruit morphology is completely formed with little difference between the various concentrations. Higher concentrations of silver led to its precipitation from solution and so were not explored. At the lowest concentration, however, a different morphology becomes prevalent, shown in Figure 3.13, which appears to lose the five-fold symmetry and instead has only two major spines which appear to be fully formed, although the other spines can still be seen, resulting in a plate-like morphology. Further study is needed to understand why this asymmetrical growth process occurs at low silver concentrations and may help to elucidate the general starfruit growth mechanism which has been only partially described up to this point.

3.6. Synthesis of Starfruit Nanowires

Given the success of the seed-mediated synthesis of starfruit structures from penta-twinned NRs, it was hypothesized that this growth procedure could be applied to much longer seeds with similar penta-twinned morphology such as the gold NWs described previously. Using these NWs as the seeds under similar silver-containing overgrowth conditions led to uniform overgrowth of the penta-branched starfruit nanowires (SNWs) with ~10 μm length with a concomitant increase in diameter from about 50 nm to 200 nm, as shown in Figure 3.14, which is the first example of such structures. The wires display a similar tip structure to SMRs, with most wires having either a sharp tip or "broken-off" appearance. This clearly shows the versatility of the silver-mediated starfruit overgrowth procedure which

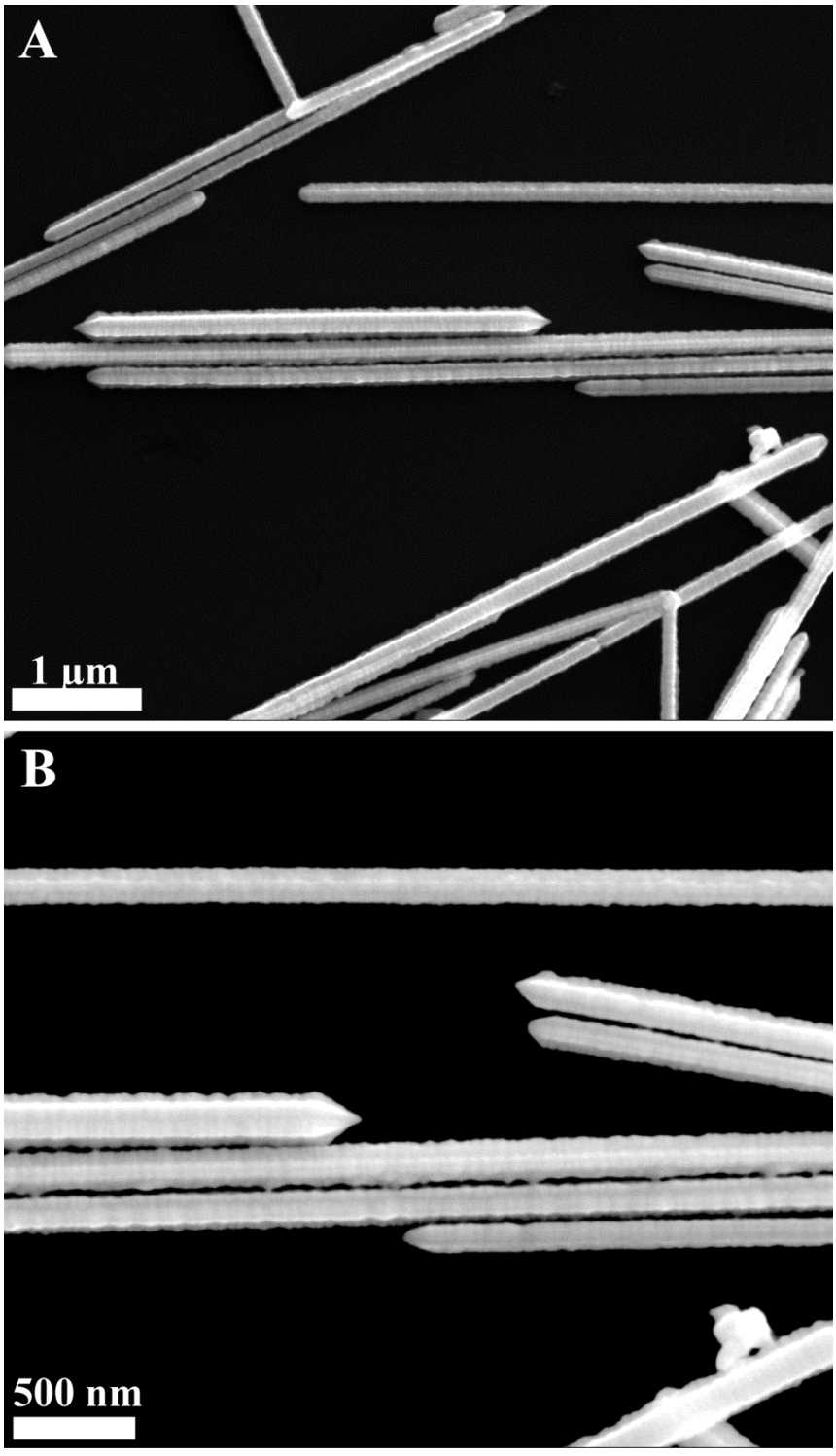

Figure 3.14. SEM images of starfruit gold nanowires at low(a) and high magnification (b).

appears to be applicable to any pentahedrally-twinned 1D gold seeds. It is important to note that overgrowth of single-crystalline rods synthesized in the presence of silver does not lead to the formation of any starfruit morphology. The presence of the starfruit morphology could have an effect on the optical and electronic properties of gold NWs. For example, the effect of these structures on plasmon propagation along the nanowire is currently under investigation and appears to be significant.

3.7. UV-Vis and SERS Properties

The starfruit particles were further characterized with UV-Visible absorption spectroscopy shown in Figure 3.15. Amplification of PNRs with a small amount of gold in the presence of silver ions led to a change in color from brownish to reddish resulting from the red-shifting of the transverse plasmon band from 500 nm to 555 nm. Full growth into SMRs leads to a further red shifting of the band to 690 nm with a large degree of broadening, granting the particles a blue-green color in solution. This plasmon band is likely due to the growing branches of the particles. The large broadening and enhanced absorption across the spectrum is likely due to the increased size of the particles leading to higher scattering as well as the presence of higher-order plasmon modes. A similar effect is visible with the growth of the SNWs. If only a small amount of growth is performed, there is a red-shift from 525 nm to 555 nm and a more pronounced red color in solution compared to the original

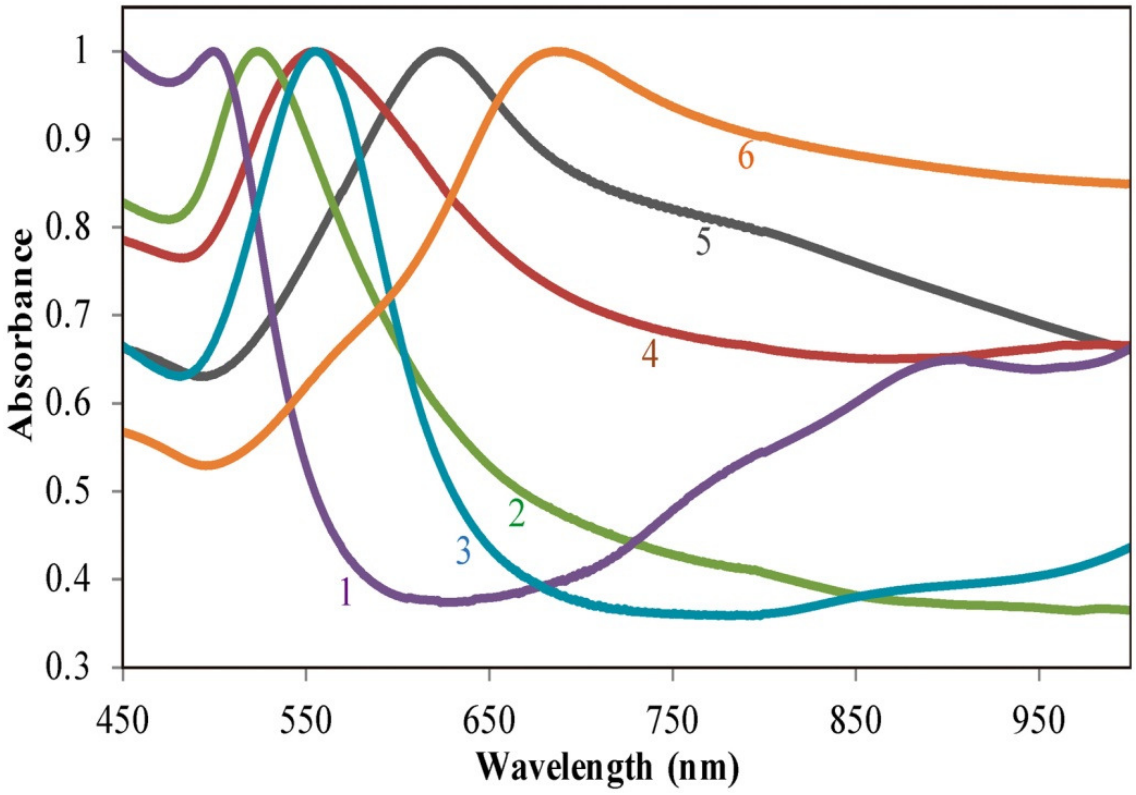

Figure 3.15. Normalized absorbance spectra of pentahedrally-twinned NRs (1), nanowires (2), small growth of starfruit NRs (3), small growth of starfruit nanowires (4), full growth of starfruit nanowires (5), and starfruit mesorods (6).

gold-brown color. Full development of the starfruit morphology leads to a further red-shifting of this band to 630 nm and a change to a blue-green color.

Finally, preliminary application of the starfruit particles to surface enhanced Raman spectroscopy (SERS) was investigated. It was expected that the increased surface roughness as well as the presence of sharp tips could lead to much higher SERS activity compared to smooth particles of a similar size and length.[12,48] In general, SERS measurements can be complicated by the presence of particle aggregates which can lead to very high enhancements.[49–51] In order to study the

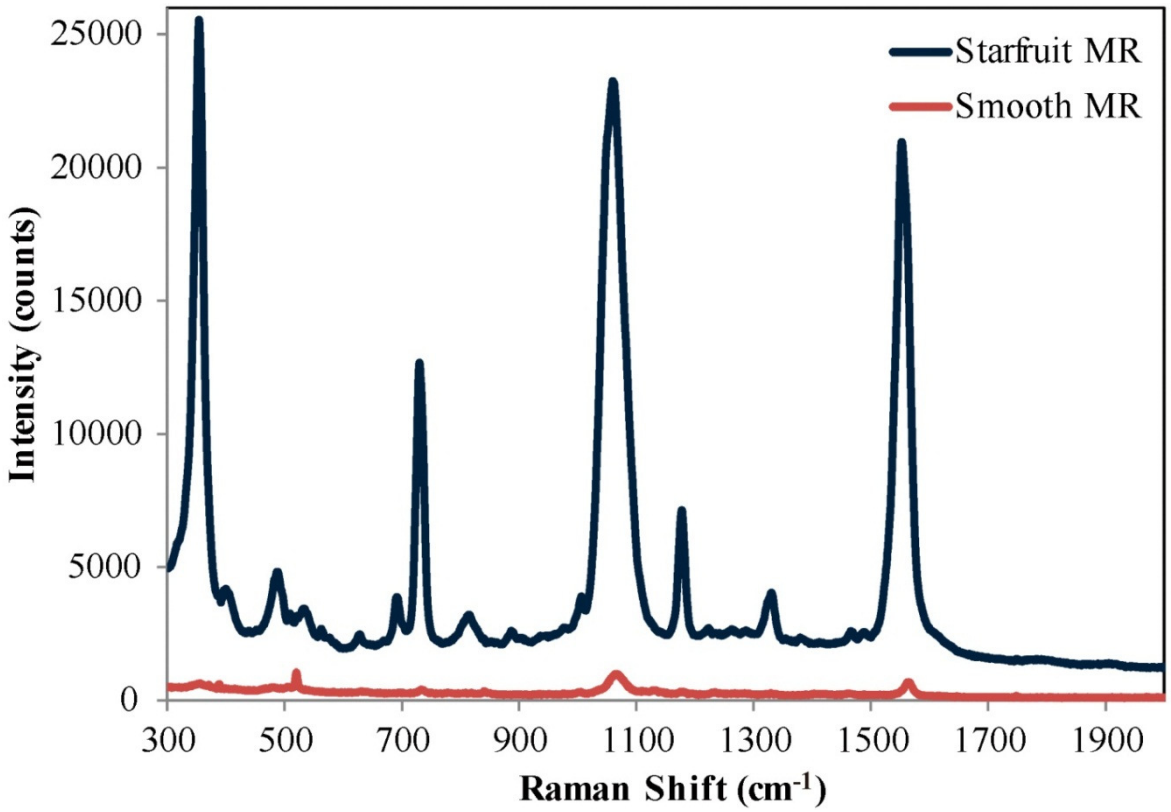

Figure 3.16. Surface-enhanced Raman spectra of an individual starfruit MR and a smooth MR deposited on benzenedithiol-coated gold film.

SERS activity of individual particles, a procedure was developed to image the area of analysis by optical microscopy and then locate the exact same area under SEM to ensure that each particle measured was indeed individual and sufficiently separated from all neighboring particles given the 2 μm spot size of the Raman laser. SERS measurements were obtained following a procedure similar to that of Rodríguez-Lorenzo et al. which takes advantage of electric field enhancement between a nanoparticle and a gold surface[6] with 1,4-benzenedithiol coating playing the role of SERS-active molecule as well as a spacer between the gold surface and the particle. Multiple single particle measurements were performed on individual starfruit MRs

as well as smooth MRs and the average SERS spectrum, shown in Figure 3.16, demonstrates significant enhancement of the bands at 1555, 1065, and 355 cm^{-1}. There is an approximately 25-fold signal enhancement for the SMRs as compared to the smooth structures, which most likely originates from the hot spots generated between the roughened branches coming in contact with the gold surface. This is true even though the smooth MRs likely contact more benzenedithiol molecules. This data indicate the potential utility of the starfruit morphology for SERS applications and the detection of various analytes.

3.8. Conclusions

This chapter described the synthesis of a variety of anisotropic gold nanostructures of various dimensions by utilizing a seed-mediated synthesis wherein the exact nature and purity of the 1D seed particles is tightly controlled. Highly-purified pentagonally-twinned NRs can be amplified in the absence of silver to make smooth MRs and NWs and in the presence of silver ions to form starfruit NRs or MRs depending on the amount of gold growth solution, while using gold NWs as a seed allows the creation of starfruit-shaped nanowires. Starfruit MRs are shown to have enhanced SERS activity compared to similarly sized smooth MRs. The synthetic scheme presented here expands the types of star-shaped particles from simple spherical objects to one-dimensional particles ranging from NRs to nanowires with lengths over 10 μm and could have applications in SERS detection and plasmonic materials. The chapter demonstrates the power of the Au(I)-CTAB

growth solution in controlling gold overgrowth onto various structures using either ascorbic acid or hydroquinone as a reducing agent at various pH levels and in the presence of different structure-directing additives.

3.9. Experimental Methods

Materials and instrumentation**.** Sodium borohydride, silver nitrate, ascorbic acid, copper(II) sulfate, iron(II) sulfate, nickel(II) sulfate and mercury(II) acetate were purchased from Sigma-Aldrich. Chloroauric acid and cetyltrimethylammonium bromide (CTAB) were purchased from Acros Organics. SEM was performed on an FEI Quanta 400. A Hitachi SU6600 FE-SEM was used for high-resolution SEM. TEM images were collected on a JEOL 1230 TEM. UV-Vis absorbance spectra were gathered on a Cary 3000 UV-Vis-NIR spectrophotometer. Raman spectra were collected on a Renishaw inVia Raman microscope.

Synthesis of PNRs**.** Synthesis and purification of these particles was carried out according to a previously published procedure.[41]

Synthesis of MRs. 500 μL of purified PNR seed was added to a growth solution consisting of 100 mL of a $2.5 \cdot 10^{-4}$ mM $HAuCl_4$ solution in 0.1M CTAB to which 550 μL of a 0.1M ascorbic acid solution (standard growth solution)has been added. Growth continued overnight after which the supernatant was decanted and the precipitated MRs redispersed in 10 mL of fresh 0.1 M CTAB solution and this sedimentation and redispersion process was repeated. Tuning of MR morphology

was accomplished by adding 1 mL of the 10 mL MR solution to 10 mL of standard growth solution and the solution was hand-stirred several times and allowed to settle overnight.

Synthesis of NWs with hydroquinone. In a typical synthesis where hydroquinone was used at 40 times the gold concentration, 100 μL of purified PNR seed solution was added to a growth solution consisting of 100 mL of a $2.5 \cdot 10^{-4}$ mM $HAuCl_4$ solution in 0.1M CTAB to which 10 mL of a 0.1M hydroquinone solution has been added. Growth continued overnight after which the supernatant was decanted and the sedimented wires redispersed in a fresh 0.1 M CTAB solution and this process was repeated.

Synthesis of starfruit-shaped gold mesorods. In a typical synthesis, a 100 mL of Au(III) solution (0.25 mM $HAuCl_4$, 0.1 M CTAB) was combined with 1 mL $AgNO_3$ solution (30 mM). To this was added 0.55 mL of ascorbic acid solution (0.1 M) and hand-stirred rapidly. Immediately after that, 0.5 mL of PNR seed solution (c = 1 mg/mL) was added and stirred. The solution was hand-stirred several times during the first few hours and the growth was allowed to continue for 24 hours. Precipitated mesorods were isolated by carefully pouring off the supernatant and redispersing the precipitate into 0.1 M CTAB aqueous solution.

Synthesis of starfruit-shaped gold nanowires**.** Gold nanowires were synthesized according to a previously published procedure.[36] A 10 mL Au (III) solution (0.25 mM $HAuCl_4$, 0.1 M CTAB) was combined with 0.1 mL $AgNO_3$ solution

(30 mM). To this was added 55 μL ascorbic acid solution (0.1 M) and hand-stirred rapidly. Immediately after that, 1 mL of nanowire solution (~0.5 mg/mL nanowires) was added and stirred. The solution was hand-stirred several times during the first few hours and the growth was allowed to continue for 24 hours. Precipitated nanowires were isolated by carefully pouring off the supernatant and redispersing in 0.1 M CTAB solution.

Surface-enhanced Raman spectroscopy. A 20 nm gold layer was evaporated onto a glass slide using an E-beam evaporator. The slide was dipped into an ethanolic solution of 1,4-benzenedithiol (1 mM) for 30 minutes and then rinsed with ethanol and dried. A drop of starfruit mesorod solution was then cast and dried on the slide and rinsed multiple times with ethanol to remove CTAB before the measurements.

3.10. References

(1) Edgar, J. A.; McDonagh, A. M.; Cortie, M. B. *ACS Nano* **2012**, *6*, 1116–1125.

(2) Kou, X.; Zhang, S.; Yang, Z.; Tsung, C.-K.; Stucky, G. D.; Sun, L.; Wang, J.; Yan, C. *J. Am. Chem. Soc.* **2007**, *129*, 6402–6404.

(3) Ni, W.; Kou, X.; Yang, Z.; Wang, J. *ACS Nano* **2008**, *2*, 677–686.

(4) Xiang, Y.; Wu, X.; Liu, D.; Feng, L.; Zhang, K.; Chu, W.; Zhou, W.; Xie, S. *J. Phys. Chem. C* **2008**, *112*, 3203–3208.

(5) Sohn, K.; Kim, F.; Pradel, K. C.; Wu, J.; Peng, Y.; Zhou, F.; Huang, J. *ACS Nano* **2009**, *3*, 2191–2198.

(6) Kim, F.; Sohn, K.; Wu, J.; Huang, J. *J. Am. Chem. Soc.* **2008**, *130*, 14442–14443.

(7) Hao, F.; Nehl, C. L.; Hafner, J. H.; Nordlander, P. *Nano Lett.* **2007**, *7*, 729–732.

(8) Senthil Kumar, P.; Pastoriza-Santos, I.; Rodríguez-González, B.; Javier García de Abajo, F.; Liz-Marzán, L. M. *Nanotechnology* **2008**, *19*, 15606.

(9) Nehl, C. L.; Liao, H.; Hafner, J. H. *Nano Lett.* **2006**, *6*, 683–688.

(10) Guerrero-Martínez, A.; Barbosa, S.; Pastoriza-Santos, I.; Liz-Marzán, L. M. *Curr. Opin. Colloid Interface Sci.* **2011**, *16*, 118–127.

(11) Trigari, S.; Rindi, A.; Margheri, G.; Sottini, S.; Dellepiane, G.; Giorgetti, E. *J. Mater. Chem.* **2011**, *21*, 6531–6540.

(12) Rodríguez-Lorenzo, L.; Álvarez-Puebla, R. A.; de Abajo, F. J. G.; Liz-Marzán, L. M. *J. Phys. Chem. C* **2010**, *114*, 7336–7340.

(13) Su, Q.; Ma, X.; Dong, J.; Jiang, C.; Qian, W. *ACS Appl. Mater. Interfaces* **2011**, *3*, 1873–1879.

(14) Hrelescu, C.; Sau, T. K.; Rogach, A. L.; Jaeckel, F.; Feldmann, J. *Appl. Phys. Lett.* **2009**, *94*, 153113/1–153113/3.

(15) Esenturk, E. N.; Hight, W. *J. Raman Spectrosc* **2009**, *40*, 86–91.

(16) Khoury, C. G.; Vo-Dinh, T. *J. Phys. Chem. C* **2008**, *112*, 18849–18859.

(17) Rodríguez-Lorenzo, L.; Alvarez-Puebla, R. A.; Pastoriza-Santos, I.; Mazzucco, S.; Stéphan, O.; Kociak, M.; Liz-Marzán, L. M.; García de Abajo, F. J. *J. Am. Chem. Soc.* **2009**, *131*, 4616–4618.

(18) LeMieux, M. C.; Lin, Y.-H.; Cuong, P. D.; Ahn, H.-S.; Zubarev, E. R.; Tsukruk, V. V. *Adv. Funct. Mater.* **2005**, *15*, 1529–1540.

(19) Alvarez-Puebla, R. a; Agarwal, A.; Manna, P.; Khanal, B. P.; Aldeanueva-Potel, P.; Carbó-Argibay, E.; Pazos-Pérez, N.; Vigderman, L.; Zubarev, E. R.; Kotov, N. a; Liz-Marzán, L. M. *Proc. Natl. Acad. Sci.* **2011**, *108*, 8157–8161.

(20) Rodriguez-Lorenzo, L.; Krpetic, Z.; Barbosa, S.; Alvarez-Puebla, R. A.; Liz-Marzan, L. M.; Prior, I. A.; Brust, M. *Integr. Biol.* **2011**, *3*, 922–926.

(21) Boca, S.; Rugina, D.; Pintea, A.; Barbu-Tudoran, L.; Astilean, S. *Nanotechnology* **2011**, *22*.

(22) Abalde-Cela, S.; Aldeanueva-Potel, P.; Mateo-Mateo, C.; Rodríguez-González, B.; Bakr, O. M.; Liz-Marzán, L. M. *J. R. Soc. Interface* **2010**, *7*, S435.

(23) Zou, X.; Ying, E.; Dong, S. *Nanotechnology* **2006**, *17*, 4758–4764.

(24) Sau, T. K.; Murphy, C. J. *J. Am. Chem. Soc.* **2004**, *126*, 8648–8649.

(25) Wu, H. L.; Chen, C. H.; Huang, M. H. *Chem. Mater.* **2009**, *21*, 110–114.

(26) Yuan, H.; Ma, W.; Chen, C.; Zhao, J.; Liu, J.; Zhu, H.; Gao, X. *Chem. Mater.* **2007**, *19*, 1592–1600.

(27) Wu, H. Y.; Liu, M.; Huang, M. H. *J. Phys. Chem. B* **2006**, *110*, 19291–19294.

(28) Jeong, G. H.; Lee, Y. W.; Kim, M.; Han, S. W. *J. Colloid Interface Sci.* **2008**, *329*, 97–102.

(29) Bakr, O. M.; Wunsch, B. H.; Stellacci, F. *Chem. Mater.* **2006**, *18*, 3297–3301.

(30) Nikoobakht, B.; El-Sayed, M. A. *Chem. Mater.* **2003**, *15*, 1957–1962.

(31) Gole, A.; Murphy, C. J. *Chem. Mater.* **2004**, *16*, 3633–3640.

(32) Busbee, B. D. D.; Obare, S. O. O.; Murphy, C. J. J. *Adv. Mater.* **2003**, *15*, 414–416.

(33) Bao, Y.; Vigderman, L.; Zubarev, E. R.; Jiang, C. *Langmuir* **2012**, *28*, 923–930.

(34) Peng, Y.; Cullis, T.; Inkson, B. *Appl. Phys. Lett.* **2008**, *93*, 183112–183113.

(35) Schwartz, O.; Oron, D. *Nano Lett.* **2009**, *9*, 4093–4097.

(36) Khanal, B. P.; Zubarev, E. R. *Angew. Chem. E. Int. Ed.* **2009**, *48*, 6888–6891.

(37) Vigderman, L.; Manna, P.; Zubarev, E. R. *Angew. Chem. E. Int. Ed.* **2012**, *51*, 636–641.

(38) Huang, X.; Neretina, S.; El-Sayed, M. A. *Adv. Mater.* **2009**, *21*, 4880–4910.

(39) Murphy, C. J.; Gole, A. M.; Stone, J. W.; Sisco, P. N.; Alkilany, A. M.; Goldsmith, E. C.; Baxter, S. C. *Acc. Chem. Res.* **2008**, *41*, 1721–1730.

(40) Dvir, T.; Timko, B. P.; Brigham, M. D.; Naik, S. R.; Karajanagi, S. S.; Levy, O.; Jin, H.; Parker, K. K.; Langer, R.; Kohane, D. S. *Nat.Nanotechnol.* **2011**, *6*, 720–725.

(41) Khanal, B. P.; Zubarev, E. R. *J. Am. Chem. Soc.* **2008**, *130*, 12634–12635.

(42) Carbó-Argibay, E.; Rodríguez-González, B.; Pastoriza-Santos, I.; Pérez-Juste, J.; Liz-Marzán, L. M. *Nanoscale* **2010**, *2*, 2377–2383.

(43) Seo, D.; Yoo, C. I.; Park, J. C.; Park, S. M.; Ryu, S.; Song, H. *Angew. Chem. E. Int. Ed.* **2008**, *47*, 763–767.

(44) Keul, H. A.; Möller, M.; Bockstaller, M. R.; Muller, M. *Langmuir* **2007**, *23*, 10307–10315.

(45) Ratto, F.; Matteini, P.; Rossi, F.; Pini, R. *J. Nanopart. Res.* **2010**, *12*, 2029–2036.

(46) Critchley, K.; Khanal, B. P.; Górzny, M. Ł.; Vigderman, L.; Evans, S. D.; Zubarev, E. R.; Kotov, N. A. *Adv. Mater.* **2010**, *22*, 2338–42.

(47) Murphy, C. J.; Thompson, L. B.; Chernak, D. J.; Yang, J. A.; Sivapalan, S. T.; Boulos, S. P.; Huang, J.; Alkilany, A. M.; Sisco, P. N. *Curr. Opin. Colloid Interface Sci.* **2011**, *16*, 128–134.

(48) Tian, Z. Q.; Ren, B.; Wu, D. Y. *J. Phys. Chem. B* **2002**, *106*, 9463–9483.

(49) Vo-Dinh, T. *Trac-Trend.Anal.Chem.* **1998**, *17*, 557–582.

(50) Kneipp, K.; Kneipp, H.; Kneipp, J. *Acc. Chem. Res.* **2006**, *39*, 443–450.

(51) Banholzer, M. J.; Millstone, J. E.; Qin, L. D.; Mirkin, C. A. *Chem. Soc. Rev.* **2008**, *37*, 885–897.

Chapter 4

Quantitative Replacement of CTAB by Cationic Thiol Ligands on the Surface of Gold Nanorods

4.1. Introduction

As mentioned previously, gold NRs have received broad attention as possible therapeutic and diagnostic agents due to their anisotropic physical properties.[1–9] However, as-synthesized NRs based on the most common synthetic approach, the seed-mediated synthesis,[10,11] are not directly useable for these applications. They are synthesized in a concentrated CTAB solution and are noncovalently coated with a CTAB bilayer (see Chapter 1.4.1).[12] For CTAB-capped rods to remain soluble, the concentration of free CTAB in solution must remain above a certain value and there is a constant dynamic exchange of CTAB molecules between the solution and NR surfaces.[13] This feature limits the usefulness of these rods for many biological

applications because free CTAB is known to be highly cytotoxic.[14,15] Various strategies have been developed to functionalize gold nanorods with a variety of different ligands to reduce their cytotoxicity.[13,16–21] Further reports have dealt with the problems of stability and biocompatibility of gold NRs by using various polymer shells,[22] polyelectrolytes,[23,24] peptides,[25] surfactants,[26] and lipids[15,27] to modify the NR surface. Partial replacement of CTAB was qualitatively confirmed in many of these cases, but the exact NR surface composition and the amount of residual CTAB was either unknown or not possible to determine. For that reason, there is always some ambiguity in interpretation of *in vitro* and *in vivo* experiments involving such NRs, especially given the large effect that surface chemistry can have on biological interactions.[28]

Understanding the exact properties and characteristics of the NR surface could be of particular importance not just for their use in biological systems, but also for many other applications such as those in plasmonics and sensing. For example, plasmonic sensors based on changes in the refractive index surrounding NRs are highly sensitive to the distance and position of the analyte in relation to the NR.[29] Sensors based on self-assembly are also driven by controlling NR surface-analyte interactions.[30–35] Controlling the distance between NRs may also be crucial to modulating their plasmonic properties for use in opto-electronic devices.[36,37] For nearly all of these systems, though, complete characterization of the NR surface has not been possible, highlighting the need to design new functionalization schemes as well as to find better strategies for the analysis of the final product.

Thus, this chapter will describe a strategy for complete exchange of CTAB for a thiolated analogue (16-mercaptohexadecyl)trimethylammonium bromide (MTAB) with which we can directly determine the chemical composition of the surface coating. Through ^{1}H NMR analysis, we were able to prove that CTAB is fully replaced by a covalent MTAB monolayer. By combining thermogravimetric analysis (TGA) with TEM size analysis of the nanorods, we were able to accurately determine the packing density of the self-assembled thiol monolayer on the surface of Au NRs.

4.2. Synthesis of MTAB-Coated Nanorods

Several reports have shown that even with systems that have successfully functionalized gold NRs, CTAB is still observed to be present on their surface.[38] We hypothesized that we could use a molecule with a structure very similar to CTAB to completely exchange the CTAB, but with the ability to bind more strongly to the NR surface. Thus, we chose to synthesize a thiolated CTAB analogue (MTAB) whose synthesis is shown in Figure 4.1. Commercially available 1,16-hexadecanediol was converted to a corresponding dibromide under standard bromination conditions, which was followed by the synthesis of its monothioester. Cleavage of the acetyl group was carried out in anhydrous methanol using *in situ* generated hydrogen chloride. The resulting 16-bromo-1-hexadecanethiol was treated with excess

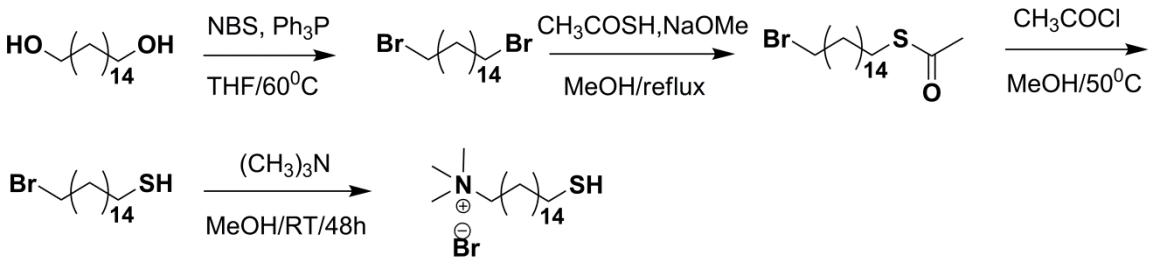

Figure 4.1. Synthesis of MTAB**.**

trimethylamine, leading to substitution of the bromide moiety. Importantly, the purified MTAB compound was found to be water-soluble, which offers an opportunity to perform ligand exchange in aqueous media. The MTAB ligand contains an entire CTAB moiety, but installs a pendant thiol group to be able to strongly anchor to the gold surface. The cross-section of this molecule is small enough to form a compact monolayer on the surface of nanorods, thus providing their solution stability.

Stabilization of gold nanorods is generally difficult because of their small surface-to-volume ratio, and finding a compound that can directly exchange with CTAB is further complicated by the high-density positive charge and the amphiphilic nature of the CTAB bilayer (Figure 4.2). In the past, researchers have exchanged only the tips of gold nanorods because of relatively weak CTAB binding there and have noted that it is much stronger on the sides.[39–41] Furthermore, as the CTAB on the sides of the rods begins to exchange, it appears that the bilayer structure breaks down and rods tend to aggregate prematurely. However, choosing a cationic ligand with a chemical structure similar to native CTAB allows for the direct exchange in

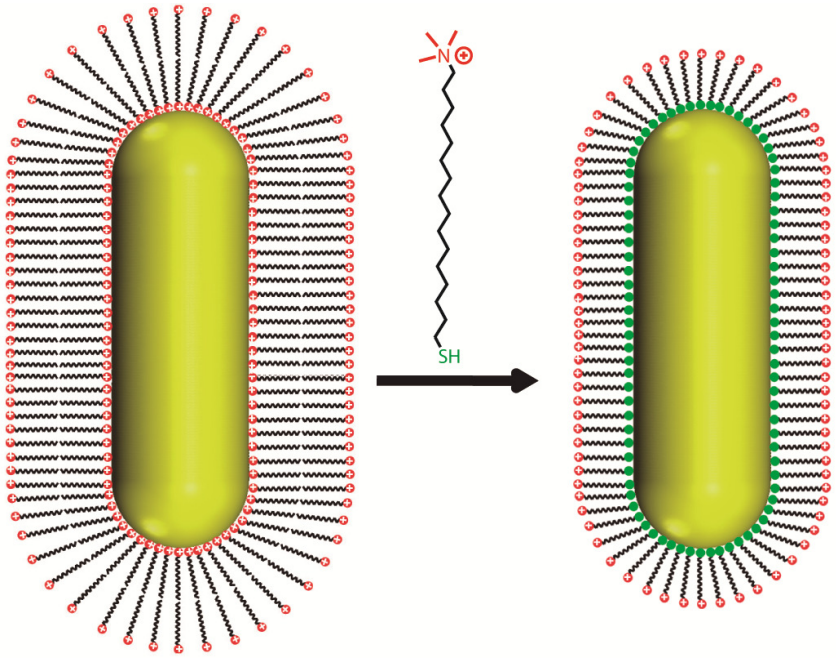

Figure 4.2. Exchange of CTAB bilayer for MTAB monolayer on the gold nanorod surface.

water to proceed smoothly as shown schematically in Figure 4.2. The noncovalent bilayer of CTAB is replaced with a compact thiolate monolayer of MTAB which is covalently anchored to the surface through gold–sulfur bonds. It is important to note that the 11 carbon equivalent of MTAB, (11-mercaptoundecyl) trimethylammonium bromide (MUTAB), was also observed to exchange CTAB and stabilize NRs quite well. Although detailed examination of MUTAB NRs was not carried out, there are certain situations where the increased solubility and ease of synthesis of MUTAB may make it preferable compared to MTAB, such as its use in Chapter 2**Error! Reference source not found.** to halt NR growth. In addition, MUTAB, unlike MTAB, is currently available for purchase from Sigma-Aldrich, which can be a significant benefit. TEM

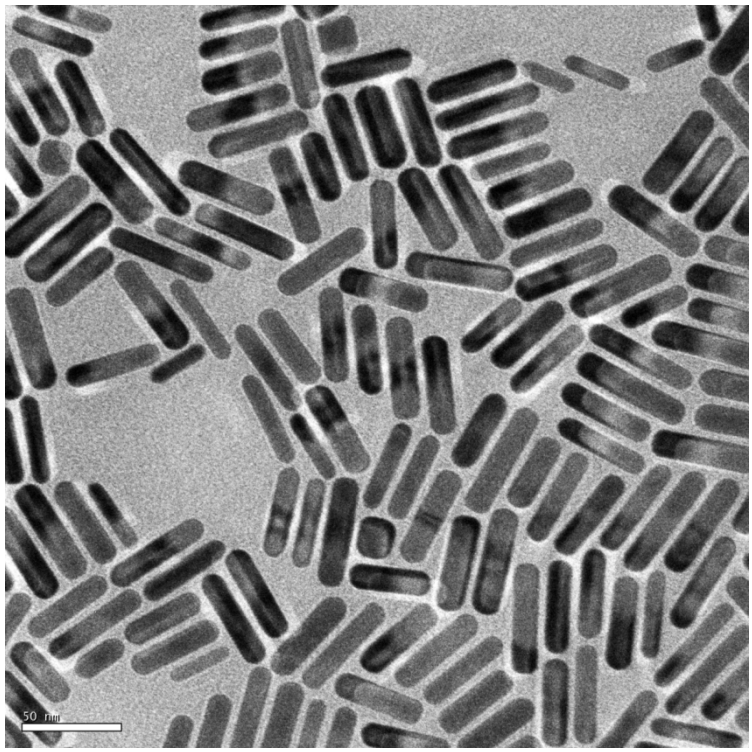

Figure 4.3. TEM image of MTAB-functionalized gold nanorods.

of the rods, shown in Fig. 4.3 demonstrates that the rod morphology has not been disturbed by the functionalization process.

Additional experiments show that these rods can be completely dried and kept in the solid state indefinitely without losing their water solubility. Surprisingly, a standard lyophilization technique can be applied to aqueous solution of MTAB NRs to produce a fluffy dark brown powder. Figure 4.4a shows a photograph of 15 mg of lyophilized Au NRs that occupy an area of several square centimeters. Most importantly, when a small amount of this powder is placed on the surface of pure water, rapid dissolution takes place as manifested by the concentration swirls and a continuous diffusion of the colored solute (Figure 4.4b). The NRs dissolve in a

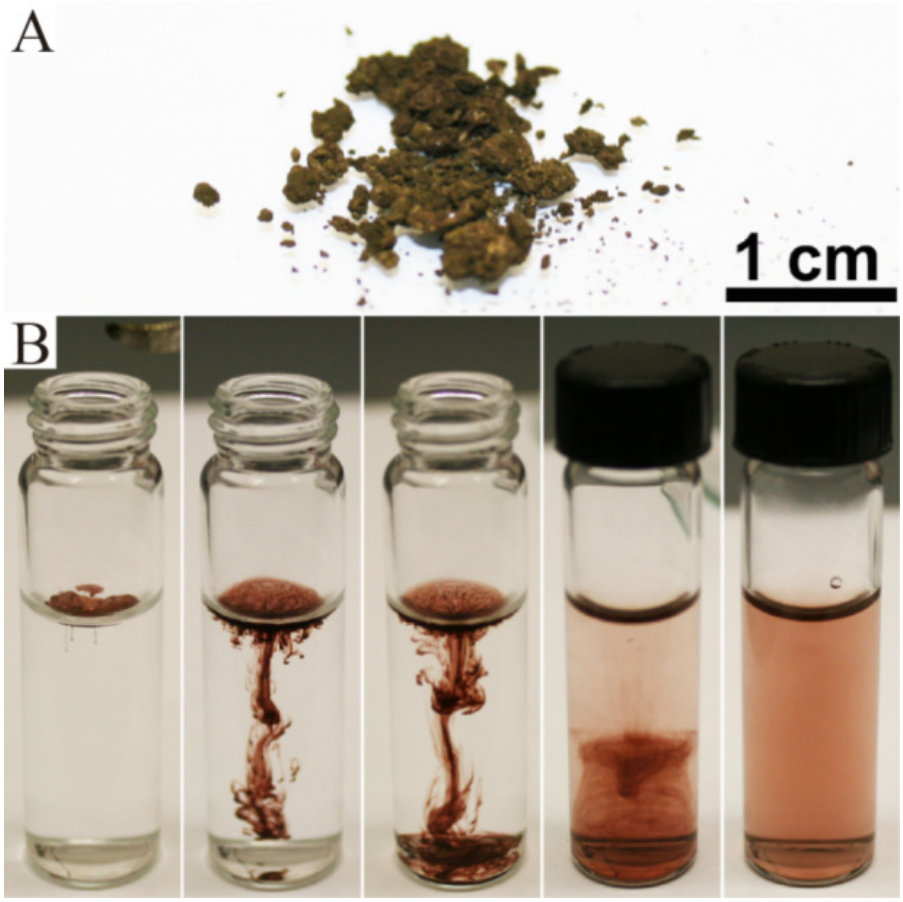

Figure 4.4. (a) Photograph of lyophilized powder of MTAB-functionalized Au NRs and (b) its spontaneous dissolution in pure water. The images were taken consecutively within intervals of five second.

matter of seconds without any heating or sonication. It is sufficient to flip the vial only once to form a homogeneous solution which does not contain any free organic molecules. The solution remains intact for at least several months as confirmed by UV/Vis analysis. This data clearly shows that a dense monolayer of small cationic thiol MTAB is capable of stabilizing large metallic particles in pure water and preventing their flocculation through entropically-driven depletion interactions.[42,43]

This data also proves for the first time that the presence of free surfactant in the solution of gold NRs is not necessary as long as their surface is covalently functionalized by a dense organic shell.

4.3. Characterization of MTAB-functionalized NRs

Characterization of the extent of surface functionalization of nanoparticles can be a difficult task, but we believe it is crucial to fully understand NRs surface chemistry to maximize their utility for a variety of applications. UV-Vis absorbance spectroscopy is often used to assess the stability of gold nanorods in solution as the intensity, the peak shape, and the peak position of the longitudinal plasmon resonance (LSPR) are sensitive to any aggregation that may occur. The UV-Vis spectrum in Figure 4.5a shows the typical absorbance spectrum for gold NRs and demonstrates what happens when excess CTAB is removed from solution after multiple rounds of centrifugation followed by dispersion in pure water. As expected, after just four rounds, the NRs have lost all solubility as evidenced by the lack of any absorbance. In stark contrast, when MTAB-modified NRs are purified by the same technique, there is no appreciable change in the absorbance spectrum even after seven rounds of centrifugation and dispersion, as seen in Figure 4.5b, indicating their much improved solution stability after completely purifying the product.

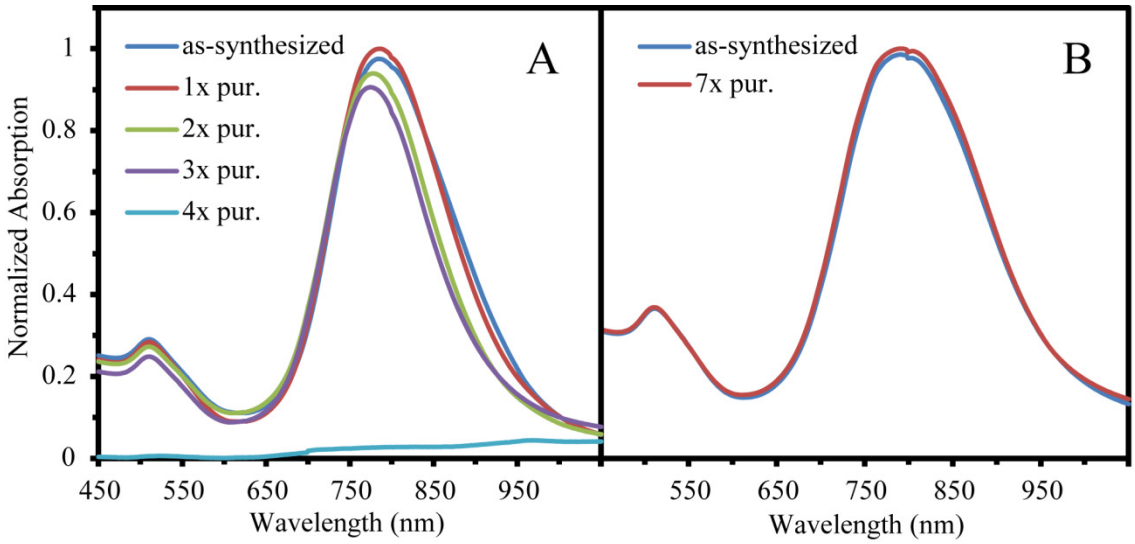

Figure 4.5. UV-vis absorbance spectrum of CTAB-NRs (a) and MTAB-NRs (b) after purification steps by high-speed centrifugation and redispersion into pure water.

Another indirect method that has often been used to characterize gold NRs is zeta potential measurement, which can qualitatively describe the charge surrounding a nanoparticle. The zeta potential of the MTAB-coated NRs was found to be +55 mV, demonstrating their cationic nature, as expected from the high concentration of quaternary ammonium groups positioned around the NR surface. However, the zeta potential is unable to distinguish between CTAB and MTAB on the surface of the rods because they both have the same cationic headgroup exposed to solution and so is useful only as a secondary confirmation of structure. We chose ^{1}H NMR spectroscopy to analyze the organic component of the MTAB-coated NRs which should be able to differentiate between the CTAB and MTAB molecules. However, organic molecules immobilized on gold nanoparticles experience reduced conformational freedom, resulting in a large broadening of peaks from protons near the gold surface and precluding a quantitative structural analysis.[44] Thus, we used

KCN to dissolve the gold NR core and release any surface-bound organic material into solution[45] after having rigorously purified the functionalized NRs. Because of the low surface-to-volume ratio as well as high density of the gold core, we performed an oxidative dissolution of 105 mg of gold NRs in one milliliter of D_2O to get enough organic material for a sufficiently strong ^1H NMR signal. The dissolution proceeded very slowly, taking approximately two weeks to dissolve all NRs, suggesting a high packing density for the MTAB surface functionality.[46] On the contrary, CTAB-coated NRs dissolved in about one hour under similar conditions. The dissolution procedure caused the organic component to precipitate from the D_2O solution, apparently because of the formation of Au/CN/MTAB complex. The NMR spectrum of the D_2O supernatant showed no signals, confirming that the entire organic component had precipitated from the solution. The NMR spectrum of this precipitate dissolved in deuterated methanol, as well as that of pure CTAB and MTAB thiol, is shown in Figure 4.6. Comparing the spectra of CTAB and MTAB, it is clear that the isolated signal from the terminal methyl group of CTAB at 0.91 ppm, highlighted in red in Figure 4.6, is not present in the MTAB spectrum, making it a convenient marker for the presence of any CTAB in solution. Analysis of the NMR spectrum of the dissolved NRs (spectrum C in Figure 4.6) clearly shows that there is no signal corresponding to this methyl group, proving that no CTAB remained on the surface of the NRs after the exchange and the following purification. Further analysis of the NMR spectrum of the dissolved NRs shows the formation of the expected disulfide of MTAB as evidenced by the triplet at 2.75 ppm corresponding

to the α-disulfide protons (instead of 2.5 ppm for α-thiol protons). Importantly, the NMR technique is capable of detecting small organic molecules at concentration close to 10^{-5} M, whereas the concentration of our solution was 10^{-2} M. This implies that even if there were some residual CTAB undetectable by NMR spectroscopy, it would not exceed 0.1 %. Therefore, for all practical purposes, one can conclude that the method described here offers an opportunity to quantitatively replace CTAB by its thiolated analogue.

Because the exact chemical composition of the NR surface agents was

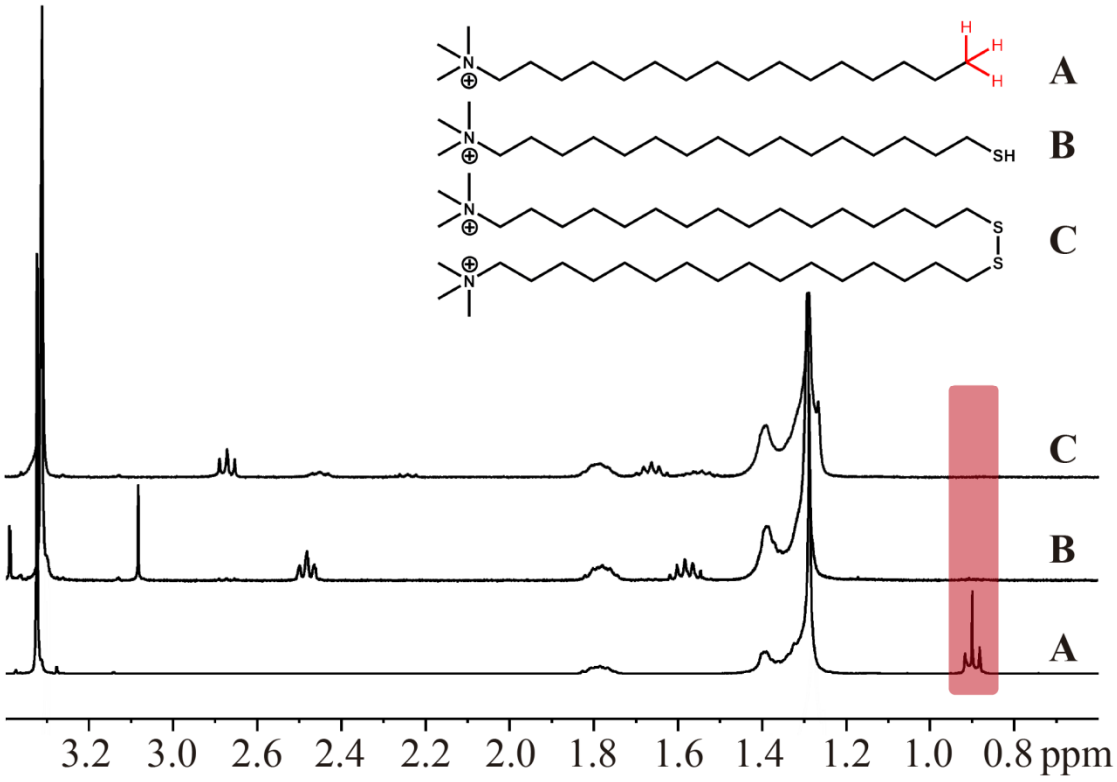

Figure 4.6. ^{1}H NMR spectra in deuterated methanol of CTAB (a), pure MTAB (b), and the organic product released upon oxidative dissolution of MTAB-coated NRs (c).

determined, it was possible to use TGA to further characterize the MTAB-coated NRs. TGA analysis is a highly useful analytical technique for hybrid inorganic–organic nanostructures because it allows one to accurately quantify the weight percentage of a nanostructure that is organic compared to inorganic core.[45,47–49] This is accomplished by heating the sample to above 600 ℃ and observing the weight loss from the sample: any organic material will generally burn off while inorganic material will remain. For our study, more than 100 mg of MTAB NRs were synthesized and functionalized to be used for TGA and NMR measurements, which is quite a large amount when it comes to gold NR synthesis, requiring a synthesis on the four liter scale. However, even this amount of material is difficult to handle, forming an almost unusable thin film when dried normally. To solve this problem, the MTAB-coated NRs were lyophilized from an aqueous solution, forming a low density powder which could be easily handled, as mentioned previously (Figure 4.4). TGA analysis of the lyophilized material, depicted in Figure 4.7, shows a weight loss of 5.3 % in the temperature range between 200 and 450 °C corresponding to the percentage of organic material in the structure following some initial weight loss at 100 °C due to residual water evaporation. Since the NMR analysis proved that no residual CTAB was left, this weight must be entirely due to MTAB ligands covalently attached to the surface of rods.

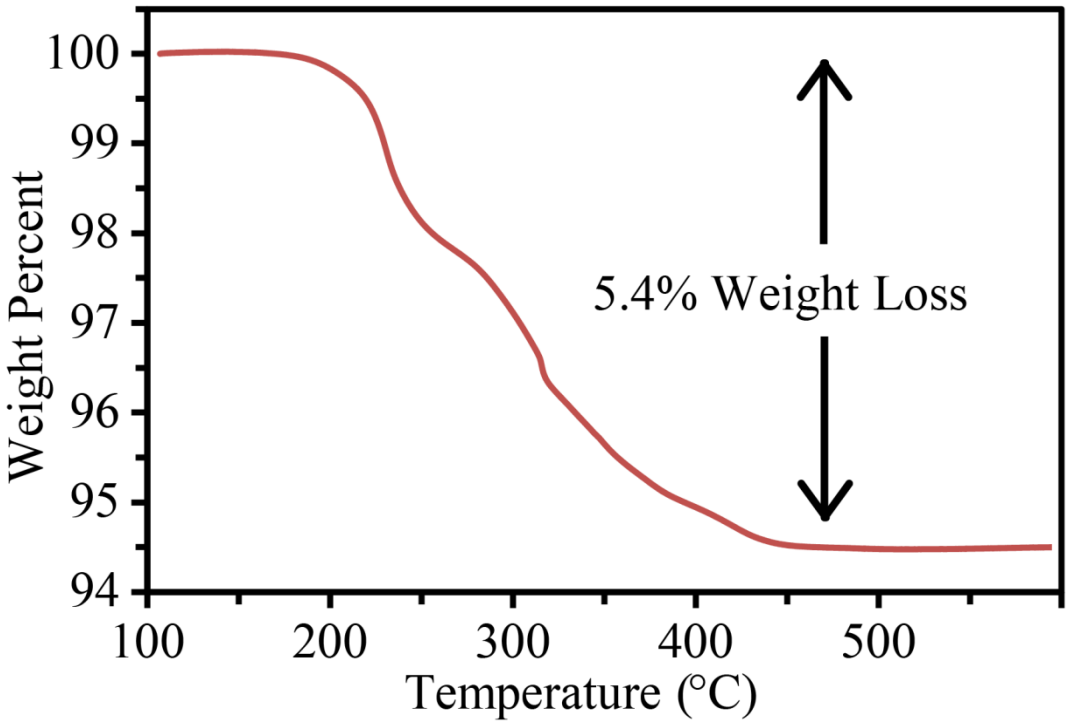

Figure 4.7. TGA curve of MTAB-coated NRs. Residual water is lost at 100 °C. Main weight loss of about 5.3 % from organic component occurs from 200 to 450 °C.

We then performed a careful TEM analysis by measuring over 300 nanorods, which determined that the average length and width of MTAB NRs were 41.9 and 9.9 nm, respectively. With this information, we were able to calculate a grafting density of about 3.7 molecules nm^{-2} for an MTAB monolayer and 5013 MTAB molecules residing on each gold NR (see Chapter 4.7.1 for detailed calculations). This is close to the grafting density of 4.5 molecules nm^{-2} for neutral alkanethiols on flat gold substrates[50] and may be slightly lower because of the repulsive forces between the positively charged headgroups. We believe this is the first proof of a dense self-assembled thiol monolayer on gold nanorods with a calculated grafting density. Estimation of the extent of thiol functionalization has been carried out on DNA-functionalized gold NRs by measuring fluorescence intensity, but such

structures contained only about 40 DNA molecules per nanorod[18] as compared to over 5000 MTAB molecules.

4.4. Limitations of MTAB

The extent with which MTAB is able to displace CTAB on the NR surface is clearly unique and potentially useful. Indeed, biological applications will be discussed in the next chapter. However, it is also important to understand the limitations of the system. First, widespread use of MTAB could be limited by its cost and availability. Few 16 carbon precursors are currently commercially available, necessitating a multi-step synthesis, with one step being a mono-substitution reaction that has inherently low yield. On the other hand, 11 carbon precursors are much more available and present an attractive alternative. Indeed, we have synthesized 11-mercaptoundecyltrimethylammonium bromide (MUTAB) and found that it is also able to effectively stabilize gold NRs through multiple rounds of centrifugation, although the full analysis of the extent of surface exchange has not been performed. One other benefit of using MUTAB is its increased solubility in aqueous media due to its smaller alkyl chain. While MTAB must be heated to 30 – 35 °C to be dissolved, MUTAB is soluble at room temperature. In fact, this was the main reason that MUTAB rather than MTAB was used in
Chapter 2 to halt NR growth.

Another limitation of using MTAB (or MUTAB) is the capability for further modification of the NR surface. The trimethylammonium bromide moiety of MTAB

cannot readily be reacted to add desired functionality such as drugs or antibodies. On the other hand, PEG-thiols, the main alternative to MTAB, can be designed to contain extra functionality such as carboxyl groups which can be coupled to other molecules while maintaining high water solubility. Depending on the application, this may be more important than the presence of residual CTAB or incomplete characterization of the NR surface. But, the similarity between the cationic surface exposed by MTAB and CTAB-capped NRs means that the layer-by-layer deposition procedure developed for CTAB-capped rods[23,24] should be equally applicable to MTAB NRs. Indeed, preliminary results showed that MTAB-coated NRs could be noncovalently functionalized with the negatively charged polyelectrolytes such as polystyrenesulfonate (PSS) and polyacrylic acid (PAA) using this procedure, as evidenced by a switch in zeta potential from +55 mV to -50 mV. PAA coating of gold NRs, in particular, has been used to attach peptides[51] and antibodies[52] to the NR surface. This combined covalent/electrostatic functionalization approach may be useful as it deals with the problem of residual CTAB and also provides a fully-characterized core onto which further chemistry can be performed.

4.5. Conclusions

In conclusion, we have synthesized highly stable, functionalized gold NRs as an alternative to CTAB-capped NRs through a direct, quantitative exchange with a thiolated CTAB analogue. The MTAB-coated NRs showed a highly increased stability to multiple rounds of purification compared to CTAB-coated NRs. Furthermore, we

were able to quantitatively prove the complete removal of CTAB through the use of ^{1}H NMR spectroscopy, and thus determined the exact composition of the organic component of the hybrid nanostructures. We also successfully performed TGA analysis to measure the exact organic versus inorganic composition of hybrid nanostructures and determined a grafting density for the MTAB thiol, proving the formation of a compact self-assembled monolayer on gold nanorods.

4.6. Experimental Methods

4.6.1. Synthesis of MTAB

Synthesis of 1,16-dibromohexadecane, **1.** A 50 mL solution of triphenylphosphine (3.93 g, 15 mmol) in anhydrous THF was added to a stirred solution of *N*-bromosuccinamide (2.67 g, 15 mmol) in 50 mL of THF at 0 $^{\circ}$C. Upon vigorous stirring, a solution of hexadecane-1,16-diol (1 g, 3.9 mmol) in 25 mL of THF was slowly added to the mixture of NBS and Ph_3P. The resulting solution was warmed to room temperature and then heated at 60 $^{\circ}$C for 3.5 hours. THF was removed by rotary evaporation and the residue was re-crystallized from ethanol to obtain 1.1 g of **2** as white powder (70 % isolated yield). ^{1}H NMR ($CDCl_3$, 400 MHz): δ 1.26-1.46 (m, 24 H), 1.85 (q, 4H), 3.41 (t, 4H).

Synthesis of 16-bromo-1-hexadecanethioacetate, **2.** One gram (2.60 mmol) of **1** was dissolved in 40 mL of methanol in a three-neck flask and the solution was degassed for one hour. Separately, 124 mg of sodium methoxide was dissolved in 12

mL dry, ice-cold methanol and mixed with 204 mg (2.6 mmol) of thioacetic acid. This mixture was transferred into a funnel. The solution in the three-neck flask was refluxed under argon atmosphere and the content in the funnel was slowly added to the solution over the course of 4 hours. After the reaction was complete, the content of the flask was cooled to room temperature and methanol was removed under reduced pressure. The yellow oil was further purified by column chromatography (20 % ethyl acetate in hexane) to obtain 480 mg of **3** (50 % yield).

Synthesis of 16-bromo-1-hexadecanethiol, **3.** To a stirred solution of **2** (400 mg, 1.05 mmol) in 10 mL of methanol, 4 mL of acetyl chloride was added drop-wise and the reaction mixture was kept at 50 $^{\circ}$C for 4 hours. After the reaction was complete, 200 mL of CH_2Cl_2 was added to the reaction mixture and excess acetyl chloride and HCl were removed by multiple extractions with DI water. The mixture was dried over sodium sulfate. Methylene chloride was evaporated under reduced pressure to obtain 284 mg of **3** as colorless oil (80 % isolated yield). ^{1}H NMR ($CDCl_3$, 400 MHz): δ 1.26-1.46 (m, 25H), 1.60 (m, 2H), 1.85 (q, 2H), 2.52 (q, 2H), 3.41 (t, 2H).

Synthesis of 16-mercaptohexadecyltrimethylammonium bromide, MTAB. To a solution of **3** (284 mg, 0.85 mmol) in 5 mL of ethyl acetate, 3 mL of 4.2 M ethanolic solution of trimethylamine was added. The mixture was vigorously stirred under argon for 4 days. The resulting white precipitate was filtered off and then washed several times with ethyl acetate to remove excess trimethylamine. The residue was vacuum dried to obtain 270 mg of MTAB (80 % isolated yield). ^{1}H NMR ($CDCl_3$, 400

MHz): δ 1.26-1.46 (m, 25H), 1.60 (m, 2H), 1.85 (m, 2H), 2.52 (q, 2H), 3.5 (s, 9H), 3.55-3.7 (m, 2H).

4.6.2. Synthesis of MTAB-Functionalized Gold Nanorods

Gold NR synthesis. Gold NRs were synthesized according to procedure described elsewhere.[47] Briefly, a seed solution was created by adding 60 µL of a 0.1 M $NaBH_4$ solution to 10 mL of $5.0x10^{-4}$ M $HAuCl_4{\cdot}3H_2O$ in 0.1 M CTAB aqueous solution upon rigorous stirring. Separately, the growth solution was prepared by adding 2 mL of 0.1 M $AgNO_3$ aqueous solution to 2,000 mL of $5.0x10^{-4}$ M $HAuCl_4{\cdot}3H_2O$ in 0.1 M CTAB solution. To this solution was added 11.5 mL of 0.1 M ascorbic acid solution and hand-stirred until the solution became clear, followed immediately by the addition of 3.2 mL of seed solution. A dark brown color indicating the presence of gold nanorods was visible after about 30 min and the solution was allowed to sit overnight before functionalization.

Gold NR functionalization with MTAB thiol**.** Four liters of Au NRs solution was concentrated to about 9 mL using centrifugation at 13,000 rpm. The concentrated NRs solution was purified by two cycles of centrifuging at 13,000 rpm, removing the supernatant and redispersing the precipitate in pure water. To this solution was added 60 mg of MTAB and the solution was stirred for 2 days. The MTAB-coated NRs were purified by seven cycles of centrifugation as described earlier and finally dispersed in 4 mL of water to a concentration of 15 mg/mL as determined by ICP-OES measurements.

4.6.3. Analysis of MTAB-NRs

For TGA analysis (TA Q-600 TGA/DSC), MTAB-NRs were first lyophilized to obtain a useable powder. 1 mL of 15 mg/mL NR solution was placed into an Eppendorf tube, flash frozen with liquid nitrogen, and lyophilized. In the TGA measurement, the temperature was held at 120 °C for 1 hour to remove any residual water and then ramped at 10 °C/min to 850 °C. For ^{1}H-NMR analysis (Bruker 400 MHz), 1.5 mL of 15 mg/mL NR solution was transferred into D_2O by two rounds of centrifugation at 13,000 rpm and redispersion into D_2O. To the D_2O solution was added 50 mg KCN and the solution stirred for two days until the solution was colorless and a white precipitate had formed. The precipitate was isolated by centrifugation and dissolved in deuterated methanol. UV-Vis analysis was carried out on a Varian Cary 500 UV-Vis-NIR Spectrophotometer. Zeta Potential measurements were carried out on a Malvern Instruments Zetasizer Nano-ZS.

4.7. Calculations

4.7.1. Calculation of MTAB Binding Parameters from TGA Data

From TEM size analysis of ~300 NRs, the average length and width were determined to be 41.88 nm and 9.87 nm, respectively. We then assumed a cylindrical shape of NR with radius (r) and height (h) plus 2 spherical caps with base radius (r) and height (a). Based on TEM, the spherical caps extend for about 2 nm on each side, therefore h = 37.88 nm, r = is 4.935 nm, and a = 2 nm. Thus, the surface

area of the rod = $\pi(r^2 + a^2) + 2\pi rh$ = 1352.6 nm^2 and the volume =($\pi/3$) a ($3r^2 + a^2$) + $\pi r^2 h$ = 3059.6 nm^3. The mass of Au per NR = 3059.6 nm^3 × 59 (atoms/nm^3) × 197 Da = $3.56 \cdot 10^7$ Da. The molecular weight of MTAB = 0.053 × (mass Au per NR + mass MTAB) = $1.99 \cdot 10^6$ Da. Number of MTAB molecules per NR = $1.99 \cdot 10^6$ Da / 397 (Da/molecule) = 5013. The molecular footprint = 1352.6 nm^2 / 5013 molecules = 0.270 nm^2 per one molecule of MTAB or 3.7 MTAB molecules per nm^2.

4.8. References

(1) Durr, N. J.; Larson, T.; Smith, D. K.; Korgel, B. A.; Sokolov, K.; Ben-Yakar, A. *Nano Lett.* **2007**, *7*, 941–5.

(2) Huang, X.; El-Sayed, I. H.; Qian, W.; El-Sayed, M. A. *J. Am. Chem. Soc.* **2006**, *128*, 2115–2120.

(3) Yu, C.; Irudayaraj, J. *Anal. Chem.* **2007**, *79*, 572–579.

(4) Liu, X.; Dai, Q.; Austin, L.; Coutts, J.; Knowles, G.; Zou, J.; Chen, H.; Huo, Q. *J. Am. Chem. Soc.* **2008**, *130*, 2780–2782.

(5) Guo, R.; Zhang, L.; Qian, H.; Li, R.; Jiang, X.; Liu, B. *Langmuir* **2010**, *26*, 5428–5434.

(6) Kawano, T.; Niidome, Y.; Mori, T.; Katayama, Y.; Niidome, T. *Bioconjugate Chem.* **2009**, *20*, 209–212.

(7) Wang, H.; Huff, T. B.; Zweifel, D. A.; He, W.; Low, P. S.; Wei, A.; Cheng, J. X. *Proc. Natl. Acad. Sci.* **2005**, *102*, 15752–15756.

(8) Zhao, L.; Pang, X.; Adhikary, R.; Petrich, J. W.; Jeffries-El, M.; Lin, Z. *Adv. Mater.* **2011**, *23*, 2844–2849.

(9) Zhao, L.; Pang, X.; Adhikary, R.; Petrich, J. W.; Lin, Z. *Angew. Chem. E. Int. Ed.* **2011**, *123*, 4044–4048.

(10) Nikoobakht, B.; El-Sayed, M. A. *Chem. Mater.* **2003**, *15*, 1957–1962.

(11) Jana, N. R.; Gearheart, L.; Murphy, C. J. *J. Phys. Chem. B* **2001**, *105*, 4065–4067.

(12) Nikoobakht, B.; El-Sayed, M. A. *Langmuir* **2001**, *17*, 6368–6374.

(13) Orendorff, C. J.; Alam, T. M.; Sasaki, D. Y.; Bunker, B. C.; Voigt, J. A. *ACS Nano* **2009**, *3*, 971–983.

(14) Cortesi, R.; Esposito, E.; Menegatti, E.; Gambari, R.; Nastruzzi, C. *Int. J. Pharm.* **1996**, *139*, 69–78.

(15) Takahashi, H.; Niidome, Y.; Niidome, T.; Kaneko, K.; Kawasaki, H.; Yamada, S. *Langmuir* **2006**, *22*, 2–5.

(16) Liao, H.; Hafner, J. H. *Chem. Mater.* **2005**, *17*, 4636–4641.

(17) Basiruddin, S. K.; Saha, A.; Pradhan, N.; Jana, N. R. *Langmuir* **2010**, *26*, 7475–7481.

(18) Wijaya, A.; Hamad-Schifferli, K. *Langmuir* **2008**, *24*, 9966–9969.

(19) Gole, A.; Murphy, C. J. *Chem. Mater.* **2005**, *17*, 1325–1330.

(20) Gentili, D.; Ori, G.; Comes Franchini, M.; Comes, F. M. *Chem. Commun.* **2009**, *39*, 5874–6.

(21) Sendroiu, I. E.; Warner, M. E.; Corn, R. M. *Langmuir* **2009**, *25*, 11282–11284.

(22) Prencipe, G.; Tabakman, S. M.; Welsher, K.; Liu, Z.; Goodwin, A. P.; Zhang, L.; Henry, J.; Dai, H. *J. Am. Chem. Soc.* **2009**, *131*, 4783–4787.

(23) Leonov, A. P.; Zheng, J.; Clogston, J. D.; Stern, S. T.; Patri, A. K.; Wei, A. *ACS Nano* **2008**, *2*, 2481–2488.

(24) Huang, H.-C. C.; Barua, S.; Kay, D. B.; Rege, K. *ACS Nano* **2009**, *3*, 2941–2952.

(25) Chanda, N.; Shukla, R.; Katti, K. V.; Kannan, R. *Nano Lett.* **2009**, *9*, 1798–1805.

(26) Alkilany, A. M.; Nagaria, P. K.; Wyatt, M. D.; Murphy, C. J. *Langmuir* **2010**, *26*, 9328–9333.

(27) Lee, S. E.; Sasaki, D. Y.; Perroud, T. D.; Yoo, D.; Patel, K. D.; Lee, L. P. *J. Am. Chem. Soc.* **2009**, *131*, 14066–14074.

(28) Khlebtsov, N.; Dykman, L. *Chem. Soc. Rev.* **2011**, *40*, 1647–1671.

(29) Lu, G.; Hou, L.; Zhang, T.; Li, W.; Liu, J. *J. Phys. Chem. C* **2011**, *115*, 22877–22885.

(30) Wanga, J.; Zhanga, P.; Lia, C. M.; Lia, Y. F.; Huang, C. Z.; Wang, J.; Zhang, P.; Li, C. M.; Li, Y. F. *Biosens. Bioelectron.* **2012**, *34*, 197–201.

(31) Wang, C.; Chen, Y.; Wang, T.; Ma, Z. *Chem. Mater.* **2007**, *19*, 5809–5811.

(32) Parab, H. J.; Jung, C.; Lee, J.-H.; Park, H. G. *Biosens. Bioelectron.* **2010**, *26*, 667–73.

(33) Fu, X.; Chen, L.; Li, J.; Lin, M.; You, H.; Wang, W. *Biosens. Bioelectron.* **2012**, *34*, 227–31.

(34) Wang, L.; Zhu, Y.; Xu, L.; Chen, W.; Kuang, H.; Liu, L.; Agarwal, A.; Xu, C.; Kotov, N. a *Angew. Chem. E. Int. Ed.* **2010**, *49*, 5472–5.

(35) Zhu, Y.; Qu, C.; Kuang, H.; Xu, L.; Liu, L.; Hua, Y.; Wang, L.; Xu, C. *Biosens. Bioelectron.* **2011**, *26*, 4387–92.

(36) Solis, D.; Willingham, B.; Nauert, S. L.; Slaughter, L. S.; Olson, J.; Swanglap, P.; Paul, A.; Chang, W.-S.; Link, S. *Nano Lett.* **2012**, *12*, 1349–53.

(37) Jain, P. K.; Huang, W.; El-Sayed, M. A. *Nano Lett.* **2007**, *7*, 2080–2088.

(38) Oyelere, A. K.; Chen, P. C.; Huang, X.; El-Sayed, I. H.; El-Sayed, M. A. *Bioconjugate Chem.* **2007**, *18*, 1490–1497.

(39) Nie, Z.; Fava, D.; Kumacheva, E.; Zou, S.; Walker, G. C.; Rubinstein, M. *Nat. Mater.* **2007**, *6*, 609–614.

(40) Caswell, K. K.; Wilson, J. N.; Bunz, U. H. F.; Murphy, C. J. *J. Am. Chem. Soc.* **2003**, *125*, 13914–13915.

(41) Sethi, M.; Joung, G.; Knecht, M. R. *Langmuir* **2009**, *25*, 1572–1581.

(42) Tuinier, R.; Rieger, J.; de Kruif, C. G. *Adv. Colloid Interface Sci.* **2003**, *103*, 1–31.

(43) LeMieux, M. C.; Lin, Y.-H.; Cuong, P. D.; Ahn, H.-S.; Zubarev, E. R.; Tsukruk, V. V. *Adv. Funct. Mater.* **2005**, *15*, 1529–1540.

(44) Terrill, R. H.; Postlethwaite, T. A.; Chen, C. hsien; Poon, C. D.; Terzis, A.; Chen, A.; Hutchison, J. E.; Clark, M. R.; Wignall, G.; Londono, J. D.; Superfine, R.; Falvo,

M.; Johnson, C. S. J.; Samulski, E. T.; Murray, R. W. *Journal of the American Chemical Society* **1995**, *117*, 12537–12548.

(45) Agasti, S. S.; You, C. C.; Arumugam, P.; Rotello, V. M. *Journal of Materials Chemistry* **2008**, *18*, 70–73.

(46) Templeton, A. C.; Hostetler, M. J.; Kraft, C. T.; Murray, R. W. *Journal of the American Chemical Society* **1998**, *120*, 1906–1911.

(47) Khanal, B. P.; Zubarev, E. R. *Angew. Chem. E. Int. Ed.* **2009**, *48*, 6888–6891.

(48) Chang, W.-S.; Slaughter, L. S.; Khanal, B. P.; Manna, P.; Zubarev, E. R.; Link, S. *Nano Lett.* **2009**, *9*, 1152–1157.

(49) Li, Z.; Huang, P.; Zhang, X.; Lin, J.; Yang, S.; Liu, B.; Gao, F.; Xi, P.; Ren, Q.; Cui, D. *Mol. Pharm.* **2009**, *7*, 94–104.

(50) Dubois, L. H.; Nuzzo, R. G. *Annu. Rev. Phys. Chem.* **1992**, *43*, 437–463.

(51) Bartczak, D.; Kanaras, A. G. *Langmuir* **2011**, *27*, 10119–10123.

(52) Kirui, D. K.; Krishnan, S.; Strickland, A. D.; Batt, C. A. *Macromol. Biosci.* **2011**, *11*, 779–788.

Chapter 5

Cytotoxicity and Cell Uptake of Anisotropic Gold Nanoparticles

5.1. Introduction

As mentioned in the previous chapter, the application of gold NRs in biological systems is hampered by the CTAB capping agent which is present on as-synthesized NRs due to issues of stability as well as toxicity.[1,2] It is possible to reduce cytotoxicity significantly by simply removing excess CTAB from solution through repeated centrifugation or extraction procedures, but a certain level of free CTAB is always necessary to keep NRs from aggregating.[3] Thus, the primary method to deal with both of these problems is to modify the surface of the NRs such that the toxic CTAB component can be either reduced sufficiently in concentration or be hidden from the outside media. As detailed in the previous chapter, many different

methods have been developed to achieve this goal including the use of polymer shells,[4] polyelectrolytes,[5,6] peptides,[7,8] surfactants,[9] and lipids.[2,10]

One of the most widely used techniques is partially replacing the CTAB coating with PEG-thiol, a simple technique which can be carried out with little risk of aggregation using commercially available components. The resulting NRs are generally highly stable and can be further functionalized if a bifunctional PEG-thiol is used.[11] However, the extent of surface functionalization is generally low due to the high molecular weight of the PEG, which generally ranges from 1000 – 20000, and can be difficult to measure. As described in the previous chapter, the cationic surface of NRs is also amenable to coating through layer-by-layer (LBL) deposition of polyelectrolytes, resulting in an anionic or cationic charge with varying deposition steps. This technique provides excellent stability with some ability to tailor surface properties, but proper analysis of the structure is difficult. Furthermore, conflicting reports exist on the biocompatibility of the resulting NRs and the long-term stability of such structures under biological conditions could be problematic, especially considering the potential for release of CTAB from the base layer.[5,12] Another strategy for increasing the biocompatibility of NRs is the non-covalent exchange of CTAB through treatment with a high concentration of lipids, although the resulting lipid bilayer has similar stability limitations compared to the original CTAB bilayer.[2,10] Finally, it is possible to modify biological molecules with thiols and directly bind them to the NR surface.[7,8] This is most typically performed with cationic or neutral peptides to keep NRs from aggregating during the surface

exchange. Attachment of such biological molecules can also be useful in encoding specific biological activity into the nanomaterial. However, as stated in the previous chapter, complete removal of CTAB through any of these methods has not been demonstrated, thus bringing uncertainty to their application in *in vivo* systems.

Beyond just low toxicity, understanding the uptake of gold nanoparticles, in general, could be important for their imaging, sensing, and therapeutic applications.[13] Specifically, there has been great interest in understanding the cellular uptake of gold NRs due to their enhanced optical properties.[3,8,14–16] For example, while functionalization with PEG does lead to substantial reduction in cytotoxicity, cellular uptake drops by as much as 94 %, and virtually no NRs can enter cells.[15] LBL deposition of polyelectrolytes does increase NR uptake and the average number of rods that enter each cell ranges from hundreds[3] to one hundred thousand.[14] However, even these NRs are taken up by cells in picogram quantities, which is only 0.1 % of a typical cell mass. This small weight fraction may explain the somewhat limited success of photothermal ablation of tumor cells,[17] which is strongly dependent on the actual number of NRs present inside the cells.

Thus, in this chapter, we demonstrate that MTAB-functionalized gold NRs, whose synthesis was described in detail in the previous chapter, are highly biocompatible and can also enter cancer cells in high quantity. Cytotoxicity of the conjugates was studied by MTT assay on breast cancer cells (MCF-7) and cell uptake was investigated by correlated optical and SEM imaging. An extremely large number of NRs (about 2×10^6 per cell) were found inside the viable cells as

confirmed by TEM and quantified by inductively coupled plasma-optical emission spectrometry (ICP-OES). Finally, we demonstrate that larger gold nanostructures such as gold NWs and MRs can also be functionalized with MTAB and are also efficiently taken up by cancer cells.

5.2. Cytotoxicity of Gold Nanorods

With the characterization complete, we performed cytotoxicity and cell uptake experiments to see if the MTAB NRs could be useful for biological applications. We first measured their *in vitro* cytotoxicity compared to regular CTAB-capped NRs using the standard MTT assay on MCF-7 breast cancer cells and the results are shown in Figure 5.1. These studies reaffirmed the cytotoxicity of regular CTAB-capped gold nanorods, which kill half of the cell population (LD_{50}) at a concentration of 10 μg/mL, and showed the decreased cytotoxicity of the thiolated rods, which are not cytotoxic even up to a concentration level of 0.1 g /L. Indeed, no LD_{50} value can be determined as the percent survival does not drop below about 85 %. This finding supports previous assertions that surface charge may not be a key factor for the cytotoxicity of nanoparticle systems.[3] Although previous reports have shown that it is mostly free CTAB that contributes to the cytotoxicity of CTAB NRs in the short term,[3] it is unknown what may happen to surface-bound CTAB in *in vivo* environment. Our system has the advantage of having quantitative CTAB replacement such that this is no longer an issue.

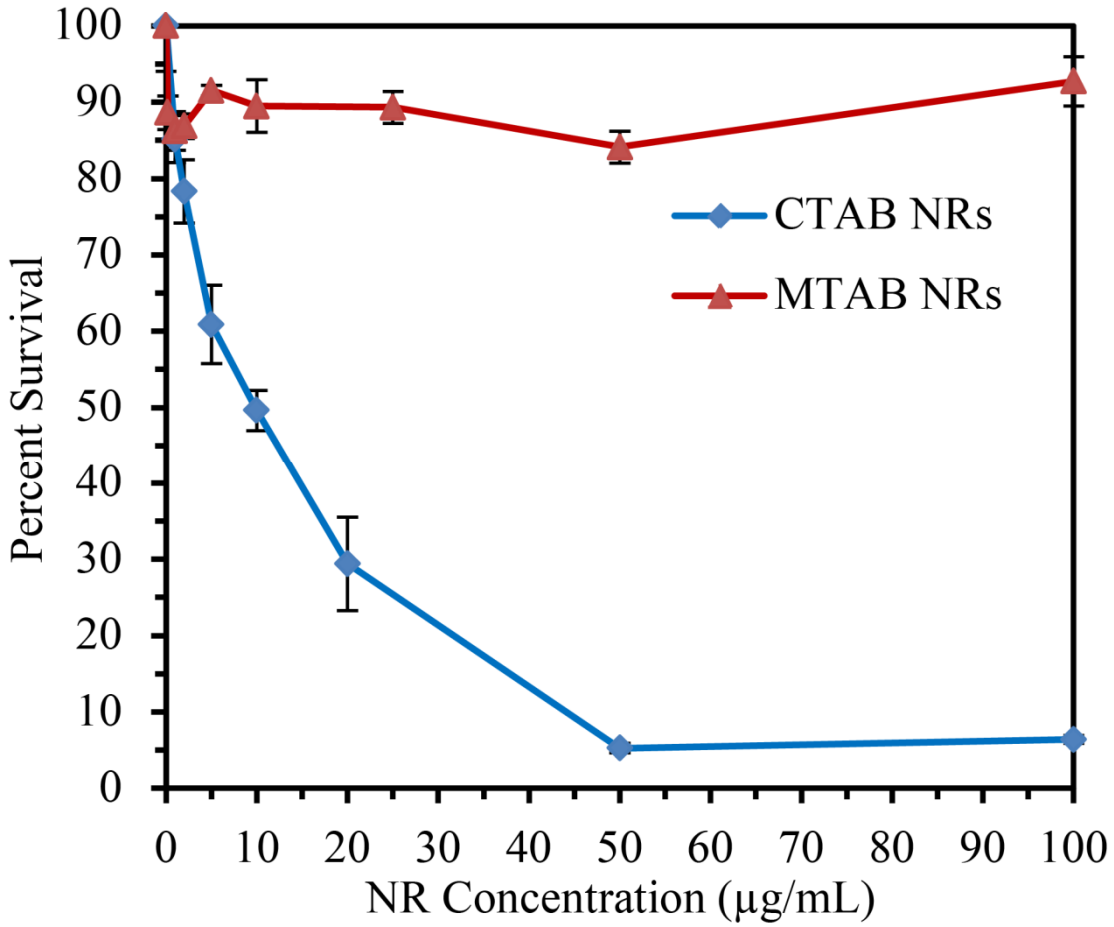

Figure 5.1 Cytotoxicity plot based on MTT analysis, which shows the percent survival of MCF-7 cells when treated with different concentrations of CTAB-NRs (blue) and MTAB-NRs (red).

5.3. Cell Uptake of Gold Nanorods

Low cytotoxicity is particularly useful if the NRs can be taken up by cells efficiently. To study the uptake, MCF-7 cells were treated with a 20 µg/mL solution of MTAB NRs in Eagle's minimum essential medium for 24 h. The cells were subsequently rinsed multiple times with PBS solution to remove the excess of NRs that did not enter the cells. After that, the cells were trypsinized, redispersed into

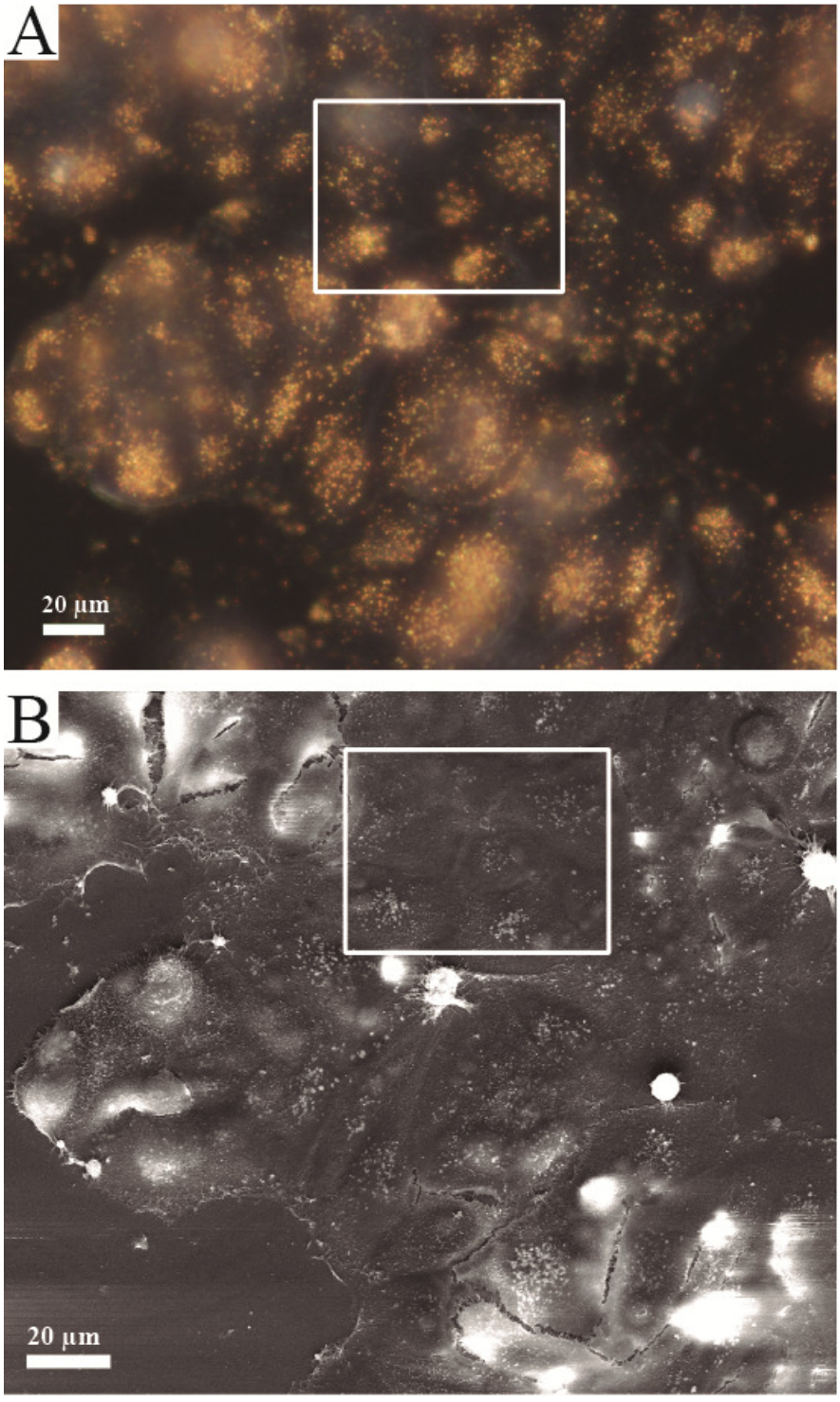

Figure 5.2. (a) Dark field optical micrograph and (b) SEM image of the same area of cells treated with MTAB NRs. Correspondence between NR positions in the optical and SEM image is highlited.

medium, and carefully plated onto a new culture slide. This approach allowed us to create a clear background without any free nanorods, which is critically important for differentiating between the internalized particles and those which are not associated with the cells.

The dark field optical image in Figure 5.2a clearly shows a large uptake of MTAB NRs and demonstrates their high scattering efficiency. It also appears that NRs are clustered together inside the cells rather than being evenly distributed throughout their interior, suggesting that the MTAB NRs enter the cells through an endosomal pathway. To perform a correlated SEM imaging of the exact same group of cells, we fixed the sample with glutaraldehyde and further cross-linked the cells with osmium tetroxide. This enabled us to prevent the collapse of cells under high vacuum conditions required for the SEM. The SEM imaging correlated with the optical experiments (Figure 5.2b) shows areas of increased brightness inside the cells because of clusters of internalized MTAB NRs. The locations of the NR clusters match up well with the bright spots seen in the optical micrograph, although there are some morphological changes that occurred during the fixation and dehydration processes. Most importantly, SEM imaging reveals that there are no MTAB NRs on the surface of the cells, which would be quite difficult to confirm by the optical microscopy alone. In contrast, the visualization of NRs residing in thicker cell areas is more efficient by optical microscopy, displaying their strong potential as imaging contrast agents.

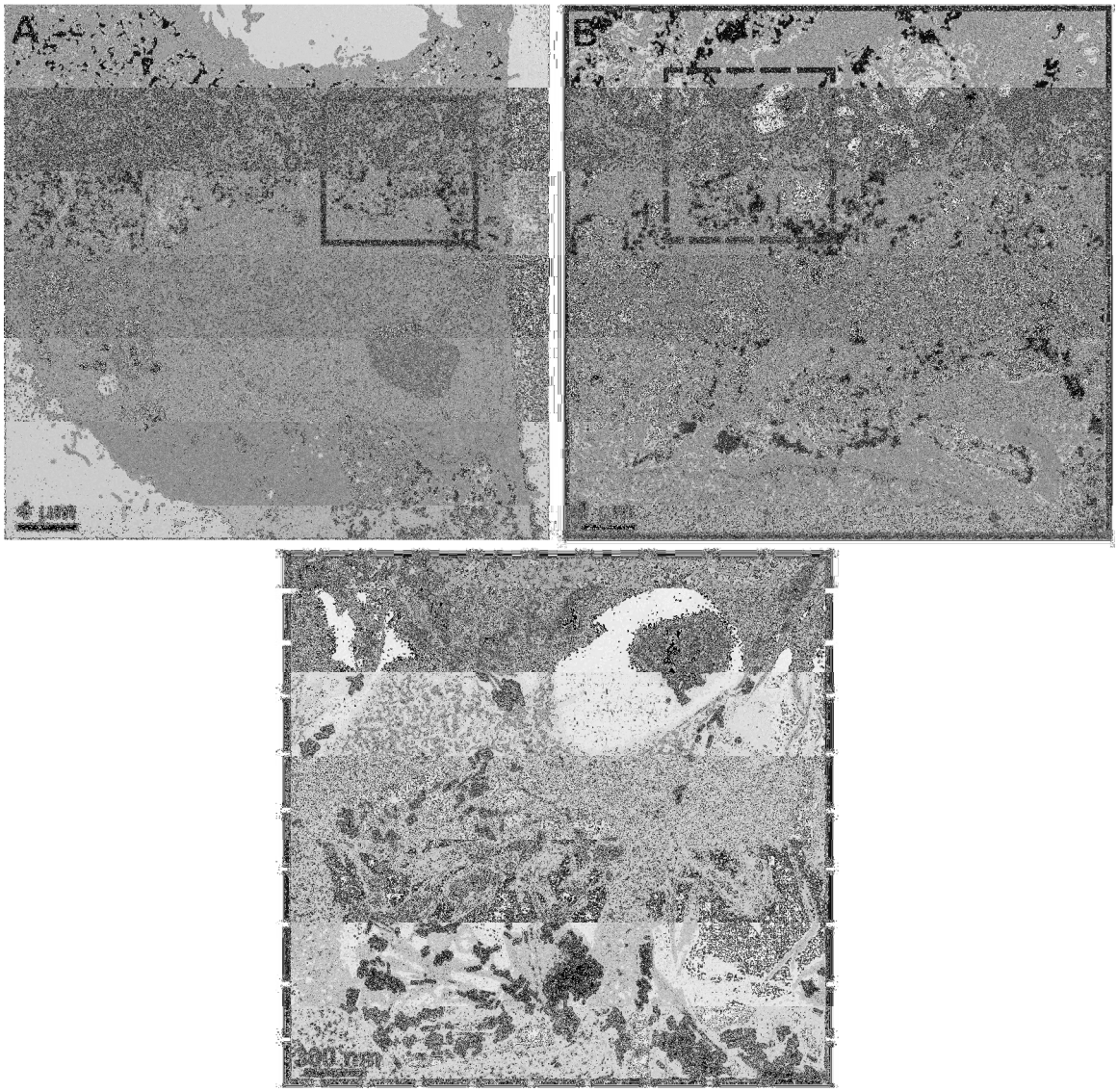

Figure 5.3. TEM images of microtomed MCF-7 cancer cells treated with the MTAB NRs (75 nm thick section). (a) View of an entire cell cross-section. (b) Magnified image of the area outlined by the black box in panel A; (c) Magnified image of the area outlined by the dashed box in panel B.

To further characterize the cellular uptake, we performed TEM imaging of cells treated with the MTAB NRs as shown in Figure 5.3. Unlike SEM and optical microscopy, TEM images of the microtomed cross-sections reveal the precise location and spatial distribution of individual NRs. We prepared 75 nm thick

sections that were cut through the center of cells. The TEM image of the entire cell cross-section (Figure 5.3a) shows an extremely large amount of NRs, which appear as dark particles. The volume of this cross-sectional sample is approximately 0.5 % of the total cell volume (20 μm in diameter), which means that the total number of nanorods inside the cell is approximately 200 times greater than that present in this image (about 10,000 NRs). Thus, even on the basis of TEM one can roughly estimate that there are at least two million NRs per cell. If confirmed by quantitative methods, it would be significantly larger than the numbers reported in the literature for nanorods of similar size, which range from several hundred[3] to one-hundred-fifty thousand NRs per cell.[14] Even at low magnification one can see that NRs do not enter the nucleus and are clustered in endosomes. Higher magnification of regions outlined by the boxes (Figure 5.3b and c) clearly shows individual NRs that do not appear to be free in the cytoplasm.[14,18–20] The amount of uptake was compared to another popular NR system, PEG NRs, which are known to resist cellular uptake and thus form a good negative control for our system. To quantify the average number of NRs taken by cells, we performed ICP-OES analysis on dissolved cells which had been treated with both MTAB NRs and their pegylated analogues. Based on these results, while almost no PEG NRs were taken up (less than 1 %), about 40 % of MTAB NRs in solution were taken up by the cells. This corresponds to a level of about 2.2 million MTAB NRs per cell that have been treated with a solution of nanorods (see Chapter 5.11.1 for detailed calculations). Such a great amount of metallic gold increases the mass of cancer cell by 0.13 ng, which is approximately

13 % of a typical cell mass (1 ng). It is particularly remarkable that the cells retain their viability and continue to proliferate with such a significant amount of gold nanostructures inside them, although further tests of their long-term health are warranted. These results show that the MTAB NRs have a very low cytotoxicity and suggest that they may be promising for further biomedical applications such as drug/gene delivery and photothermal therapy.

5.4. Factors Affecting Cell Uptake of Gold Particles

Since it is clear that MTAB NRs have a high propensity to enter cells, our next question was whether other gold nanostructures similarly functionalized with MTAB could also be taken up into cells. In general, cell uptake of nanoparticles can be affected by many factors including the surface coating as well as the size and shape of the nanoparticles.[21–23] Surface charge, in particular is thought to have a great effect on the cellular uptake. Cationic nanoparticles, in particular, have been known to have a high uptakes, presumably due to interactions with the negatively charged cell membrane. Recent research has actually called into question this simplistic view, showing that nanoparticles placed in a biological medium become rapidly coated with a protein corona that changes due to nanoparticle surface characteristics and also evolves with time.[22] This suggests that, beyond just the charge of the particles, the specific protein adsorbed on their surface is an important factor. Still, it is clear that the MTAB coating is highly effective at promoting cell uptake regardless of the actual mechanism of endocytosis.

The effect of size and shape on nanoparticle uptake has also received significant of attention.[13,21–23] However, in the case of gold nanoparticles, these studies are usually limited to the study of spherical particles which can typically be synthesized with sizes under 100 nm. Very few studies of the uptake of larger gold particles have been published. In addition, little has been shown regarding the effect of the shape of gold particles on their uptake. The most studied anisotropic particles to date are gold NRs given their more accessible synthesis. However, the size of these particles is typically limited to below 50 nm and is not readily tunable. Several examples do exist of cell uptake of template-synthesized NWs with length of 600 nm to 8 μm and diameter of 200 nm.[24,25] These studies demonstrated the ability of HeLa cells to uptake gold NWs regardless of their length, showing that the expected size limitations for this process should be reevaluated. However, no reports exist on the uptake of chemically synthesized NWs with much smaller diameters and significantly different surface chemistry.

5.5. Surface Functionalization of Nanowires and Mesorods with MTAB

Chapter 3 detailed the synthesis of larger gold particles based on the chemical overgrowth of purified PNR seeds. One of the main advantages of this synthetic technique was the ability to synthesize MRs and NWs with smooth and starfruit-like morphology in high purity. That high level of purity offers the anisotropic particles for use in a variety of applications such as their cellular uptake.

Indeed, the reason that only template-synthesized NWs have been studied for biological applications up to this point is that other chemical methods of NW synthesis simply do not yield a pure enough product. Given our experience with MTAB NR cell uptake, we wanted to see if MTAB surface functionalization of MRs and NWs could be successfully performed.

Indeed, treatment of MRs and NWs with MTAB followed by purification by several steps of sedimentation followed by supernatant removal was found to be an effective way of stabilizing the as-synthesized, CTAB-capped particles. Qualitatively, it is clear that this procedure worked because the particles remained stable and dispersible after several rounds of purification while CTAB-capped MRs and NWs have a very high tendency to aggregate at low CTAB concentration due to their large size and high rate of sedimentation. NWs, in particular, tend to form large bundles even at higher CTAB concentrations due to their extremely high aspect ratio. Quantitative analysis of the extent of MTAB exchange similar to what was performed for gold NRs was not conducted for either the MRs or NWs due to the impracticality of carrying out such experiments. The reduced surface-to-volume ratio of these structures would necessitate the synthesis and dissolution of very large amounts of material in order to carry out TGA and NMR experiments. Still, it is expected that the surface functionalization should occur in a similar manner as it did for NRs. One particular difference is that NRs have a single-crystalline structure while MRs and NWs both have pentahedrally-twinned structures. This feature

determines which crystal facets are exposed to CTAB and MTAB binding, but it is unknown if this affects the surface capping process.

5.6. Cell Uptake of MTAB Mesorods

Next, MCF-7 cancer cells were treated with MTAB MRs purified from excess CTAB and MTAB. After incubation overnight, the cells were fixed and processed as in the NR uptake experiments and imaged with TEM. Figure 5.4 shows TEM images of cells treated with MTAB MRs at a concentration of about 10 μg/mL. The representative low-magnification image in Figure 5.4a demonstrates the large amount of MRs which can be taken up into cells, an amount which is significantly higher than that observed for template-synthesized gold microstructures; in those papers only a few particles per cells were shown.[24,25] This can be partly attributed to the limited yield of particles that can be produced from a template-based synthetic procedure, as discussed in Chapter 1.4.3, which would limit the total amount of MRs that can be used in an experiment. MRs synthesized wet-chemically through our seed-mediated procedure, on the other hand, can be synthesized in larger quantities that scale in three dimensions rather than two, as is the case for the template-based synthesis. Besides affecting the total amount of material which is taken up into cells, any eventual use of such particles would have to be accompanied by a reasonably scalable synthesis for it to be practical. Other than total amount of material which can be produced, it is likely that the MTAB surface coating is an important factor in inducing cell uptake of the particles, similar to what

was observed in the case of MTAB NRs. Figure 5.4b-d show higher magnification images demonstrating that the dark shapes observed in the low magnification images are indeed MRs. The orientation of the MRs is not limited to parallel to the substrate as is generally observed in normal TEM images. Many

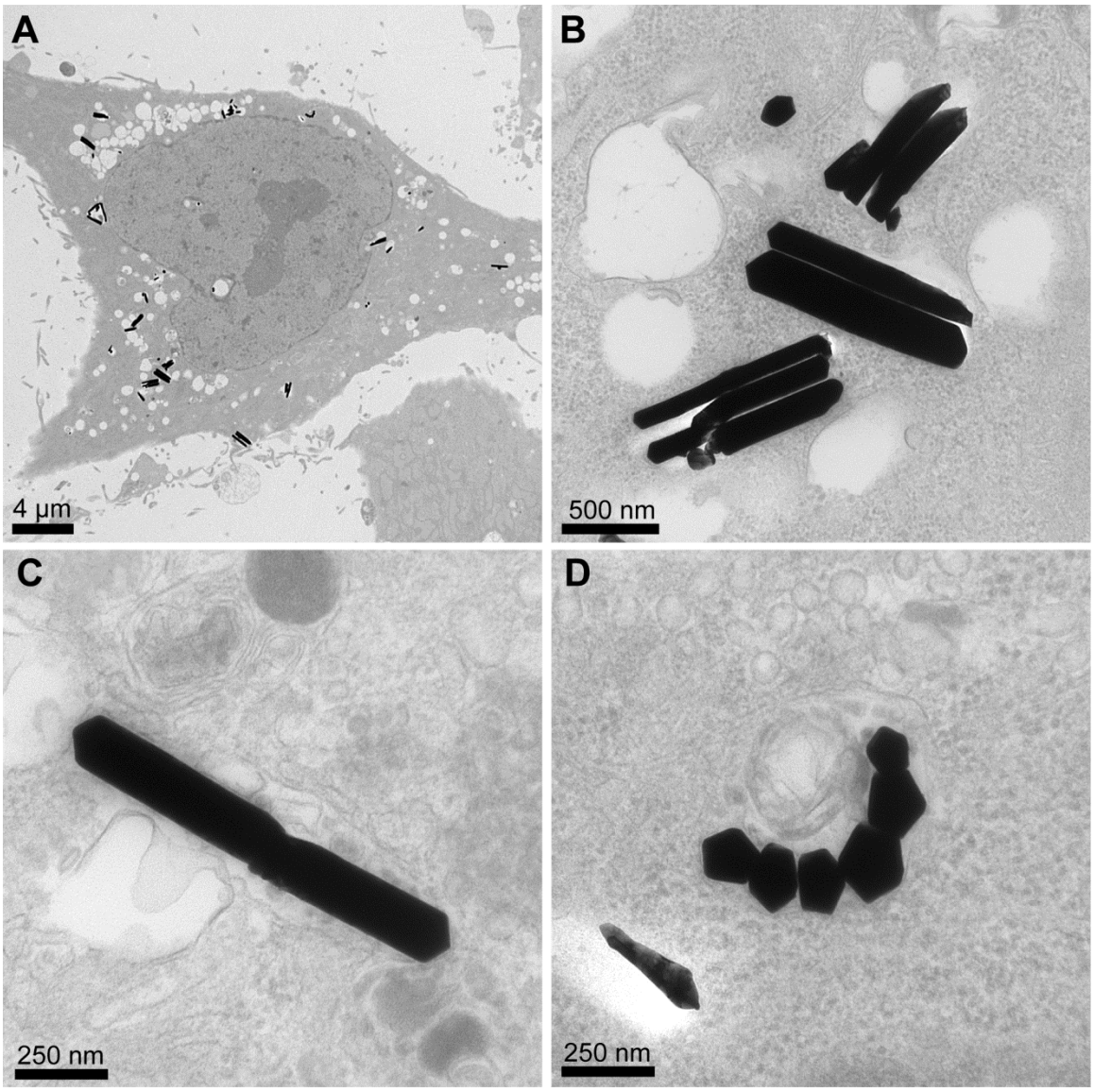

Figure 5.4. Low (a) and high (b-d) magnification TEM images of gold MRs that have been taken up into cells.

smaller fragments as well jagged breaks exist where tilted MRs appear to have been imperfectly cut by the microtome. In fact, Figure 5.4d shows several MRs which are oriented perpendicularly to the substrate, clearly showing their pentahedral cross-section. One area of interest for these experiments is to determine whether the size of these particles has an effect on method of uptake or intracellular fate. As shown previously, MTAB NRs all appeared to be contained inside vesicles, suggesting a standard endocytosis process. On the other hand, MRs do not display the same obvious encapsulation inside cells. While many MRs in Figure 5.4a do appear to be surrounded by or at least located in the vicinity of large vesicles, the high magnification images, especially Figure 5.4c and d, appear to show MRs located free in the cytoplasm outside of any vesicles. Although these results are not conclusive, they do suggest that the cell uptake process or intracellular fate of MRs is different than NRs. However, similar to the NRs, it appears that MRs are not able to penetrate the nucleus of the cell.

5.7. Cell Uptake of MTAB Nanowires

To see if this could be observed with a different particle type, we treated cancer cells with MTAB NWs of 6 – 10 μm length and 60 nm diameter and again imaged them by TEM, as shown in Figure 5.5. The low-magnification image in Figure 5.5a shows a very similar uptake pattern to the MRs, with a large number of wires having been internalized by the cell. The length of the visible wires is highly variable, which can be explained in a couple of ways. First, NWs do have a higher

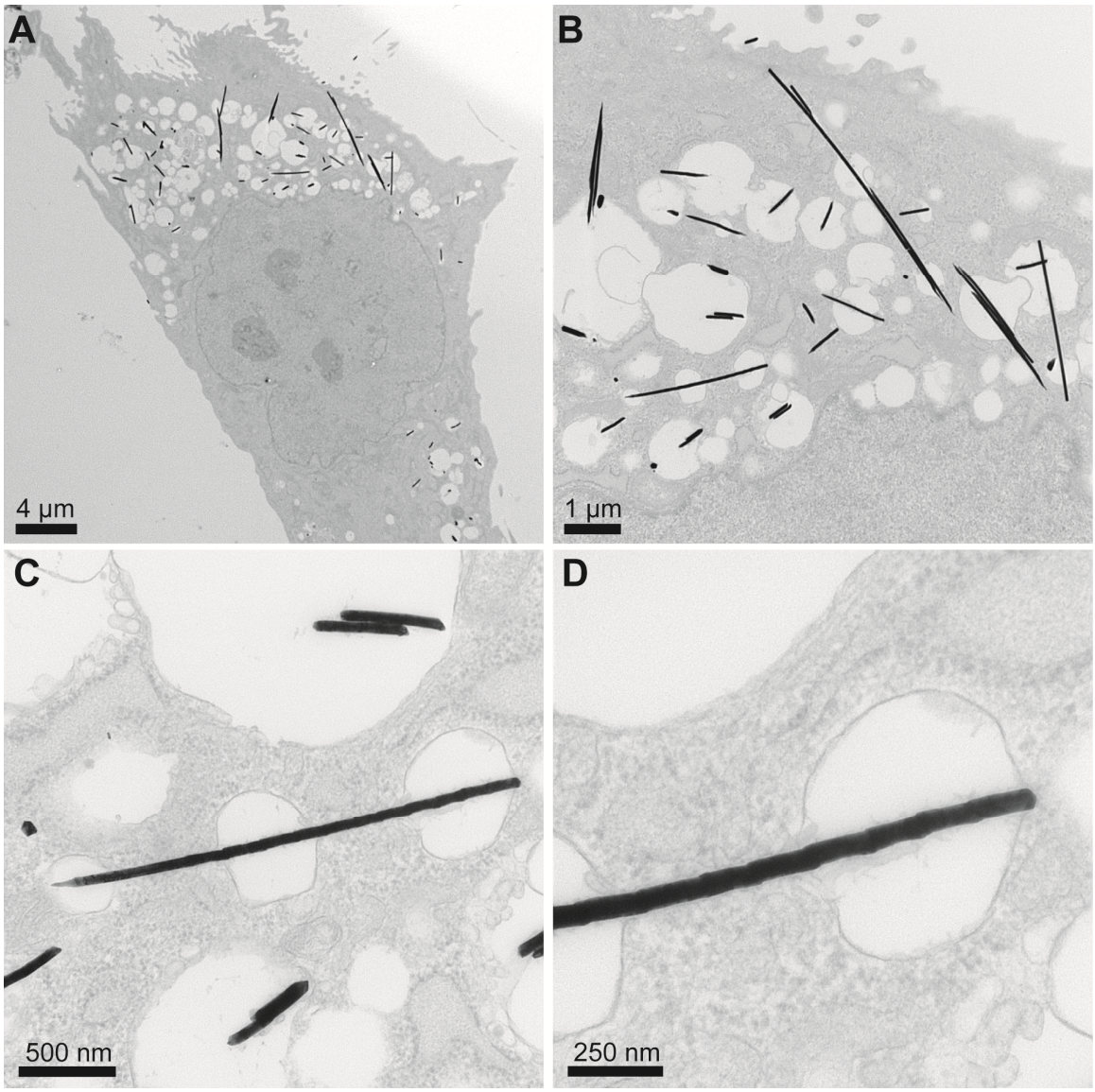

Figure 5.5. Low (a), medium (b), and high (c-d) magnification TEM images of MTAB NWs inside of cancer cells.

polydispersity in terms of length compared to either NRs or MRs and small NWs are always present along with larger ones. Second, NWs should have a high propensity for fragmentation during the microtoming process because of their length. Interestingly, NWs seen in the high-magnification images in Figure 5.5c-d displayed a zigzag-like morphology which appears to be an artifact of the microtoming

process. The distribution of NWs throughout the cell is similar to that seen for both MRs and NRs: again, no NWs are visible in the nucleus. The high-magnification TEM images seem to indicate that wires are not located inside of vesicles, which might not be surprising given their extreme length. However, a closer examination indicates that a membrane layer of some sort does appear to completely encircle each NW and that each NW is attached to at least one circular vesicle structure. In fact, the NW shown in Figure 5.5c can be seen traversing three separate vesicles and the higher magnification view of the same wire in Figure 5.5d shows that not only does the vesicle membrane warp around the tip of the wire, but it also appears to travel along the wire in between the vesicles without breaks.

5.8. Analysis of the Uptake of Larger Gold Particles

The results discussed for the cell uptake of MTAB-capped gold MRs and NWs are still at the preliminary stage. We were able to demonstrate that both of these types of gold particles have a high propensity for internalization by MCF-7 cancer cells, but further work needs to be done to better understand the mechanism of uptake as well as its effect on the health of the cells. However, some general conclusions can be drawn from our results. First, it is clear that none of our particles were able to enter the nucleus, which suggests that this is a general limitation that MTAB-capped particles share with many other nanoparticle systems.[13,21,22] In general, it appears that some sort of specific targeting moiety is necessary to deliver nanoparticles to the nucleus. For instance, El-Sayed and

coworkers utilized a nuclear targeting peptide to direct NRs towards the nucleus.[8] Although cytotoxicity measurements still have to be performed, the particles did not appear to destroy the cell structure. TEM images of cells that have internalized NWs and MRs appear similar to images of NR-loaded cells which are not cytotoxic. Of course, one large question is how the uptake process is affected by the size and shape of the MRs and NWs. Both types of particles are large enough that due to the high density of gold they tend to settle out of solution. This could enhance cell uptake by placing a large portion of particles in solution directly on top of the cells. On the other hand, this lack of solution stability could also be a limitation for *in vivo* applications. Finally, although the method of cell uptake is not currently known, it appears that a single, large vesicle is not responsible for the NW uptake due to their large length and aspect ratio. However, the NWs are still attached to at least one vesicle and also appear to be entirely covered in a thin membrane, suggesting, perhaps, that wires are initially pulled in through a normal endocytotic process after which the rest of the wire is internalized in a different way. On the other hand, some MRs appear to exist outside of any membrane-structure, suggesting that the initial membrane could have been lost after uptake or that mechanism of internalization could be different. The ability of non-phagocytotic cells like the breast cancer cells used in our experiments to take up such large particles is an important finding which supports recent results from other groups that disprove the traditionally held view that particles must be below 100 nm in size to be internalized.[23] It is important to note than one difference between our experiments and many others

dealing with microparticle uptake is that the density of our gold particles is much higher than that of other systems, which typically employ polymeric materials.[22,23,26] The effect of this difference could be an important area of research in the future.

5.9. Conclusions

In this chapter, we demonstrated the uptake into cancer cells of a variety of anisotropic gold particles including NRs, MRs, and NWs that have been surface functionalized with the cationic thiol MTAB. NRs, in particular, were shown to be nontoxic by MTT assay and could be taken up in amounts surpassing 2 million NRs per cell as shown by a comprehensive combination of optical microscopy, SEM, TEM, and ICP-OES data. Much larger MRs and NWs were also found to enter cells in significant numbers, possibly through a unique internalization process, as demonstrated by TEM imaging. More work still needs to be done to better understand the mechanism of internalization of these MTAB particles, especially in the case of MRs and NWs. In fact, the ability to tune MR and NW sizes over a wide range may render them particularly useful in understanding the effect of size and shape on the cell uptake process.

5.10. Experimental Methods

5.10.1. Cytotoxicity of MTAB NRs

MCF-7 cells were cultured in Eagles Minimum Essential Medium with non-essential amino acids, 2 mM L-glutamine, 1 mM sodium pyruvate, and fetal bovine serum to a final concentration of 10 %. MCF-7 cells were plated into a 96-well plate at 15,000 cells per well and 6 wells per each concentration. Cells were treated with an appropriate amount of MTAB NRs or CTAB NRs in medium for 24 hours, followed by the addition of 25 μL of a 5 mg/mL MTT solution in PBS. After incubating for 4 hours, the medium was removed, the cells were lysed with DMSO, and the absorbance measured on a plate reader at 570 nm.

5.10.2. Optical and SEM Imaging of NR Cell Uptake

For cell uptake imaging experiments, MCF-7 cells were plated into a 6-well plate at 500,000 cells per well and treated with 2 mL of a 20 μg/mL solution of NRs in medium for 24 hours, trypsinized, and then plated onto a culture slide. For quantification of NR uptake by ICP-OES, cells were treated with 2 mL of an 80 μg/mL solution of NRs in medium for 24 hours, washed several times with PBS, trypsinized, pelleted, dissolved with aqua regia, and the gold concentration measured by ICP. For SEM imaging, the cells were first fixed by using 2.5 % glutaraldehyde in PBS for one hour followed by 0.4 % osmium tetroxide solution. Next, cells were dehydrated by consecutive treatment with 25 %, 50 %, 70 %, 95 %,

and 100 % ethanol followed by 50 % and 100% hexamethyldisilazane and allowed to dry overnight.

5.10.3. MR and NW Synthesis and MTAB Functionalization

MRs were synthesized according to the procedure in Chapter 3.9. NWs were synthesized similar to the procedure in Chapter 3 but with the standard ascorbic acid reducing agent rather than hydroquinone. Briefly, 100 μL purified PNR seed was added to a growth solution consisting of 100 mL of a $2.5 \cdot 10^{-4}$ mM $HAuCl_4$ solution in 0.1M CTAB to which has been added 550 μL of a 0.1M ascorbic acid solution. Growth continued overnight after which the supernatant was decanted and the sedimented wires redispersed in fresh 0.1M CTAB solution and this sedimentation and redispersion process was repeated at least 3 more times. To a solution of purified MRs and NWs, MTAB was added to reach a final concentration of ~5-10 mg/mL and the particles were allowed to exchange overnight with several sonication steps to redisperse them into solution. Purification was carried out by repeated rounds of sedimentation, removal of the supernatant, and redispersion in pure water.

5.10.4. TEM Imaging of MTAB-Capped Particle Cellular Uptake

MCF-7 cells were plated into a 6-well plate at 500,000 cells per well and treated with 2 mL of a 20 μg/mL solution of MTAB NRs, MRs, or NWs per well in the medium for 24 hours. Cells were washed several times with PBS and fixed with a solution containing 3% glutaraldehyde and 2% paraformaldehyde in 0.1 M

cacodylate buffer, pH 7.3, for 1 hour. After fixation, the samples were washed and treated with 0.1% Millipore-filtered cacodylate buffered tannic acid, postfixed with 1% buffered osmium tetroxide for 30 min, and stained en bloc with 1% Millipore-filtered uranyl acetate. The samples were dehydrated in increasing concentrations of ethanol, infiltrated, and embedded in LX-112 medium. The samples were polymerized in a 70 ^{o}C oven for 2 days. Ultrathin sections were cut in a Leica Ultracut, stained with uranyl acetate and lead citrate in a Leica EM Stainer, and examined in a JEM 1010 transmission electron microscope (JEOL) at an accelerating voltage of 80 kV. Digital images were obtained using AMT Imaging System (Advanced Microscopy Techniques Corp). All steps after the initial fixation were carried out by MD Anderson High Resolution Electron Microscopy Facility in Houston.

5.11. Calculations

5.11.1. Calculation of the Amount of NRs Taken Up per Cell

500,000 cells were treated with 2 mL of medium containing 80 μg/mL MTAB-NR in medium. From ICP-OES, the total amount of up-taken gold was determined to be 40% of 160 μg or 64 μg Au / 500,000 cells = $1.28 \cdot 10^{-4}$ (μg Au/cell). Given the density of gold and the previously calculated volume per NR of 3060 nm^3 × 1.93·10-14 (μg Au/nm^3) = 5.91·10-11 (μg Au/NR). So, $1.28 \cdot 10^{-4}$ (μg Au/cell) / $5.91 \cdot 10^{-11}$ (μg Au/NR) = $2.17 \cdot 10^{6}$ NR per cell.

5.12. References

(1) Cortesi, R.; Esposito, E.; Menegatti, E.; Gambari, R.; Nastruzzi, C. *Int. J. Pharm.* **1996**, 139, 69–78.

(2) Takahashi, H.; Niidome, Y.; Niidome, T.; Kaneko, K.; Kawasaki, H.; Yamada, S. *Langmuir* **2006**, 22, 2–5.

(3) Alkilany, A. M.; Nagaria, P. K.; Hexel, C. R.; Shaw, T. J.; Murphy, C. J.; Wyatt, M. D. *Small* **2009**, 5, 701–708.

(4) Prencipe, G.; Tabakman, S. M.; Welsher, K.; Liu, Z.; Goodwin, A. P.; Zhang, L.; Henry, J.; Dai, H. *J. Am. Chem. Soc.* **2009**, 131, 4783–4787.

(5) Leonov, A. P.; Zheng, J.; Clogston, J. D.; Stern, S. T.; Patri, A. K.; Wei, A. *ACS Nano* **2008**, 2, 2481–2488.

(6) Huang, H.-C. C.; Barua, S.; Kay, D. B.; Rege, K. *ACS Nano* **2009**, 3, 2941–2952.

(7) Chanda, N.; Shukla, R.; Katti, K. V; Kannan, R. *Nano Lett.* **2009**, 9, 1798–1805.

(8) Oyelere, A. K.; Chen, P. C.; Huang, X.; El-Sayed, I. H.; El-Sayed, M. A. *Bioconjugate Chem.* **2007**, 18, 1490–1497.

(9) Alkilany, A. M.; Nagaria, P. K.; Wyatt, M. D.; Murphy, C. J. *Langmuir* **2010**, 26, 9328–9333.

(10) Lee, S. E.; Sasaki, D. Y.; Perroud, T. D.; Yoo, D.; Patel, K. D.; Lee, L. P. *J. Am. Chem. Soc.* **2009**, 131, 14066–14074.

(11) Alkilany, A. M.; Thompson, L. B.; Boulos, S. P.; Sisco, P. N.; Murphy, C. J. *Adv. Drug Deliv. Rev.* **2012**, 64, 190–199.

(12) Rayavarapu, R. G.; Petersen, W.; Hartsuiker, L.; Chin, P.; Janssen, H.; van Leeuwen, F. W. B.; Otto, C.; Manohar, S.; van Leeuwen, T. G. *Nanotechnology* **2010**, 21, 145101.

(13) Dykman, L.; Khlebtsov, N. *Chem. Soc. Rev.* **2012**, 41, 2256–2282.

(14) Hauck, T. S.; Ghazani, A. A.; Chan, W. C. *Small* **2008**, 4, 153–159.

(15) Parab, H. J.; Chen, H. M.; Lai, T. C.; Huang, J. H.; Chen, P. H.; Liu, R. S.; Hsiao, M.; Chen, C. H.; Tsai, D. P.; Hwu, Y. K. *J. Phys. Chem. C* **2009**, 113, 7574–7578.

(16) Huff, T. B.; Hansen, M. N.; Zhao, Y.; Cheng, J. X.; Wei, A. *Langmuir* **2007**, 23, 1596–1599.

(17) Kennedy, L. C.; Bickford, L. R.; Lewinski, N. A.; Coughlin, A. J.; Hu, Y.; Day, E. S.; West, J. L.; Drezek, R. A. *Small* **2011**, 7, 169–183.

(18) Shukla, R.; Bansal, V.; Chaudhary, M.; Basu, A.; Bhonde, R. R.; Sastry, M. *Langmuir* **2005**, 21, 10644–10654.

(19) Verma, A.; Uzun, O.; Hu, Y.; Hu, Y.; Han, H. S.; Watson, N.; Chen, S.; Irvine, D. J.; Stellacci, F. *Nat.Mater.* **2008**, 7, 588–595.

(20) Nativo, P.; Prior, I. A.; Brust, M. *ACS Nano* **2008**, 2, 1639–1644.

(21) Lévy, R.; Shaheen, U.; Cesbron, Y.; Sée, V. *Nano Rev.* **2010**, 1, 4889.

(22) Albanese, A.; Tang, P. S.; Chan, W. C. W. *Annu. Rev. Biomed. Eng.* **2012**, 14, 1–16.

(23) Petros, R. A.; DeSimone, J. M. *Nat. Rev. Drug Disc* **2010**, 9, 615–627.

(24) Kuo, C.-W.; Lai, J.-J.; Wei, K. H.; Chen, P. *Adv. Funct. Mater.* **2007**, 17, 3707–3714.

(25) Kuo, C.-W.; Lai, J.-J.; Wei, K. H.; Chen, P. *Nanotechnology* **2008**, 19, 025103.

(26) Gratton, S. E. A.; Ropp, P. A.; Pohlhaus, P. D.; Luft, J. C.; Madden, V. J.; Napier, M. E.; DeSimone, J. M. *Proc. Natl. Acad. Sci.* **2008**, 105, 11613–11618.